UNIVERSITY OF CALIFORNIA, SAN DIEGO

The Effects of Chemistry on the Colloidal Behavior of Alumina Slurries and Copper Nanohardness for Copper Chemical Mechanical Planarization

A dissertation submitted in partial satisfaction of the requirements for the degree of

Doctor of Philosophy

in

Chemical Engineering

by

Robin Veronica Ihnfeldt

Committee in charge:

Professor Jan B. Talbot, Chair
Professor Pao Chau
Professor Richard Herz
Professor Paul Linden
Professor Vitali Nesterenko

2008

The dissertation of Robin Veronica Ihnfeldt is approved, and it is acceptable in quality and form for publication on microfilm:

_____

_____

_____

_____

_____
Chair

University of California, San Diego

2008

Dedicated to my parents.

TABLE OF CONTENTS

LIST OF SYMBOLS AND ABBREVIATIONS

A	real contact area between pad asperities and wafer (m^2)
a	mean asperity area (μm^2)
a'	correction factor to calculate cohesive strength, has values between 6-8
A_0	total contact area between pad and wafer (m^2)
A_B	cross-sectional breaking plane in the agglomerate (nm^2)
a_P	radius of projected area of contact between abrasive and wafer (nm)
A_S	surface area of contact between the abrasive and the wafer (nm^2)
a_P	radius of projected area of contact between abrasive and pad (nm)
b	mean separation between pad and wafer (nm)
C_0	material removal due to chemical etching (nm/min)
C_{L1}	chemical etch rate of Cu(I) in water-complexing agent system (nm/min)
C_{L2}	chemical etch rate of Cu(II) in water-complexing agent system (nm/min)
C_S	cohesive strength of the agglomerate (MPa)
C_{W1}	chemical etch rate of Cu(I) in water (nm/min)
C_{W2}	chemical etch rate of Cu(II) in water (nm/min)
D	diameter of wafer (mm)
d	diameter of the agglomerate (nm)
D_{max}	maximum agglomerate size (nm)
d_p	primary particle diameter (nm)
d_s	dilution ratio of slurry to DI water
D_{SUM}	number of asperities per unit area of pad (cm^{-2})
e	offset between platen and wafer (cm)
E^*	equivalent modulus of elasticity (Pa)
E_i	elastic modulus of i (GPa)
E_P	Young's modulus of the pad (MPa)
E_{SP}	reduced Young's modulus of the abrasive/pad pair (MPa)
E_W	Young's modulus of the wafer (Pa)
F	applied force (N)
f	slurry flow rate (ml/min)

F_B	force required to break apart the agglomerate (N)
F_N	normal force on the agglomerate (N)
F_S	shear force of wafer sliding over the agglomerate (N)
F_{SP}	force between the particle and pad (N)
F_{SW}	force between the particle and wafer (N)
F_U	force on agglomerates during ultrasonication (N)
g	gap between the wafer and the pad (nm)
G_1	volume concentration of abrasives (ml^{-1})
H	Hamaker constant (J)
h	slurry film thickness (μm)
h	copper layer thickness (nm)
H_i	nanohardness of compound *i* (GPa)
H_N	hardness necessary to obtain the experimental MRR (GPa)
H_P	hardness of the pad (MPa)
H_W	hardness of the wafer (GPa)
IEP	iso-electric point
K_P	Preston's constant
l	height of asperities (μm)
M_0	mechanical removal rate of Cu metal (nm/min)
M_2	mechanical removal rate of Cu(I) (nm/min)
M_1	mechanical removal rate of Cu(II) (nm/min)
MRR	material removal rate (nm/min)
$m_{s\text{-}a}$	concentration of slurry before dilution (%)
MW_{Cu}	molecular weight of copper metal of 63.5g/mol
N	number of active abrasives
n	total number of abrasives
P	applied pressure (Pa)
P_0	wafer down pressure (Pa)
P_C	total contact pressure on pad asperities (Pa)
q	area density of the abrasives (nm^{-2})

R	radius of asperities (μm)
R	radius of indentor (nm)
r	primary particle radius (nm)
R_a	roughness (μm)
S	cross sectional area of the material deformed by the abrasive (nm^2)
t	polishing time (min)
V	volume removed by a single abrasive (m^3)
v	relative velocity (m/s)
v_{sa}	volume concentration of abrasives in slurry (vol abrasives/vol slurry)
w_k	wear constant
x	abrasive diameter (nm)
x_{act}	diameter of active abrasives (nm)
x_{avg}	average abrasive diameter (nm)
x_{max}	diameter of the largest abrasives (nm)
y	tip displacement (μm)
z	asperity height (μm)

Greek letters

α	surface tension of the liquid (dyn/cm)
β	density ratio of the surface film and the wafer
δ	separation distance of the particles in the primary medium (nm)
Δ	total penetration depth of abrasive into wafer and pad(μm)
δ_{max}	maximum indentation depth (nm)
δ_{min}	minimum indentation depth (nm)
Δ_P	penetration depth of abrasive into pad (nm)
Δ_W	penetration depth of abrasive into wafer (nm)
ε	porosity of the agglomerate
ξ	tolerance parameter
μ	slurry viscosity (Pa·s)

μ_f	coefficient of friction between wafer surface and contacting asperity tips
μ_s	static coefficient of friction between alumina particles
ν_i	Poisson's ratio of *i*
ν_P	Poisson's ratio of the pad
ν_W	Poisson's ratio of the wafer
$\phi(z)$	distribution function of asperity heights
ρ_a	density of the abrasive (g/cm^3)
ρ_{Cu}	density of copper (8.933 g/cm^3)
ρ_s	density of the slurry before dilution (g/cm^3)
ρ_W	density of the wafer (g/cm^3)
σ	standard deviation of the abrasive size distribution (nm)
σ_i	yield strength of *i* (MPa)
σ_s	standard deviation of asperity heights (μm)
τ	shear stress (Pa)
υ	vibration frequency (μm)
ω	effective wafer rotation speed (m/s)
Ω_P	platen rotation speed (rpm)
Ω_W	wafer rotation speed (rpm)

LIST OF FIGURES

LIST OF TABLES

Acknowledgements

This work was sponsored by FLCC Consortium through a UC Discovery grant. The authors gratefully acknowledge all the companies involved in the UC Discovery grant: Advanced Micro Devices, Applied Materials, ASML, Atmel Corporation, Cadence, Canon, Cymer, Cypress, Dupont, Ebara Technologies Inc., Hitachi Global Storage Technologies, Intel Corporation, KLA-Tencor, Mentor Graphics, Nikon Research Corporation of America, Novellus Systems Inc., Panoramic Technology, Photronics, Synopsys, and TEL USA.

The collaboration of Professors Komvopoulos and Doyle and their research groups from the University of California, Berkeley is greatly appreciated. I would also like to thank Professor Dornfeld and his group from University of California, Berkeley for the use of their polishing apparatus and for the help that was provided to set up the copper CMP experiments. Professor Bavarian and his research group from California State University, Northridge, provided the Hysitron Instrument for our hardness experiments and their time and expertise is very much appreciated. Professor Talke and his research group from University of California, San Diego also provided a nanoindentor for our initial hardness measurements, and their help is also appreciated. Additional thanks to Professor Arrhenius from University of California, San Diego for providing the cuprite samples and Evelyn York for the EDX analysis. Professor Nesterenko from University of California, San Diego provided his expertise in developing the criteria to determine when agglomerates break up, and his help is very

much appreciated. Also, I would like to acknowledge Cabot Corporation for providing the slurry for our experiments.

Chapter 3, in full, is a reprint of the material as it appears in the Journal of the Electrochemical Society, Robin Ihnfeldt and Jan B. Talbot, Vol. 153, Issue 11, pg. G948 (2006). The dissertation author was the primary investigator and author of this paper.

Chapter 4 is a reprint of the material as it appears in the Journal of the Electrochemical Society, Robin Ihnfeldt and Jan B. Talbot, Vol. 154, Issue 12, pg. H1018 (2007), with some additional information. The dissertation author was the primary investigator and author of this paper.

Chapter 5 is a reprint of the material as it appears in the Journal of the Electrochemical Society, Robin Ihnfeldt and Jan B. Talbot, Vol. 155, Issue 6 (2008), also with some additional information. The dissertation author was the primary investigator and author of this paper.

Chapter 6, in full, has been submitted for publication of the material as it may appear in the Journal of the Electrochemical Society, Robin Ihnfeldt and Jan B. Talbot, 2008. The dissertation author was the primary investigator and author of this paper.

Vita

2001	Bachelor of Science, Colorado School of Mines
2001-2003	Engineer, Micron Technology, Boise, Idaho
2003-2008	Graduate Student Researcher, University of California, San Diego
2005	Master of Science, University of California, San Diego
2008	Doctor of Philosophy, University of California, San Diego

Publications

Modeling Material Removal Rates for Copper CMP Using Copper Nanohardness and Etch Rates, R.V. Ihnfeldt and J.B. Talbot, *J. Electrochemical Soc.*, submitted March 2008.

Effect of CMP Slurry Chemistry on Copper Nanohardness, R.V. Ihnfeldt and J. B. Talbot, *J. Electrochemical Soc.*, **155**, H412 (2008).

Modeling of Copper CMP Using the Colloidal Behavior of an Alumina Slurry with Copper Nanoparticles, R.V. Ihnfeldt and J.B. Talbot, *J. Electrochemical Soc.*, **154**, (12) H1018 (2007).

The Effects of Copper CMP Slurry Chemistry on the Colloidal Behavior of Alumina Abrasives, R. Ihnfeldt and J.B. Talbot. *J. Electrochemical Soc.*, **153**, G948 (2006).

Modeling Copper CMP Material Removal Rates Using Copper Surface Nanohardness, R. V. Ihnfeldt and Jan B. Talbot, to be presented at the 213th Meeting of the Electrochemical Society, Phoenix, Arizona, May 18-23, 2008.

Copper CMP Removal Rate Predictions Using Alumina Agglomerate Size Distributions, R.V. Ihnfeldt and J.B. Talbot, VLSI Multilevel Intercon. Conf.(VMIC), Sept.25-27, 2007, Fremont, CA.

Effects of CMP Slurry Chemistry on Agglomeration of Alumina and Copper Surface Hardness, R. Ihnfeldt and J.B. Talbot, The 210th Meeting of the Electrochemical Society, Cancun, Mexico, Oct. 29-Nov. 3, 2006, **3** (41), 21.

2nd Place ICPT 2006 Outstanding Poster Award - *Copper Removal Rate Predictions Using Alumina Agglomerate Size Distribution and Copper Nanohardness Measurements*, R. Ihnfeldt and J.B. Talbot. 2006 International Conference on Planarization/CMP Technology, Oct. 12-13, Foster City, CA.

Comparison of HILIC and Fluorinated Columns Using LC and SFC for the Separation of Polar Basic Compounds in Drug Development, R. Ihnfeldt, Y. Zhao, M. Coutant, C. Aurigemma. The 30th International Symposium on High Performance Liquid Phase Separations and Related Techniques, San Francisco, CA, Jun. 17-22, 2006.

ABSTRACT OF THE DISSERTATION

The Effects of Chemistry on the Colloidal Behavior of Alumina Slurries and Copper Nanohardness for Copper Chemical Mechanical Planarization

by

Robin Veronica Ihnfeldt

Doctor of Philosophy in Chemical Engineering

University of California, San Diego, 2008

Professor Jan B. Talbot, Chair

Chemical mechanical planarization (CMP) is used in integrated circuit manufacturing to remove excess material and provide a globally planarized wafer surface. The CMP process requires slurry containing nanometer-sized abrasive particles and chemical additives which produce a mechanical and chemical synergistic effect that is responsible for the material removal rate (MRR). Because copper has become the interconnect material of choice, the focus of our research is on copper CMP. The chemical additives in the slurries control the state of the copper (CuO, Cu^{2+}, etc.) on the surface of the wafer and in the slurry and also affect the dispersion characteristics of the abrasives. This research investigated the influence of common additives (glycine, H_2O_2, etc.), solution pH, and presence of copper on the colloidal behavior of alumina suspensions. The colloidal behavior was characterized through measurement of zeta potential and agglomerate size distributions. The effects of common slurry additives and solution pH on the nanohardness and etch rate of the copper surface were also studied.

It was found that with the addition of copper into the slurry, an increase or decrease in agglomeration of the alumina was observed depending on the state of the copper in the solution. With the addition of chemical additives and changes in the pH of the solution, the nanohardness of the copper film was observed to range from 0.05 – 20 GPa, due to the formation of different films (CuO, Cu_2O, etc.) and/or changes in the compactness of the surface film from complexing reactions or dissolution.

Additionally, experimental results were incorporated into a model of CMP to predict MRR and predictions were compared to experimental copper CMP data. The CMP model accounts for the chemical activity of the slurries through the abrasive size and distribution, hardness and chemical etch rate parameters. The model MRR predictions only agreed with experiment for slurries with pH>8 and small etch rates. However, for acidic slurries and slurries with large etch rates, model predictions did not agree with experiment, most likely due to using nanohardness measured under quiescent conditions.

CHAPTER 1

INTRODUCTION

Chemical mechanical planarization (CMP) is used in integrated circuit manufacturing to remove excess material and provide a globally planarized wafer surface. The CMP process requires slurry containing nanometer-sized abrasive particles and chemical additives which produce a mechanical and chemical synergistic effect that is responsible for the material removal rate (MRR). CMP occurs when the wafer surface to be polished is forced against a polishing pad, which is typically a porous polymer material. The polishing pad is covered with a liquid slurry and the wafer is rotated relative to the slurry-covered pad [1]. CMP was first introduced into semiconductor manufacturing in the mid 1980's by IBM to planarize inter-level dielectrics [2]. With continually shrinking device dimensions and the implementation of multilevel metallization, the increasing topography from accumulated unevenness at feature, die, and wafer level, created an uneven surface [3]. This created depth of focus problems during photolithography, which in turn, affected the performance of the chip [2]. A process to planarize the wafer surface became necessary for devices with dimensions less than 0.35μm [3]. There are different degrees of planarization on a wafer surface. For an unplanarized surface, chemical etching can be used to obtain local smoothing and planarization. However, only the CMP process will provide "global" planarization across the entire wafer [4]. Figure 1.1 shows a device fabricated without and with CMP, where the difference in topography is very apparent [3, 5]. CMP provided a way to achieve local and global planarization across a wafer surface

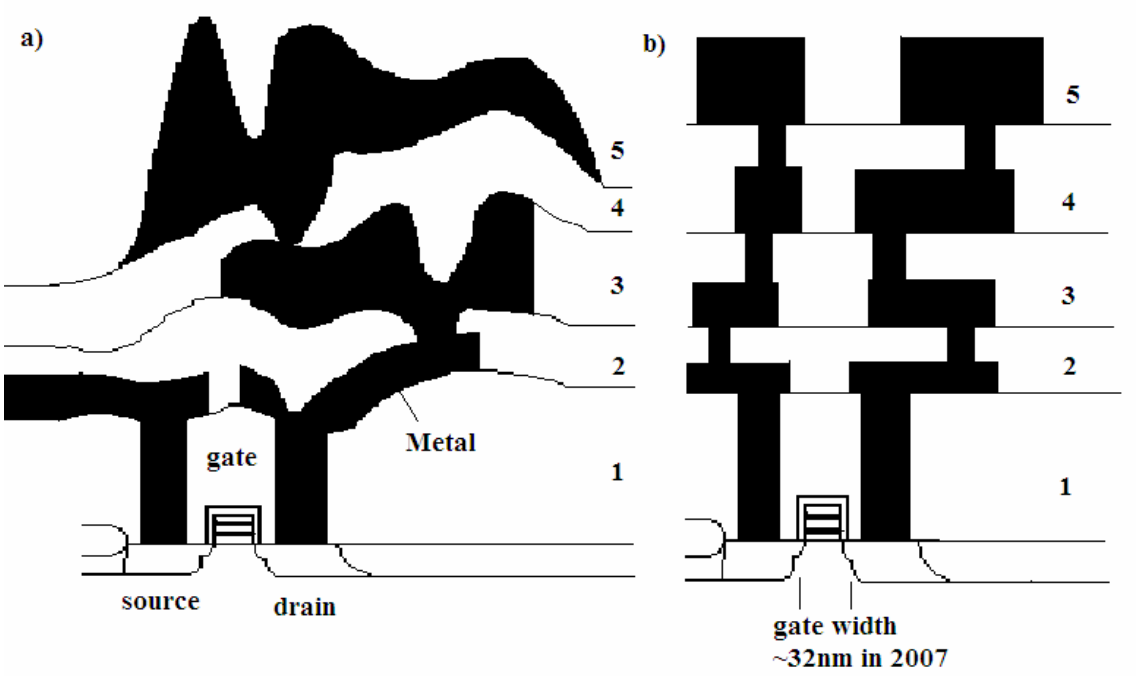

Figure 1.1 Comparison of a device with layers fabricated a) without and b) with CMP [3, 5].

which reduced the depth of focus problems of photolithography, thus enabling the production of more advanced devices [4].

Before its implementation in polishing single crystal silicon wafers, the process of CMP was traditionally used in glass polishing [6]. The technology of glass polishing provided the hardware, consumables and process of CMP, but the application and enormous growth of the CMP process has been done without a scientific understanding of the polishing mechanisms, either for silicon dioxide and other dielectrics, or for metals [2]. The semiconductor industry has effectively adapted its CMP technology for the 300 mm wafer [6], even though, to date, a comprehensive model of individual CMP polishing events does not exist [2]. Several models have been proposed in literature, but most of them focus on a specific aspect of the CMP process.

The goal of this research is to provide a fundamental understanding of the effects of chemical additives on both the colloidal properties of the abrasives and the hardness of the copper surface. Because copper has become the interconnect material of choice, the focus of our research is on copper CMP. Previous work in our research group was done by Tanuja Gopal to investigate the colloidal behavior of CMP slurries through the measurement of zeta potential and particle size distributions as a function of slurry chemistry [7, 8]. This research is a continuation of the preliminary work done by Gopal [7, 8]. The chemical additives in the slurries control the state of the copper (CuO, Cu^{2+}, etc.) on the surface of the wafer and in the slurry and also affect the dispersion characteristics of the abrasives. This research investigated the influence of common slurry additives (glycine, H_2O_2, benzotriazole, etc.), pH of the solution, and the presence of copper on the colloidal behavior of alumina suspensions. The effects of common slurry additives and pH of the solution on the nanohardness and etch rate of the copper surface were also studied. The experimental results were incorporated into the Luo and Dornfeld model of CMP to predict MRR [1, 9]. Experimental CMP on copper was also performed in order to compare the Luo and Dornfeld model MRR predictions to experimental MRR data.

This dissertation is organized as follows. Chapter 2 presents a background of the CMP process. A brief history of CMP as well as the important process parameters used in CMP are discussed. A detailed background on CMP has been given previously [10], however, the newest developments for CMP processes, including electrochemical CMP, or ECMP, are described in Chapter 2. A review of the current and future

direction of the CMP slurry market is also given. A derivation of the Luo and Dornfeld model is given as well as a review of several other CMP models developed to date.

Each of Chapters 3-6 is self-contained material which has been published or submitted for publication [11-14]. Chapter 3 discusses the effects of copper CMP slurry chemistry on the colloidal behavior of alumina abrasives. A review of the work done by Gopal [7, 8] is given along with a summary of our previous work [10]. In this work, the same slurry chemistries as Gopal are used, but also in the presence of copper nanoparticles [11]. The zeta potential and abrasive size distributions are measured under quiescent conditions with the addition of chemical additives and at different pH values.

In Chapter 4 the colloidal behavior of the alumina slurry with and without the copper nanoparticles is used in a model of CMP [12]. The modeling work done by Gopal is also reviewed [15]. In this chapter, a method is developed to determine the force on the abrasives during CMP versus the force required to break apart the agglomerated abrasive particles. It is shown for the conditions of our CMP experiments the agglomerates do not break up, and therefore our agglomerate size distribution measurements can be used in the model [12].

Chapter 5 presents the effects of CMP slurry chemistry on copper surface nanohardness [13]. The nanohardness and etch rates of copper samples are measured after exposure to the same slurry solutions used in the previous studies.

Chapter 6 incorporates the nanohardness and etch rate measurements into the Luo and Dornfeld model along with the abrasive size distributions [14]. A discussion of the behavior of the Luo and Dornfeld model with respect to hardness, etch rate,

abrasive size and abrasive size distribution is given. Model predictions are compared to experimental MRR of copper CMP.

In Chapter 7, the results of surface analysis of copper samples before and after exposure to aqueous solution containing 0.1M glycine, 2.0wt% H_2O_2, and 1mM KNO_3, by electron spectroscopy for chemical analysis (ESCA) are discussed.

The conclusions of this study and proposed future work are discussed in Chapter 8.

REFERENCES

1. J. Luo and D. Dornfeld, *Integrated Modeling of Chemical Mechanical Planarization (CMP) for Integrated Circuit Fabrication: from Particle Scale to Feature, Die and Wafer Scales*, Report, University of California, Berkeley (October 2003).

2. M. R. Oliver, *Chemical-Mechanical Planarization of Semiconductor Material*, Springer-Verlag, Berlin, Germany (2004).

3. Y. Li editor, *Microelectronic Applications of Chemical Mechanical Planarization*, John Wiley & Sons, Inc., Hoboken, New Jersey (2008).

4. J. M. Steigerwald, S. P. Murarka, and R. J. Gutman, *Chemical Mechanical Planarization of Microelectronic Materials*, John Wiley & Sons, New York (1997).

5. G. M. Borsuk and T. Coffey, *Defense Horizons*, **30**, 1 (2003).

6. P. B. Zantye, A. Kumar, and A. K. Sikder, *Materials Science and Engineering*, **R45**, 89 (2004).

7. T. Gopal, PhD Thesis, University of California, San Diego (2004).

8. T. Gopal and J. B. Talbot, *J. Electrochemical Soc.*, **153**, G622 (2006).

9. J. Luo and D. Dornfeld, *IEEE Trans. Semi. Manuf.*, **14**, 112 (2001).

10. R. Ihnfeldt, Masters Thesis, University of California, San Diego (2005).

11. R. Ihnfeldt and J. B. Talbot, *J. Electrochemical Soc.*, **153**, G948 (2006).

12. R. V. Ihnfeldt and J. B. Talbot, *J. Electrochemical Soc.*, **154**, (12) H1018 (2007).

13. R. V. Ihnfeldt and J. B. Talbot, *J. Electrochemical Soc.*, **155**, 6 (2008).

14. R. V. Ihnfeldt and J. B. Talbot, *J. Electrochemical Soc.*, to be published (2008).

15. T. Gopal and J. B. Talbot, *J. Electrochemical Soc.*, **154**, H507 (2007).

CHAPTER 2

BACKGROUND ON CHEMICAL MECHANICAL PLANARIZATION

2.1 History of CMP

Chemical mechanical polishing (CMP) was first introduced as a new planarization technique for integrated circuit (IC) manufacturing in the mid 1980's [1]. Initially, CMP was used as an enabling technology for IC manufacturing to fabricate high performance, multiple level metal structures. Because of more complex technology and shrinking device sizes, depth of focus issues associated with topography on IC's were experienced at the photolithography step. The topography introduced problems with step coverage, deposition, yield and reliability. The CMP process for IC manufacturing is designed to remove areas of elevated topography more quickly than the lower areas which cannot be achieved by chemical etching alone [2].

A brief history of CMP from simple glass polishing to more complicated metal polishing of high performance structures has been reviewed previously [3]. There have been many publications in the past two decades featuring CMP. The first book on CMP was published in 1997 by Steigerwald et al. [4]. In 2004 Oliver published a book [2] and the most recent publication of CMP edited by Li in 2008 provides a comprehensive review of the past decade advances in CMP technology along with future challenges [5]. Additionally, the Materials Research Society (MRS) features an annual symposium on CMP technology [6]. The Electrochemical Society also features a symposium every other year on CMP technology, the most recent (fall 2006) of which highlighted advances in copper CMP processing including electropolishing and fixed abrasive

polishing, and also emphasized fundamental studies of slurry interactions [7]. Articles on the numerous aspects of CMP are published in journals such as *Microelectronic Engineering*, *Thin Solid Films*, *Journal of Colloid and Interface Science*, and *Semiconductor International*.

A review of the types of CMP, with a focus on copper CMP, and the various parameters in the process, including the role of the abrasive particles and the currently available commercial slurries for copper CMP as of ~2005 can be found elsewhere [3]. The following discussion will outline the developments in CMP technology since ~2005, including new developments in CMP processes, the current and future directions of CMP slurries, and the new models of CMP.

2.2 The CMP Process

The CMP process involves four main items: the wafer, the pad, the conditioning disk and the slurry. The slurry provides both the chemical and mechanical action on the wafer. The pad, which is typically made of a polymeric material, provides a medium to carry the chemicals and abrasives across the surface of the wafer. The conditioning disk is a hard abrasive surface typically embedded with a matrix of diamonds points, which is rotated across the pad surface before and during CMP to roughen it. Figure 2.1 shows a schematic of a typical rotary CMP machine with all of the main components except the conditioner [2].

Typical wafer or head velocities are 30 to 120 rpm with the carrier down pressure from 1 - 9 psi. Platen velocities range from 30 to 120 rpm. The conditioner down pressure is usually 1 to 5 psi with the diamond size of 70 to 180 μm. Slurry flow

rates are usually 50 to 300 ml/min [4]. The different types of slurries, pads and conditioning disks were previously reviewed [3], and a detailed discussion of the newest advances in CMP consumables can be found elsewhere [5]. A discussion of new slurry technology is given in the next section.

CMP is a complex process which is influenced by a number of process variables. Table 2.1 lists the basic variables of a typical CMP process. The results of CMP that are affected by these processing variables are the material removal rate (MRR), wafer uniformity, and type and number of polishing defects. Polishing defects include scratches, residual slurry, particles embedded or adhering to the surface, ripout of material on the surface, and dishing or erosion due to overpolish in areas on the wafer [8]. Typical MRR for industrial copper CMP ranges from 50 – 1000 nm/min [2, 5]

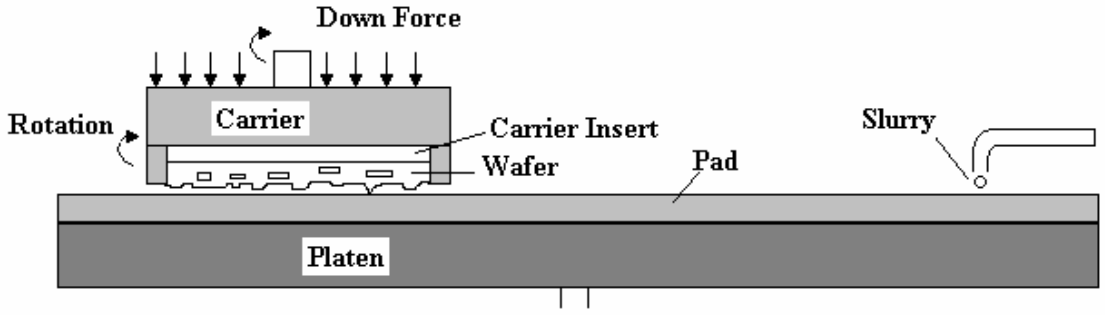

Figure 2.1 Schematic of a basic rotary CMP machine, showing wafer, carrier, pad and platen [2].

Table 2.1 Basic process variables for a typical CMP process.

Component	Variable
Wafer/Head	Wafer surface – material, uniformity, step height, etc.
	Wafer velocity
	Head down pressure on pad
	Internal head pressures on wafer
Pad/Platen	Pad hardness, roughness
	Platen velocity
Conditioning Disk	Conditioner down pressure
	Embedded matrix size and shape
	Conditioning time before and during polish
Slurry	Slurry flow rate
	Slurry dispensing position on platen
	pH of solution
	Chemical additives
	Abrasive type, size, concentration
	Viscosity of solution
Other	Temperature

The ability to control this extensive list of process variables is the reason CMP is considered to be more of an art than a science. It is a complex process that requires experienced engineers and technicians to operate the tools [2]. Research has been done in many areas of CMP. Because the slurry is such an important part of the CMP process and there are many variables introduced through just this one component, our research has been focused on the abrasives and chemistry of these slurries for copper.

2.3 Types of CMP

CMP can be divided into two basic areas, oxide (dielectric and polysilicon) CMP and metal CMP. Oxide CMP processes are the most widely used in industry and the best understood. Metal CMP is used to fabricate “damascene” structures (microscopic inlaid metal features) that serve as wiring to connect individual electronic components, such as transistors that were previously formed in an underlying

semiconductor substrate [2]. Previous work has described the different types of CMP processes (interlayer-dielectric (ILD), shallow trench isolation (STI), tungsten, copper, etc.) and their purpose in IC manufacturing as of ~2005 [3]. A timeline for the introduction of each of the different CMP processes into IC manufacturing is also given elsewhere [5]. Recently, challenges for CMP due to changes in underlying materials have led to new developments within the CMP processes.

Copper CMP, which was introduced in 2001, is now used in manufacturing around the world and semiconductor manufacturers and polishing system suppliers are aggressively developing processes incorporating copper interconnect technology [5]. The advantage of the damascene copper interconnect is that it eliminates all metal mask steps, which are a part of the typical aluminum interconnect and tungsten plug strategies [9]. Because copper has become the interconnect material of choice and it is the least understood CMP process, our research is focused on studying copper CMP.

The damascene copper interconnect is typically fabricated using the usual tungsten plugs, followed by a dielectric deposition. An image of the interconnect layer is then etched back, and a barrier layer (typically tantalum or tantalum nitride) is deposited, followed by the deposition of a copper layer. Figure 2.2 illustrates the copper damascene process where copper deposition is followed by copper CMP [2]. To achieve practical copper material removal rates, pressures greater than 3 psi are often required, which do not delaminate or deform the conventional dielectric material. However, the introduction of porous low-k (low dielectric constant) materials requires a small down pressure (<1 psi) to maintain the structural integrity of the device [5]. To meet the copper planarization requirements imposed by low-k materials,

electrochemical mechanical planarization (ECMP) has been developed. ECMP is a combination of mechanical abrasion and electrochemical removal of the copper film from the wafer to achieve planarization. In ECMP a passive film is formed across the copper surface by electrochemistry from an applied potential. In the recessed areas on the wafer, the passive film prevents dissolution of the copper surface, while in the protruded areas the passive film is removed by mechanical abrasion of the polishing pad, which then allows electrochemical dissolution of the copper. The ECMP planarization efficiency depends on the electrolyte chemistry and its operating voltage. The charge flowing through the polishing cell is controlled so that the passive film formed is thick enough to prevent current from passing through in the recessed areas and at the same time soft enough to be removed by the mechanical abrasion of the pad at low down pressures [2].

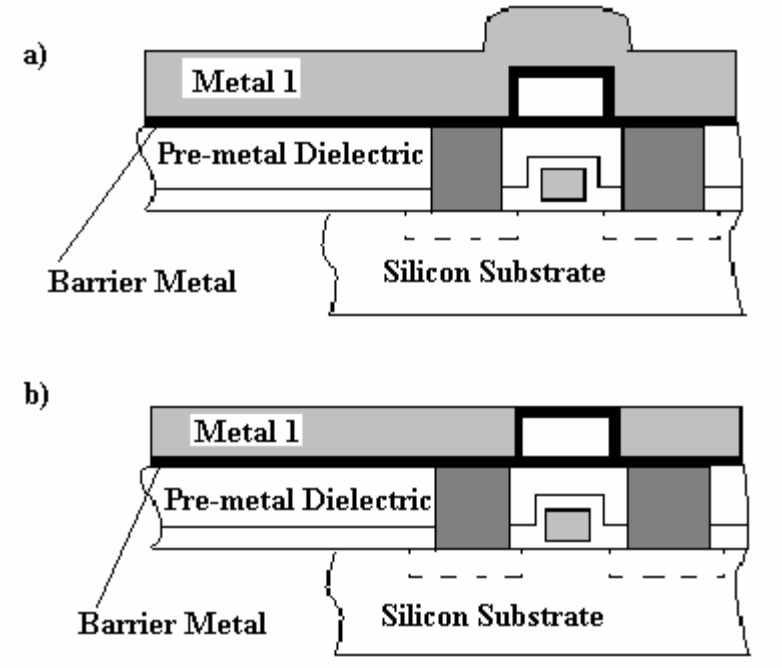

Figure 2.2 Copper damascene fabrication with (a) copper deposition and (b) after copper CMP [2].

Additionally, some slurry suppliers have started developing slurries capable of achieving high removal rates of bulk copper at low down pressures that can be used in traditional CMP, without the voltage-activated electrochemical reactions (ECMP). These new slurries are discussed in the following section.

2.4 CMP Slurries

During CMP the slurry provides both the mechanical and chemical action of material removal. The mechanical action of removal is done through the nanometer-sized abrasive particles, typically alumina or silica. The chemical action of removal is done through the chemical additives, which for copper CMP includes glycine, H_2O_2, benzotriazole, etc. [2]. Previous work reviewed the various types of abrasive particles and their use in the various slurries, i.e. alumina is typically used to remove harder materials because it is a very hard material (mohs hardness of 9 [10]), while the softer silica abrasive (mohs hardness 6-7 [10]) may be used to polish softer dielectric materials [3]. The demands of planarization of new materials have created a wide variety of options for abrasives in slurries. Even in the past three years the slurry market has changed dramatically. The CMP slurry market value has almost doubled in the past three years from approximately $600 million in 2005 to greater than $1 billion in 2008 [5], and is expected to be worth more than $1.9 billion in 2009 [11]. The market value of materials related to IC manufacturing is now over $10 billion. Figure 2.3 shows the market distribution of the materials used in IC manufacturing [5]. The figure shows that CMP slurries account for ~7% of the market, and CMP pads and slurries together account for ~11% of the materials used in IC manufacturing. This

indicates that CMP technology has become a key component in the semiconductor manufacturing process [5]. The type of particle used in CMP slurries has also changed. Previous work showed for the 2005 global CMP slurry market 40% of the slurries contained fumed silica, 34% contained colloidal particles, 18% contained alumina particles, and 8% had some other type of abrasive or no abrasives [3]. Since 2005, there has been an increase in fixed abrasive processing, no abrasive slurries, and ECMP slurries for copper CMP [11]. Fixed abrasive processing uses a polishing pad where the abrasive is incorporated into the pad and the polishing fluid only contains the chemicals needed to etch the wafer surface. This process bypasses the problem of particle suspension that occurs with slurries [2]. Many manufacturers are also using non-standard abrasives such as ceria (CeO_2), manganese sesquioxide (Mn_2O_3), manganese dioxide (Mn_2O_2), and zirconia (ZrO_2) as well as combinations of different abrasives [2, 12]. However, manufacturers now consider the type and concentration of the abrasives in their slurries proprietary information, which makes it difficult to determine the most commonly used abrasives. Market research was performed by Techcet in 2007 on CMP consumables [13] and BCC research is expected to publish a report in July 2008 on CMP equipment and materials [14]. These reports may contain more information on the types of abrasives currently used by manufacturers for CMP slurries.

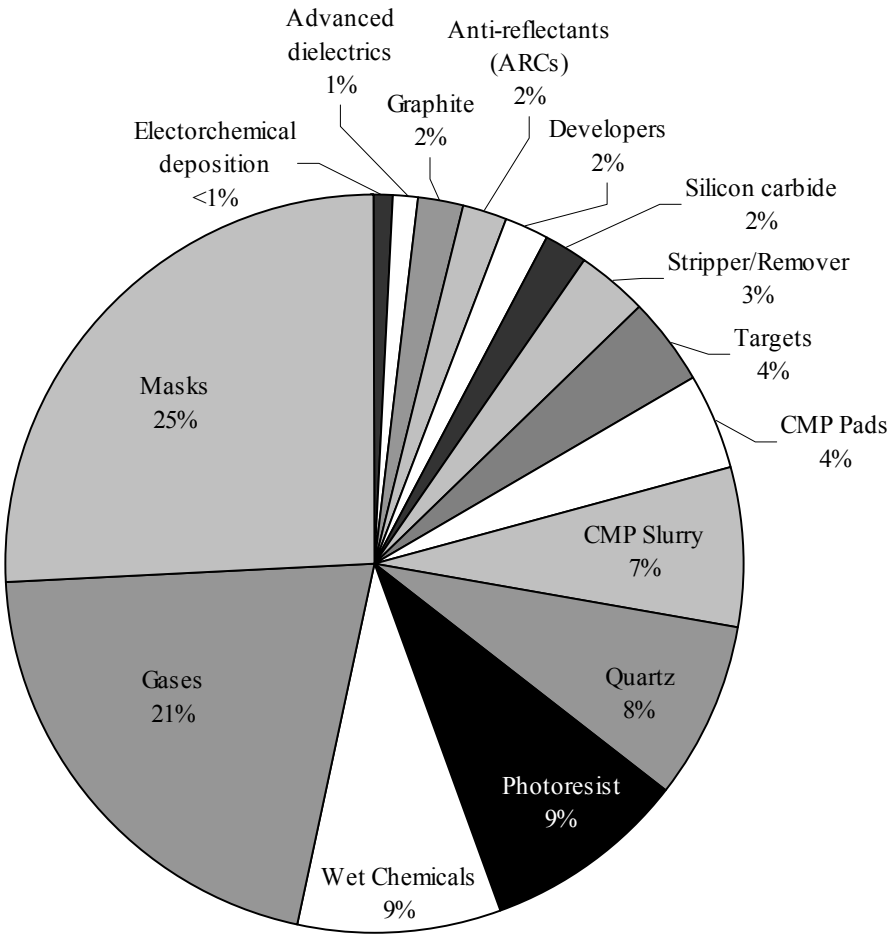

Figure 2.3 Market value distribution of materials used in the IC manufacturing process [5].

As the industry develops smaller and smaller circuitry, CMP technology has become more fragmented which can be attributed to the introduction of new materials. As the industry currently transitions from 90 to 65 nm circuitry, more than 10 new materials have been introduced. In the future, the transition from 65 to 45 nm circuitry is expected to have more than 30 new materials introduced [11]. The new materials and variation in products between customers have caused the CMP industry to need to customize its products for each customer [11]. Cabot Microelectronics is currently the

leading company in the slurry market [15]. However, more companies are entering the CMP slurry market due to the introduction of copper as an interconnect and the many possibilities of slurry formulations for different applications [11, 16]. Cabot Microelectronics currently manufactures fumed silica slurries for dielectric CMP, and they also have a line of copper polishing slurries both with and without abrasives [17]. DA Nanomaterials is currently producing alumina [18], colloidal silica [19], and abrasive free slurries for copper CMP [20, 21]. They also have several slurries using nonstandard abrasives for other CMP processes, including cerium oxide abrasives for STI [22, 23] and ILD [24] CMP, an aluminum powder slurry for tungsten CMP [25], as well as a proprietary inorganic metal oxide slurry for tungsten CMP [26]. Hitachi Chemical offers an abrasive free slurry for both the copper and barrier (TaN) polish [27]. Fujimi manufactures both silica and alumina slurries [28]. Planar Solutions manufactures a colloidal silica slurry for copper CMP, as well as many abrasive-free copper CMP slurries for use with low-k films [29]. JSR Micro has developed a new abrasive particle, the Soft-brasive™, which is a composite colloidal silica and polymer particle, and works well when polishing copper on low-k materials [30]. Currently, the ECMP market is dominated by Applied Materials, which manufactures the Reflexion ECMP tool [31] that is used with a simple electrolyte solution manufactured by Praxair [16].

These new slurry technologies and the increase in options for slurries for polishing copper over the last few years indicate the difficulty of this process. The abrasives in a slurry may scratch and cause defects on the wafer, while abrasive-free solutions may cause corrosion and typically have low MRRs [16]. Slurries containing

abrasive particles need to be tailored so that the particle sizes and their distributions are small enough to not cause scratches. The chemistry in abrasive free solutions needs to be optimized for minimal corrosion and maximum MRR. Therefore, fundamental studies of abrasive size distributions and the effects of chemistry (Chapter 3), as well as chemical effects on the wafer surface (Chapter 5), will be useful in developing technology to planarize the next generation of semiconductors.

Previous work (in our research group) by T. Gopal investigated the effect of common copper CMP slurry additives on the colloidal behavior of alumina suspensions [8, 32]. A short summary of Gopal's work is given in Chapter 3; a more detailed summary can be found elsewhere [3]. This research is an extension of the preliminary work done by Gopal [8, 32]. As stated above, alumina was the most commonly used abrasive for copper CMP slurries several years ago, while currently there are many different types of abrasives used for polishing copper. However, in this research, only alumina suspensions were studied.

2.5 CMP Models

The CMP process involves many parameters, such as wafer and platen velocity, wafer and pad hardness, wafer down pressure, slurry chemistry, and particle characteristics that affect the MRR. Researchers have shown through microscopic observations of polished surfaces that the material removal in CMP occurs as a result of a combination of chemical reaction of the slurry chemicals with the wafer surface and the repeated sliding and indentation of the abrasive particles against the wafer surface [2]. Chemical action by itself also removes material by etching, but typically at a much

lower rate than is observed when mechanical action is also present [5]. Numerous models of CMP have been proposed in the past two decades [33-48]. The earliest and simplest model for MRR developed is known as Preston's equation:

$$MRR = K_P P v \qquad [2.1]$$

where K_P is Preston's coefficient (Pa^{-1}), P is the down pressure (Pa), and v is the relative wafer velocity (cm/s) [2]. This model predicts MRR over the entire wafer, and thus, is known as a wafer-scale model. Researchers have also developed models to describe the MRR during CMP over individual features, or feature-scale models [35, 39, 40, 46]. These models were developed in order to predict the change in step height over time, the amount of dishing of the material being polished, and the amount of erosion of material that should not be polished. In this research, we are only concerned with MRR over the entire wafer, therefore, only wafer-scale models will be discussed.

Previous work (in Ihnfeldt's MS thesis) discussed the history of wafer scale CMP models, from the development of Preston's equation, which only accounted for the mechanical removal during CMP, to more advanced models which account for both the chemical and mechanical removal [3]. A comprehensive review of the existing models and the parameters that are utilized as of 2004 was given by Gopal [8]. Oliver also provided an outline of models developed for metal CMP processes as of 2004 [2]. Many of the early CMP models treated the chemical and mechanical effects of the slurry separately [2]. This approach works well for processes that are not very chemically active, such as SiO_2 CMP and ILD CMP, but for copper CMP the MRR is greatly influenced by the chemistry [37]. To model the mechanical effects of CMP the type of contact between the pad and the wafer must be considered. There are two

different contact modes that are observed during CMP, which are hydrodynamic and solid-solid, as shown in Figure 2.4. The hydrodynamic mode occurs when the wafer down pressure is small and the relative velocity of the wafer is large [35, 45]. The slurry film thickness for this contact mode has been predicted as 45-95 μm by L. Zhang et al. [36], which is much larger than the size of the abrasive particles. In this mode the wafer surface, the abrasives and slurry chemicals, and the pad are one with rotation. The material removal is due to the floating abrasives in the slurry and chemical etching by the slurry chemicals. The solid-solid contact mode occurs when the wafer down pressure is large and the relative velocity of the wafer is small [35, 45]. The slurry film thickness is much smaller (typically <20 μm [36]) than that of the hydrodynamic mode and the majority of the removal is due to the static abrasion of the wafer surface as it slides over the abrasive particles, which are embedded into the pad.

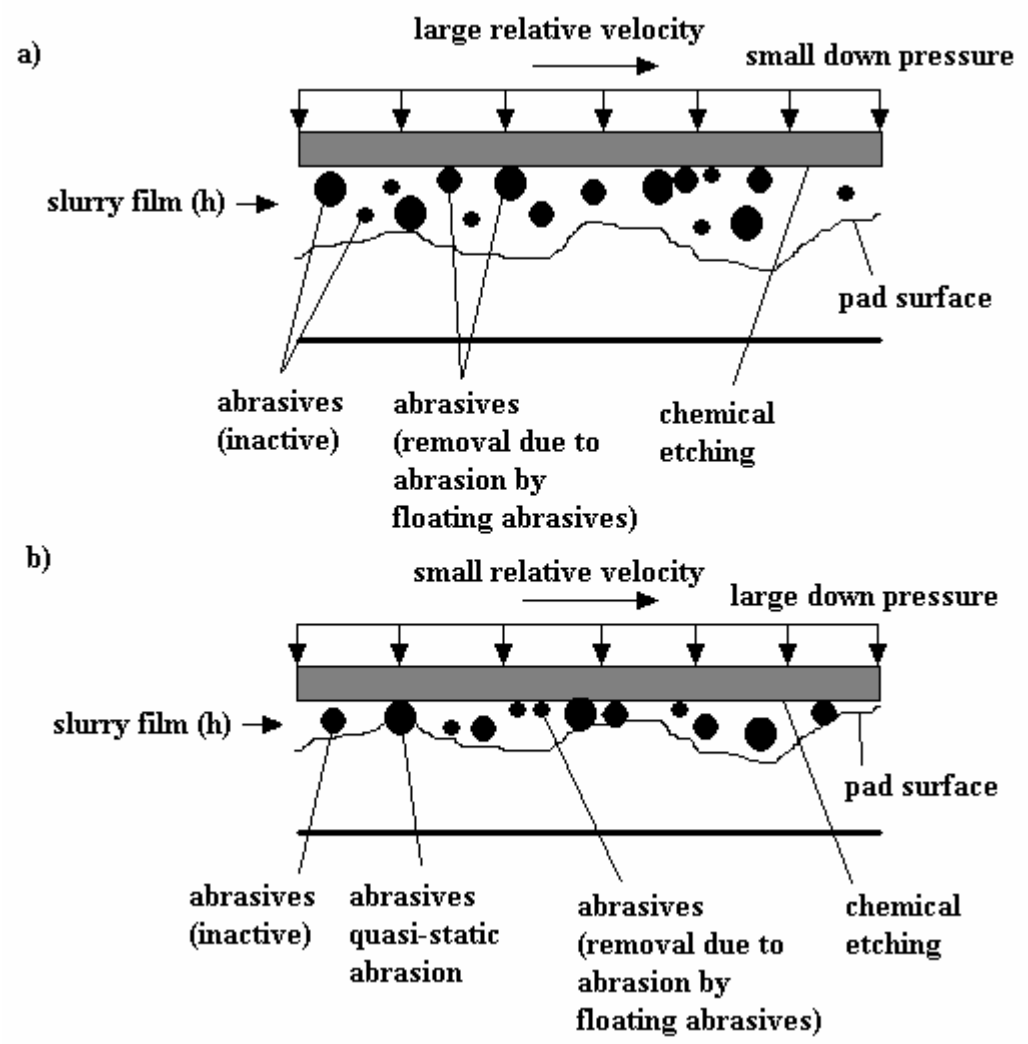

Figure 2.4 Two contact modes of CMP (a) hydrodynamic contact mode and (b) solid-solid contact mode [35, 45].

Previous work discussed a hydrodynamic model of copper CMP removal rates developed by Subramanian et al. using abrasive-free slurries [36], which only accounts for the chemical component of the material removal process [3]. A discussion of a more comprehensive hydrodynamic model of copper CMP developed by Thakurta et al. [34], which included both the chemical component of material removal and the mechanical abrasion of the surface, has also been previously discussed [3]. This model

is only applicable to acidic slurry solutions containing H_2O_2 [34]. A more recent model of copper CMP was developed by Paul et al. which attempts to describe the highly chemically active nature of the copper CMP process by incorporating the kinetic reactions of the copper surface with both oxidizers and etchants (complexing agents), and also incorporates the mechanical abrasion of the surface into the model [37]. Paul et al. proposed that the MRR is the sum of the mechanical rate of removal of the surface, plus the rate of removal due to chemical etching, where each of the different states of copper on the surface (Cu metal, Cu_2O, CuO) will have a different mechanical removal rate and a different etch rate [37]. The overall MRR equation is given by the following:

$$MRR = M_0 + M_1 + M_2 + C_{W1} + C_{L1} + C_{W2} + C_{L2} \quad [2.2]$$

where M_0, M_1 and M_2 are the mechanical removal rate of Cu metal, Cu(I), and Cu(II), respectively, and C_{W1} is the chemical etch rate of Cu_2O by this reaction:

$$Cu_2O + 2H^+ \rightarrow Cu + Cu^{2+}(aq) + H_2O \quad [2.3]$$

and C_{L1} is the chemical etch rate of Cu_2O by this reaction:

$$Cu_2O + 2HL \rightarrow Cu + CuL_2(aq) + H_2O \quad [2.4]$$

where L is a complexing agent such as glycine [37]. C_{L1} is proportional to the concentration of the complexing agent, [L]. Similarly C_{W2} and C_{L2} are the chemical etch rates of CuO given by the following reactions

$$3CuO + 2H^+ \rightarrow Cu_2O + Cu^{2+}(aq) + H_2 + O_2 \quad [2.5]$$

$$3CuO + 2HL \rightarrow Cu_2O + CuL_2(aq) + H_2 + O_2 \quad [2.6]$$

where C_{L2} is also proportional to [L] [37]. The mechanical and chemical etch rates (M_0, M_1, M_2, C_{W1}, C_{L1}, C_{W2}, C_{L2}) are proportional to the number of ions (Cu metal, Cu_2O, and CuO) on the wafer surface and the rate constants of the reactions, which must be experimentally measured. The rate of formation of Cu_2O and CuO on the surface due to exposure to hydrogen peroxide, H_2O_2, given by the following reactions, is also accounted for in the model [37].

$$2Cu + H_2O_2 \rightarrow Cu_2O + H_2O \quad [2.7]$$

$$Cu_2O + H_2O_2 \rightarrow 2CuO + H_2 + O_2 \quad [2.8]$$

Details of the model derivation can be found elsewhere [37]. The overall MRR equation developed by Paul et al. takes the form shown below

$$MRR = \frac{a_0 + a_1[H_2O_2] + a_2[H_2O_2]^2}{a_3 + a_4[H_2O_2] + [H_2O_2]^2} \quad [2.9]$$

where the a_i depend on the mechanical and chemical rates, and [H_2O_2] is the concentration of hydrogen peroxide [37]. This model, as for the hydrodynamic models developed to date, does not account for the effect of the abrasive size on the MRR. For hydrodynamic systems, the abrasive size tends not to have as much of an effect on the MRR compared to the chemistry and, therefore, these models have worked well for the particular slurry systems studied [37]. However, it is difficult to apply these models to other slurry systems because they have been developed for a specific kinetic reaction scheme. Use of different chemical additives or even changes in concentration of the additives may require the development of a new kinetic reaction model.

Additionally, early models have assumed that the MRR remains constant during CMP processing, while experimental data has shown that the MRR can vary with time

due to pad surface topography evolutions [33]. Attempts have been made to model the dynamic MRR during CMP [46, 49], however, these models only account for the mechanical component of removal and do not consider the chemical effects of the slurry on the wafer surface [33].

Prior to 2004, very few models of CMP had been developed for a solid-solid contact mode that accounted for both the mechanical and chemical components of removal. The Luo and Dornfeld model of CMP, first developed in 2001, focuses on the mechanical effects, or the material removal mechanism by the abrasive particle, during solid-solid contact mode [35, 45]. This model is based upon the physical principles of CMP and it incorporates both particle-particle and particle-surface interactions of the abrasives and the wafer surface through the average abrasive size, the abrasive size distribution, and the wafer surface hardness, in order to predict the MRR [35, 45]. A brief outline of the model assumptions and its derivation are given below. The simplified model equation for the MRR is given by:

$$MRR = \rho_W NV + C_0 \qquad [2.10]$$

where ρ_W is the density of the wafer, N is the number of active abrasives, V is the volume removed by a single abrasive, and C_0 is the MRR due to chemical etching. The removal due to chemical etching is neglected because it is usually small compared to the overall MRR [35, 45].

In considering the pad-wafer interface, the Luo and Dornfeld model assumes that the pad is soft and elastically deforms to the wafer surface, and that the abrasive particles are small so that the pad asperities deform around them. The pad asperities are assumed to be uniformly distributed with a known density, D_{SUM}, and have the same

height, l, and radius, R [35, 45]. The total contact area between the wafer and the pad, A_0, is equal to $\pi D^2/4$, where D is the diameter of the wafer [35, 45]. The contact area, A, between the pad asperities and the wafer surface is modeled by Hertzian contact and is given by [35, 45]:

$$A = \pi\left(\frac{3R}{4D_{SUM}}\frac{P_0}{E^*}\right)^{\frac{2}{3}} D_{SUM} A_0 = b_1\left(\frac{P_0}{E^*}\right)^{\frac{2}{3}} A_0 \qquad [2.11]$$

where

$$b_1 = \pi\left(\frac{3R}{4}\right)^{\frac{2}{3}} D_{SUM}{}^{\frac{1}{3}} \qquad [2.12]$$

and E^* is a combined Young's modulus of the wafer and the pad given by:

$$E^* = \frac{1}{\frac{(1-\upsilon_w)^2}{E_w} + \frac{(1-\upsilon_p)^2}{E_p}}. \qquad [2.13]$$

where E_W and E_P are the Young's modulus of the wafer and the pad, respectively, and ν_W and ν_P are the Poisson's ratio of the wafer and the pad, respectively [35, 45]. Because the Young's modulus of the wafer is typically much larger (E_W~20 GPa for silicon) than the Young's modulus of the pad (E_P~2.3 MPa for pad material such as IC1000), and the Poisson's ratio of the pad is close to ν_P~0.5 for polymer materials, $E^* = 4E_P/3$ in Eq. 2.13 [45].

The total contact pressure is given by:

$$P_C = \frac{P_0 A_0}{A} = \frac{1}{b_1} E^{*\frac{2}{3}} P_0^{\frac{1}{3}}. \qquad [2.14]$$

In considering the particle-wafer interface, the model assumes that the particles plastically deform the wafer surface; this is reasonable because small cutting depths (<1 μm) cause brittle materials to be removed in a ductile manner [35, 45]. The force F applied on an abrasive is equal to the contact pressure times the abrasive area as given by the following equation:

$$F = \frac{\pi P_c x^2}{4} = \frac{\pi}{4}\left(\frac{1}{b_1}\right)\left(\frac{4}{3}\right)^{\frac{2}{3}} E_P^{2/3} P_0^{1/3} x^2 \qquad [2.15]$$

where the diameter of the abrasive is x [35, 45]. Figure 2.5 shows a schematic of the contact between a spherical abrasive particle, wafer and pad where the particle penetrates both the wafer and the pad. The mean contact pressure applied by the abrasive onto the pad and the wafer are equal to their hardness, H_W and H_P, respectively [35, 45]. The force applied on the abrasive is given by:

$$F = \frac{\pi a_W^2 H_W}{2} = \pi a_P^2 H_P \qquad [2.16]$$

where a_W and a_P are the radii of the projected circle of contact between the spherical abrasive and the wafer and pad surfaces, respectively [35, 45]. Since the penetration depths, Δ_W and Δ_P, of the spherical abrasive into the wafer and pad surfaces are much smaller than the diameter of the abrasive x ($\Delta_W << x$ and $\Delta_P << x$), it can be shown that $x\Delta_W = a_W^2$ and $x\Delta_P = a_P^2$. So the penetration depths are given by

$$\Delta_W = \frac{2F}{\pi x H_W} \qquad [2.17]$$

$$\Delta_P = \frac{F}{\pi x H_P} \qquad [2.18]$$

and the total penetration depth Δ is given by

$$\Delta = \Delta_W + \Delta_P = \frac{F}{\pi x}\left(\frac{2}{H_W} + \frac{1}{H_P}\right). \quad [2.19]$$

The mean value of Δ_W can be approximated by the final roughness, R_a, of the polished wafer. For a polishing process with down pressure P_0, relative velocity V, and mean size x_{act} of active abrasives, the average volume removed by a single abrasive per unit time can be calculated using the following equation:

$$V = \Delta_W a_W v = R_a a_W v = \frac{\sqrt{2} x_{act}^2 E_P}{3(b_1 H_W)^{\frac{3}{2}}} \sqrt{P_0} v. \quad [2.20]$$

It is also assumed that the abrasives are spherical and have normally distributed agglomerate sizes, the size of the abrasives that are actively removing material, x_{act}, is constant, and the active abrasive size is equal to the average abrasive size, x_{avg}, plus three times the standard deviation, σ, of the abrasive size distribution, $x_{act}=x_{avg}+3\sigma$ [35, 45]. The volume removed by a single abrasive is given by:

$$V = K\left(x_{avg}^2 + 6\sigma x_{avg} + 9\sigma^2\right)\sqrt{P_0} v \quad [2.21]$$

where

$$K = \frac{\sqrt{2} E_P}{3(b_1 H_W)^{\frac{3}{2}}} \quad [2.22]$$

This shows that as x_{avg} increases the volume removed increases parabolically. Similarly, as σ increases, x_{act} increases, and the volume removed also increases parabolically.

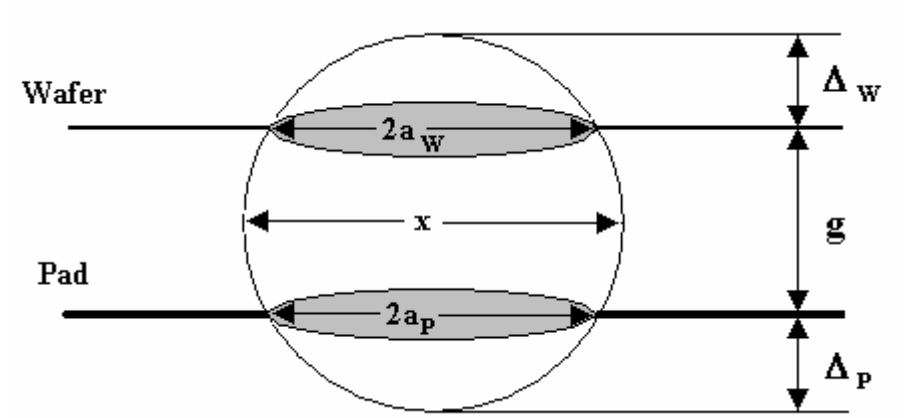

Figure 2.5 A schematic of the contact between a spherical abrasive particle, wafer and pad [35, 45].

The number of active abrasives *N* is calculated assuming the abrasive sizes are normally distributed and satisfy the normal probability density functions given by the following equations [35, 45]:

$$p\{x = x_a\} = p(x_a) = \frac{1}{\sqrt{2\pi}} \exp\left(-\frac{1}{2}\left(\frac{x - x_{avg}}{\sigma} \right)^2 \right) \qquad [2.23]$$

and

$$p\{x \le x_a\} = \Phi(\frac{x_a - x_{avg}}{\sigma}) = \frac{1}{\sqrt{2\pi}} \int_{-\infty}^{\frac{x_a - x_{avg}}{\sigma}} \exp\left(-\frac{1}{2} t^2 \right) dt \,. \qquad [2.24]$$

The number of active abrasives *N* over the wafer-pad interface is given by:

$$N = n\left[\Phi\left(\frac{x_{\max} - x_{avg}}{\sigma} \right) - \Phi\left(\frac{x_{\max} - \Delta - x_{avg}}{\sigma} \right) \right] \qquad [2.25]$$

where x_{max} is the diameter of the largest abrasives and is assumed equal to $x_{avg}+3\sigma$, and *n* is the total number of particles in the wafer pad contact area and is given by:

$$n = G_1 A_0 D_{SUM} al \,, \qquad [2.26]$$

where a is the mean asperity area, and G_1 is the total number of abrasives per volume of slurry [35, 45]. The abrasive concentration G_1 can be calculated using the following:

$$G_1 = \frac{d_s \rho_s m_{sa}}{\rho_a \frac{\pi}{6} x_{avg}^3} \quad [2.27]$$

where d_s is the dilution ratio of slurry to DI water, ρ_s is the density of the slurry before dilution, m_{sa} is the concentration of slurry before dilution, and ρ_a is the density of the abrasive [35, 45].

The material removal rate based on thickness (nm/min) is then given by:

$$MRR = \frac{MRR_{mass}}{\rho_w A_0} = \frac{VN}{A_0} \quad [2.28]$$

which can be expanded to consider the effects of x_{avg} and σ to :

$$MRR = \underbrace{A_1 \left(\frac{1}{x_{avg}} + \frac{6\sigma}{x_{avg}^2} + \frac{9\sigma^2}{x_{avg}^3} \right)}_{\text{Thickness Removed}} \underbrace{\left[1 - \Phi\left(3 - A_2 \frac{\left(x_{avg} + 3\sigma \right)}{\sigma} \right) \right]}_{\text{Probability of Active Abrasives}} \quad [2.29]$$

where

$$A_1 = \frac{2\sqrt{2} d_s \rho_s m_{s-a} D_{SUM} a l}{\rho_a \pi} \frac{E_P}{\left(b_1 H_W \right)^{\frac{3}{2}}} \sqrt{P_0} v, \quad [2.30]$$

and

$$A_2 = 0.25 \left(\frac{4}{3} \right)^{2/3} \left(\frac{1}{H_P} + \frac{2}{H_W} \right) \frac{E_P^{2/3}}{b_1} P_0^{1/3}. \quad [2.31]$$

The product of the first two terms of the model equation represents the thickness removed per unit time, while the third term represents the probability of active

abrasives. Eq. 2.29 shows that this model has a linear dependence on the velocity, v, while the down pressure, P_0, dependence is much more complicated with a square root dependence in the A_1 term and a dependence to the 1/3 power in the probability density function [35, 45]. Researchers have suggested that the Luo and Dornfeld assumption of $x_{act}=x_{avg}+3\sigma$ in Eq. 2.21 may not be valid, and that the active abrasive size can vary between $x_{avg}+\sigma$ to $x_{avg}+2\sigma$, depending on the applied down pressure, pad properties, and particle size distribution [33]. In our research the Luo and Dornfeld model is used without modification, however, future work with this model may require altering the Luo and Dornfeld model by assuming $x_{act}=x_{max}-\Delta$, and $x_{max}=x_{avg}+3\sigma$, and then substituting Eq. 2.19 in for Δ where x is equal to x_{max}. However, this would produce a more complicated MRR equation.

The Luo and Dornfeld model accounts for the chemical effects of the slurry on the wafer surface through the hardness parameter, H_W [35, 45]. However, this model assumes a static MRR and does not account for the decrease in MRR that is typically observed over time [33]. In our research the Luo and Dornfeld model is used to predict MRR. Further discussion of the Luo and Dornfeld model is given in Chapters 4 and 6. More information on the Luo and Dornfeld model can also be found elsewhere [35, 45]. To compare the Luo and Dornfeld model to other solid-solid contact models the volume concentration of the abrasives in the slurry, v_{sa}, is given by

$$v_{sa} = \frac{d_s \rho_s m_{sa}}{\rho_a} \qquad [2.32]$$

Then model Eqs. 2.29-2.31 can be simplified to:

$$MRR = \frac{8\sqrt{2}v_{sa}D_{SUM}^{\frac{1}{2}}al}{3\pi^{\frac{5}{2}}R}\frac{E_P}{H_W^{\frac{3}{2}}}\left(\frac{1}{x_{avg}}+\frac{6\sigma}{x_{avg}^2}+\frac{9\sigma^2}{x_{avg}^3}\right)\left[1-\Phi\left(\frac{g-x_{avg}}{\sigma}\right)\right]\sqrt{P_0}v$$

[2.33]

where g is the gap between the pad and wafer, as shown in Figure 2.5.

Another CMP model assuming a solid-solid contact mode was developed by Zhao and Chang [48]. This model was developed about the same time as the Luo and Dornfeld model, ~2001, and follows the same basic model equation (Eq. 2.28). However, calculation of both the number of active abrasives, *N*, and the volume removed by an abrasive, *V*, are much different. To calculate *N* in the Luo and Dornfeld model it is assumed that the abrasive particles are entrapped in the wafer-pad contact area and are clustered together so that only a fraction of the abrasives are considered active, those with size larger than g [35,45]. The Zhao and Chang model assumes that the abrasives entrapped in the wafer-pad contact area are uniformly spaced, as they are in the slurry, and not clustered together [48]. Since the particles are separated away from each other with sufficient distance, then all particles are considered active. The number of particles participating in the material removal of the wafer surface is equal to the total area of pad/wafer contact, *A*, times the area density of the particles, *q*,

$$N = Aq = A\left(\frac{6v_{sa}}{\pi x_{avg}^3}\right)^{\frac{2}{3}}. \qquad [2.34]$$

Zhao and Chang also calculate the real area of pad/wafer contact differently than Luo and Dornfeld. In the Luo and Dornfeld model the heights of the pad asperities were assumed constant [35,45]. Zhao and Chang assume varying height of the pad

asperities as shown in Figure 2.6 [48]. To calculate the real area of pad/wafer contact, *A*, Zhao and Chang use the Greenwood and Williamson elastic model of contact between a rough surface (the pad) and a smooth surface (the wafer) [48]. The real area of contact is given by:

$$A = \pi D_{SUM} A_0 R \int_b^\infty (z-b)\phi(z)dz \qquad [2.35]$$

where *b* is the mean separation between pad and wafer, z is the asperity height, $\phi(z)$ is the distribution function of asperity heights. For a Guassian distribution of asperity heights $\phi(z)$ is given by

$$\phi(z) = \frac{1}{\sqrt{2\pi}} \exp\left(-\frac{1}{2}\left(\frac{z-b}{\sigma_s} \right)^2 \right) \qquad [2.36]$$

where σ_s is the standard deviation of the asperity heights.

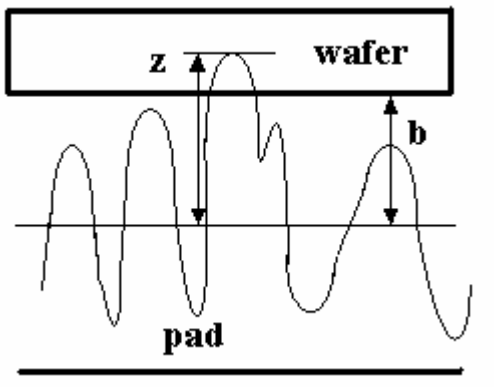

Figure 2.6 Schematic of pad/wafer contact with varying height pad asperities from the model of Zhao and Chang [48].

To calculate the volume removed by a single abrasive, the Zhao and Chang model assumes elastic deformation of the abrasive into the pad, and plastic deformation of the abrasive into the wafer [48]. These assumptions are identical to the Luo and Dornfeld model, however, the contact system of Zhao and Chang is different. Figure 2.7 shows the interaction of the pad/abrasive/wafer proposed by Zhao and Chang, where the polishing pad completely surrounds the abrasive particle [48]. The volume removed by a single particle is given by:

$$V = w_k S v t \qquad [2.37]$$

where t is the polishing time, w_k is the wear constant, which is the probability that displaced material is detached from the surface and can be approximated as:

$$w_k \approx \frac{3}{\pi}\sqrt{\frac{\Delta_W}{x_{avg}}}, \qquad [2.38]$$

and S is the cross-sectional area of the material deformed by the abrasive which is approximated as:

$$S \approx \frac{1}{2}\Delta_W a_W \approx \Delta_W \sqrt{\Delta_W x_{avg}} \qquad [2.39]$$

To calculate the indentation depth of the abrasive into the wafer, Δ_W, Zhao and Chang balanced the force between the particle and pad, F_{SP}, with the force between the particle and the wafer, F_{SW} :

$$F_{SP} = \frac{4}{3}E_{SP}\left(\frac{x_{avg}}{2}\right)^{\frac{1}{2}}\Delta_P^{3/2} \qquad [2.40]$$

$$F_{SW} = H_W \pi x_{avg} \Delta_W \qquad [2.41]$$

where E_{SP} is the reduced Young's modulus of the abrasive particle/pad pair [48]. For the contact system defined by Zhao and Chang,

$$x_{avg} = \Delta_W + \Delta_P . \qquad [2.42]$$

Setting Eq. 2.40 equal to Eq. 2.41, then substituting in Eq. 2.42 and rearranging yields:

$$\Delta_W^3 + \left(\frac{9\pi^2 H_W^2}{8E_{SP}^2} - 3 \right) x_{avg} \Delta_W^2 + 3x_{avg}^2 \Delta_W - x_{avg}^3 = 0 \qquad [2.43]$$

which can be used to calculate the indentation depth of the particle into the wafer. The overall MRR equation for the Zhao and Chang model is given by

$$MRR = \beta 9.9 \left(\frac{v_{sa}}{\pi} \right)^{\frac{2}{3}} \left(\frac{\Delta_W}{x_{avg}} \right)^2 \left(D_{SUM} R \int_b^\infty (z-b)\phi(z)dz \right) v \qquad [2.44]$$

where β is the density ratio of the surface film divided by the density of the wafer [48]. This model has a linear dependence on velocity, similar to the Luo and Dornfeld model, but the model does not explicitly depend on the applied down pressure, P_0. The down pressure is accounted for through the deformation of the pad asperities, b, which will vary as P_0 varies. Additionally, this model does not account for the effects of varying abrasive size distribution. The chemical effects of the slurry are accounted through a wafer hardness parameter, H_W, and also through the composition of the wafer surface material, β [48]. This model also assumes a static MRR and does not account for the dynamic MRR decay [48].

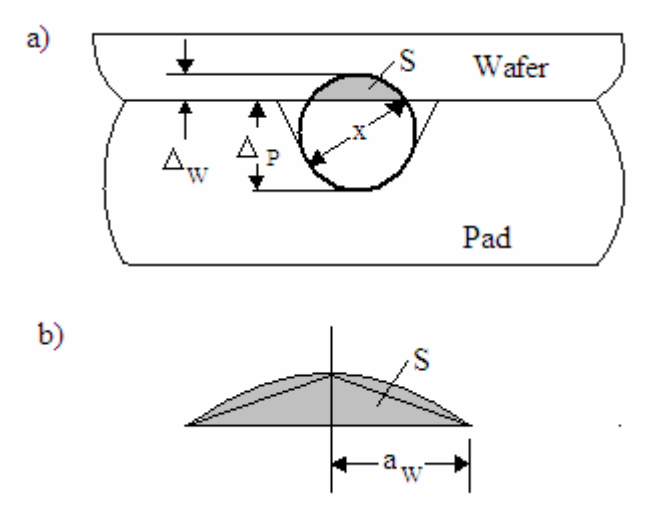

Figure 2.7 Schematic of a) the pad/abrasive/wafer contact and b) the cross-sectional area of the deformed material for the model proposed by Zhao and Chang [48].

The most recently developed model of CMP, proposed by Wang et al., follows the same overall MRR equation, Eq. 2.28, and incorporates the approaches of both Luo and Dornfeld and Zhao and Chang [33]. To calculate the number of active abrasives, *N*, the model assumes that the abrasives entrapped within the pad/wafer interface are uniformly spaced a sufficient distance away from each other so that all particles are active, which is similar to the Zhao and Chang assumption [33, 48]. However, Wang et al. does not assume the abrasives are the same size [33]. Instead, it is assumed that the abrasive size varies randomly, similar to the Luo and Dornfeld model, so that the total number of active abrasives entrapped within the jth contact area is given by:

$$N_j = \frac{6v_{sa}x_{\max}A_j}{\pi x_{avg}^3} \qquad [2.45]$$

where A_j is the circular contact area given by

$$A_j = \begin{Bmatrix} \pi[z_j - b(t)]R, z_j > b(t) \\ 0, z_j \le b(t) \end{Bmatrix}, \quad [2.46]$$

and z_j is the height of the jth asperity, which is also assumed to vary randomly [33]. The total pad contact area, $A_j(t)$, is given by:

$$A_j(t) = \pi D_{SUM} A_0 R \int_{b(t)}^{\infty} [z_j - b(t)]\phi(z_j, t)dz \quad [2.47]$$

which is a function of time because the height of the asperities varies with time [33].

The volume removed by a single particle is calculated similar to Zhao and Chang (Eq. 2.37) without the wear constant w_k, and is also different for each particle. Hence for the ith particle within the jth local contact area, the volume removed is given by:

$$V_{i,j} = S_{i,j} vt \quad [2.48]$$

where S is defined in Eq. 2.39 from Zhao and Chang [48], and Δ_W is defined in Eq. 2.17 from Luo and Dornfeld [35, 45]. Substituting Eqs. 2.39, 2.17, and 2.15 into Eq. 2.48 gives:

$$V_{i,j} = \left(\frac{1}{2H_W}\right)^{\frac{3}{2}} vt \cdot x_{i,j}^2 \cdot Pc_j^{\frac{3}{2}} \quad [2.49]$$

where Pc_j is the local contact pressure over the jth contact area, and $x_{i,j}$ is the diameter of the ith particle in the jth contact area [33]. The total material removed by the abrasives, TM, is given by the following

$$TM = \left(\frac{1}{2H_W}\right)^{\frac{3}{2}} vt \cdot \sum_{j=1}^{D_{sum}A_0} \left[Pc_j \sum_{i=1}^{N_j} x_{i,j}^2 \right] \quad [2.50]$$

The overall MRR equation developed by Wang et al. is given by

$$MRR = \frac{32\sqrt{2}v_{sa}D_{SUM}R^{\frac{1}{4}}}{9}\left(\frac{E_P}{\pi H_W}\right)^{\frac{3}{2}}\frac{x_{\max}}{x_{avg}}\left(\int_{b(t)}^{\infty}[z_j - b(t)]\phi(z_j,t)dz\right)v \qquad [2.51]$$

The details of the Wang et al. model derivation can be found elsewhere [33]. This model has a linear dependence on the velocity, v, and the applied down pressure, P_0, is accounted through the pad asperity deformation, $b(t)$ [33]. The chemical effects of the slurry are accounted through a wafer hardness parameter, H_W. The model also accounts for the dynamic MRR decay over time by incorporating the time-dependent parameter for the height of the pad asperities [33]. The effects of the abrasive size and size distribution are accounted in the x_{max} and x_{avg} terms, where x_{max} can be taken as $x_{avg}+3\sigma$ [33]. In this model, an assumption on the size of the active abrasives x_{act}, is not needed, as it is in the Luo and Dornfeld model. A model for the wear rate of the asperity height with time was also developed by Wang et al., which can be used in the model equation [33].

One of the disadvantages of the models incorporating the chemical reaction kinetics on the wafer surface is that the kinetic reaction steps must be known, and therefore, the chemical additives in the slurry must also be known. When using the solid-solid contact mode, the chemical effects of the slurry are accounted through a wafer surface hardness parameter and the abrasive size and distribution. Therefore, only the abrasive size distribution and the wafer surface hardness is needed to obtain MRR predictions, and the composition of the slurry, which can be difficult to obtain if using commercial slurries, is not needed. However, while obtaining agglomerate size distributions that are representative of the slurry during CMP is possible, as shown in

Chapter 4, obtaining a representative hardness of the wafer surface during CMP is much more difficult (Chapter 6). Additionally, most of these models have only been conceptually verified, meaning experimental data were used to obtain the unknown parameters, and then using these fitted values, model predictions are interpolated or extrapolated [33, 35, 36, 45]. While this approach shows that the model is capable of predicting the trend of experimental data, it does not verify the model for any CMP process. In Chapters 4 and 6, the Luo and Dornfeld model will be used with measured parameters from either literature, or from our experiments, in an attempt to determine the model's ability to predict MRR for copper CMP.

REFERENCES

1. Y. Moon, "Mechanical Aspects of the Material Removal Mechanism in Chemical Mechanical Polishing (CMP)", PhD Thesis, University of California, Berkeley (1999).

2. M. R. Oliver, *Chemical-Mechanical Planarization of Semiconductor Material*, Springer-Verlag, Berlin, Germany (2004).

3. R. Ihnfeldt, MS Thesis, University of California, San Diego (2005).

4. J. M. Steigerwald, S. P. Murarka, and R. J. Gutman, *Chemical Mechanical Planarization of Microelectronic Materials,* John Wiley & Sons, New York (1997).

5. Y. Li editor, *Microelectronic Applications of Chemical Mechanical Planarization*, John Wiley & Sons, Inc., Hoboken, New Jersey (2008).

6. C. Borst, L. Economikos, A. Philipossian, and G. Zwicker, *MRS Symposium Proceedings*, **991**, (2007).

7. S. Seal, V. Desai, Y. Obeng, and K. Sundarum, *The 210th Meeting of the Electrochemical Society*, Cancun, Mexico, Oct. 29-Nov. 3, 2006, **3** (41), 21.

8. T. Gopal, PhD Thesis, University of California, San Diego (2004).

9. W. R. Morrison, S. Joshi, and R. Tolles, *Copper and STI CMP Technology: The Challenges and the Cost*, Future Fab International, Volume 11 (2001).

10. A. Szymanski and J. M Szymanski, *Hardness Estimation of Minerals Rocks and Ceramic Materials*, Elsevier Science Publishers B. V., New York, NY (1989).

11. M. McCoy, *Chemical and Engineering News*, **84** (26), 17 (2006).

12. M. Corbett, *Solid State Technology,* **43**, 72 (December 2000).

13. Karey Holland, *CMP Consumables 2007 a Techcet Group Critical Materials Report*, Techcet Group, LLC., Genoa, Nevada, Control #ISMT022807 (2007).

14. *Chemical Mechanical Polishing (CMP) Equipment and Materials*, BCC Research, Wellesley, Massachusetts, Report ID# AVM047B, expected July (2008).

15. A. S. Mutschler, *Electronic News*, **52** (44), 3 (2006).

16. L. Blanchfield, *ICIS Chemical Business Americas*, **271** (1), 36 (2007).

17. www.cabotcmp.com (accessed February 2008).

18. DuPont Air Products NanoMaterials L.L.C. Material Safety Data Sheet, Trade Name BTX-301-I, Tempe, Arizona (2007).

19. DuPont Air Products NanoMaterials L.L.C. Material Safety Data Sheet, Trade Name CoppeReady® CU300™, Tempe, Arizona (2007).

20. DuPont Air Products NanoMaterials L.L.C. Material Safety Data Sheet, Trade Name CoppeReady® CU3900™, Tempe, Arizona (2007).

21. www.nanoslurry.com (accessed February 2008).

22. DuPont Air Products NanoMaterials L.L.C. Material Safety Data Sheet, Trade Name MicroPlanar® STI2100™, Tempe, Arizona (2007).

23. DuPont Air Products NanoMaterials L.L.C. Material Safety Data Sheet, Trade Name MicroPlanar® STI2100F™, Tempe, Arizona (2007).

24. DuPont Air Products NanoMaterials L.L.C. Material Safety Data Sheet, Trade Name MicroPlanar® IMD2400™, Tempe, Arizona (2007).

25. DuPont Air Products NanoMaterials L.L.C. Material Safety Data Sheet, Trade Name CR90X™, Tempe, Arizona (2007).

26. DuPont Air Products NanoMaterials L.L.C. Material Safety Data Sheet, Trade Name MicroPlanar® CMP3200X™, Tempe, Arizona (2007).

27. www.hitachi-chem.co.jp/english/products/srm/004.html (accessed February 2008).

28. www.fujimico.com/products/abrasives.html (accessed February 2008).

29. www.planarsolutions.com (accessed February 2008).

30. www.jsrmicro.com/pro_CMP_slurry.html (accessed February 2008)

31. www.appliedmaterials.com (accessed February 2008).

32. T. Gopal and J. B. Talbot, *J. Electrochemical Soc.*, **153**, G622 (2006).

33. C. Wang, P. Sherman, and A. Chandra, *Int. J. Manufacturing Technology and Management,* **7** (5), 504 (2005).

34. D. G. Thakurta, D. W. Schwendeman, R. J. Gutmann, S. Shandar, L. Jiang, and W. N. Gill, *Thin Solid Films*, **414**, 78 (2002).

35. J. Luo and D. Dornfeld, *Integrated Modeling of Chemical Mechanical Planarization (CMP) for Integrated Circuit Fabrication: from Particle Scale to Feature, Die and Wafer Scales*, Report, University of California, Berkeley (October 2003).

36. L. Zhang and R. S. Subramanian, *Thin Solid Films*, **397**, 143 (2001).

37. E. Paul, F. Kaufman, V. Brusic, J. Zhang, F. Sun, and R. Vacassy, *Journal of the Electrochemical Society*, **152** (4), G322 (2005).

38. Y. Wang, Y. Zhao, and J. Gu, *Journal of Materials Processing Technology*, **183**, 374 (2007).

39. R. Saxena, D.G. Thakurta, R. J. Gutmann, and W. N. Gill, *Thin Solid Films*, **449**, 192 (2004).

40. D. Mejia and S. Beaudoin, *Journal of the Electrochemical Society*, **150** (2), G96 (2003).

41. C. Cho, S. Park, and Y. Ahn, *Thin Solid Films*, **389**, 254 (2001).

42. A. R. Mazaheri and G. Ahmadi, *Journal of the Electrochemical Society*, **150** (4), G233 (2003).

43. J. Seok, C. P. Sukam, A. T. Kim, J. A. Tichy, and T. S. Cale, *Wear*, **257**, 496 (2004).

44. J. Seok, C. P. Sukam, A. T. Kim, J. A. Tichy, and T. S. Cale, *Wear*, **254**, 307 (2003).

45. J. Luo and D. Dornfeld, *IEEE Transactions on Semiconductor Manufacturing*, **14** (2), 112 (2001).

46. Y. Guo, A. Chandra, and A. F. Bastawros, *Journal of the Electrochemical Society*, **151** (9), G583 (2004).

47. P. H. Chen, B. W. Huang, and H. C. Shih, *Thin Solid Films*, **476**, 130 (2005).

48. Y. Zhao and L. Chang, *Wear*, **252**, 220 (2002).

49. G. Fu and A. Chandra, *Journal of Electronic Materials*, **31** (10), 1 (2002).

CHAPTER 3

EFFECTS OF COPPER CMP SLURRY CHEMISTRY ON THE COLLOIDAL BEHAVIOR OF ALUMINA ABRASIVES

3.1 Abstract

The effects of common slurry additives on the colloidal behavior of alumina suspensions used for copper chemical mechanical planarization (CMP) were investigated. The alumina suspensions were characterized by zeta potential and agglomerate size distribution measurements with various chemical additives. To simulate the slurry during copper CMP, the effect of the addition of ~100 nm diameter copper particles was studied. The presence of 0.12 mM copper caused a decrease in agglomeration for pH values less than 6.5 and an increase in agglomeration ranging from 200-1000 nm for pH values greater than 7 in aqueous solutions. Addition of glycine caused the formation of a soluble Cu-glycine complex that decreased agglomeration at pH values less than 4. The addition of 0.1 wt% H_2O_2 did not affect the effective alumina agglomerate size without copper, but with copper in the solution the majority of the alumina agglomerated to ~2 μm for all pH values. However, increasing H_2O_2 concentration to 2.0 wt% decreased the agglomerate size by 100-400 nm. The pH of the slurry had the largest effect on the zeta potential and agglomerate size distributions.

3.1 Introduction

Chemical mechanical planarization (CMP) is used in integrated circuit manufacturing to remove excess material and provide a globally planarized wafer

surface. The CMP process uses a slurry containing abrasive particles and chemical additives which produces a mechanical and chemical synergistic effect that causes material removal [1]. Since copper has become the interconnect material of choice, the focus of our research is on copper CMP. Material removal rates (MRR) for copper CMP are significantly affected by the addition of chemicals to the slurries. These additives need to be optimized so that both the interactions with the wafer surface and the effects on the abrasive particle in the slurry will provide an adequate MRR and planarized surface with minimal defects [2]. In order to understand the effects of the chemical additives on the overall copper CMP process, the chemical and colloidal effects of the additives on the abrasive particles in the slurry were studied.

The colloidal properties of the slurry particles can be measured through zeta potential and effective particle size distributions. The zeta potential is indicative of the charge on the surface of a particle. The magnitude of the zeta potential depends on the particle material and the solution ionic composition, especially pH [3]. When the absolute magnitude of the zeta potential is small, less than 10 mV, the repulsive forces between the particles are small, allowing the particles to approach each other and eventually agglomerate. This agglomeration occurs near the iso-electric point (IEP), which is the pH at which the zeta potential is zero. In contrast, when the absolute magnitude of the zeta potential is large (>30 mV), the colloids remain dispersed [2, 3]. The zeta potential can be affected by chemical additives in a slurry, which generally act as surfactants, inhibitors, complexing agents, oxidizers, microemulsions, and catalysts [2].

The effects of various chemical additives and pH of the slurry on the MRR during CMP has been investigated [4-17]. Ramarajan et al. demonstrated the importance of the electrostatic interactions between the slurry particles and the wafer surface by measuring changes in the MRR as the ionic strength of the slurry was varied while the pH was held constant [13]. Studies by Aksu and Doyle showed the copper surface can form a variety of oxides and hydroxides depending upon the pH and chemical additives in the slurry [18-20].

There are a few studies of both zeta potential and particle size distribution [13-17]. D. Lee et al. studied the behavior of alumina slurries by measuring settling rate, particle size, and zeta potential at various pH values [17]. They found that agglomerate sizes were typically small (less than 300 nm) for pH values less than 6 and large (200 – 1000 nm) for pH values above 8. The measured IEP was found to be pH 9-10 for all of the slurries studied. The addition of nonionic surfactants to the alumina slurries did not have much effect on the zeta potential, but did cause a 5-10% decrease in the agglomerate size [17].

3.3 Review of Gopal's Work

A systematic study of the effects of slurry chemistry on alumina particles was conducted by Gopal [21, 22]. The colloidal behavior of the alumina abrasive in a commercial EKC Tech aqueous slurry was first studied, and then in the presence of common copper CMP slurry additives. All solutions contained a 1 mM KNO_3 electrolyte to give a constant ionic strength, as the pH was varied from 2 to 12 with either KOH or HNO_3 [21, 22]. Without additives, the IEP was pH~9 for the EKC Tech

alumina (~100 nm diameter). The zeta potential was greater than 20 mV for pH values less than 7. The average agglomerate size was less than 400 nm for pH values less than 8. Between the pH values of 8.5 and 10 the particle size increased to greater than 2 μm and the largest agglomerate size (~3 μm) was observed at the IEP [21].

The colloidal behavior with the addition of common copper slurry additives was also measured [21]. Glycine, a complexing agent, was added in concentrations ranging from 1 to 100 mM. It was found that glycine stabilized the zeta potential and effective particle size measurements at all pH values giving better reproducibility. The addition of hydrogen peroxide, an oxidizer, in both a 0.1 and 2.0 wt% concentration with 0.1 M glycine and 1 mM KNO_3 was found to lower the magnitude of the zeta potential from that of the solution with only glycine, but agglomerate size was unaffected. The addition of sodium-dodecyl-sulfate (SDS), an anionic surfactant, caused the zeta potential to become negative for all pH values and the particle size to remain constant at ~200-230 nm. The change in zeta potential behavior has been attributed to the adsorption of SDS onto alumina. The addition of benzotriazole (BTA), a corrosion inhibitor, was found to have no effect on the colloidal properties of the EKC Tech alumina, and the addition of ethylene-diamine-tetra-acetic-acid (EDTA), another complexing agent, increased the agglomerate size to greater than 1 μm for all pH values, while the magnitude of the zeta potential was less than 10 mV for all pH values [21]. Since CMP slurries usually have a combination of many additives the combination of the EKC Tech alumina slurry with 0.01 wt% BTA, 10^{-3} M SDS, 0.1 wt% H_2O_2, 1 mM KNO_3 and either 0.1 M glycine, or 0.01 M EDTA was also studied. The mixture of additives containing glycine had much smaller particle sizes with

glycine than with EDTA, as the magnitude of the zeta potential was larger with glycine than with EDTA [21].

3.4 Review of Previous Work

The study by Gopal showed that chemical additives can significantly affect the properties of the slurry and particle suspension. This paper is a continuation of the research done by Gopal [21, 22] by investigating the colloidal properties of an alumina abrasive in solution with the chemical additives previously studied but also in the presence of copper. The addition of copper to the solutions was done in order to better simulate the slurry during the CMP process. Typical copper concentrations in the slurry, [Cu], were calculated from the MRR using the following equation:

$$[Cu] = \frac{\pi(MRR)\cdot(D)^2\cdot(\rho_{Cu})}{4\cdot f\cdot MW_{Cu}} \qquad [3.1]$$

where D is the wafer diameter, f is the slurry flow rate, ρ_{Cu} is the copper density of 8.933 g/cm^3 and MW_{Cu} is the molecular weight of Cu, 63.5 g/mol. Assuming a typical copper removal rate ranging from 50-300 nm/min and a slurry flow rate range of 150-300 ml/min, the average concentration of copper in the slurry for a standard wafer diameter (100, 150, 200, and 300 mm) is ~10 mM Cu. This calculation assumes a fresh constant supply of slurry to the wafer surface and is used in order to obtain an approximate concentration of copper in solution to use in our experiments.

A previous study of copper in CMP slurries was done by Du et al. which used dissolved $CuSO_4$ to give Cu^{2+} in solution [23]. Our initial zeta potential measurements used dissolved $CuSO_4$ and it was found that the solution with the dissolved $CuSO_4$ had

a lower IEP than the solution containing the copper nanoparticles [24]. This is believed to be due to the addition of SO_4^{2-} from the $CuSO_4$ which has been shown in previous work to lower the IEP of alumina [25]. Due to this effect of $CuSO_4$, copper nanoparticles were used for the experimental investigation.

3.5 Experimental

Experiments were performed following a similar procedure to Gopal [21]. A ZetaPlus (Brookhaven Instruments Corporation) was used to measure both the zeta potential and effective particle size distribution. Zeta potential was measured by an electrophoretic light scattering (ELS) technique, also known as laser doppler velocimetry (LDV) [26], and particle size was measured using a quasi-elastic light scattering (QELS) technique [27]. The ZetaPlus machine is capable of measuring the zeta potential from -150 to +150 mV with ±2% accuracy [26]. The instrument can measure particle size within the range of 2 nm to 3 μm with a ±1% accuracy [27].

All solutions were prepared with filtered de-ionized (DI) water with 1 mM KNO_3 (from Acros Organics) to maintain a constant ionic strength. The DI water was filtered through 20 μm Nalgene cellulose nitrate non-fiber filters [21]. The desired additives were mixed with the solution and a small amount (~0.048 wt%) of alumina particles added [24]. For all of the experiments the alumina from a dispersion manufactured by Cabot Corporation containing 40 wt% α-alumina in DI water was used [24]. The median aggregate diameter of the alumina is 150 nm, which consists of a primary spherical particle of 20 nm diameter and forms globular type aggregates, as reported by Cabot Corporation [28]. The pH of the solution was adjusted between 2

and 12 using KOH (from Acros Organics) or HNO_3 (from Fisher Scientific). The pH of the solution was measured using an Orion model SA 720 pH meter. The solutions were ultrasonicated, using a Bransonic Cleaner model 1200, for 5 minutes. Then ~10 ml was pipetted into disposable cuvettes for effective particle size and zeta potential measurements [24].

The agglomeration as a function of time after 5 min of ultrasonication was measured. Figure 3.1 shows the agglomerate size vs. time for the alumina in a 1mM KNO_3 solution at various pH values. It was found that for pH values near the IEP (pH~7.5) the average agglomerate size increases with time until the agglomerates become very large (>5μm) and begin to settle. This occurs within 2 hours of ultrasonication. For pH values outside of this range (pH 4 and 10) the agglomerate size reaches steady state within 5 minutes of ultrasonication. For a typical industrial copper CMP process the copper wafer surface will be exposed to the slurry solution for approximately 5-10 minutes [2]. In order to compare our experiments to the copper CMP process all solutions were measured 10 minutes after ultrasonication.

Zeta potential and particle size measurements were performed using the Cabot alumina slurry and the concentrations of additives as listed in Table 3.1. Additionally, experiments were also performed in the presence of copper nanoparticles (<100 nm in diameter, from Aldrich). The concentration of alumina in the slurry during CMP is typically 0.4-4 wt% [29]. The required concentration of the alumina in the samples used to measure zeta potential and particle size is ~0.048 wt%. In order to maintain a similar ratio of copper to alumina as during a typical CMP process, a concentration of 0.12 mM Cu was used in the samples [24]. Although the required concentration of

alumina in the measured samples is much lower than in a CMP slurry our results may be comparable to slurries with higher solid content. According to the criterion established by Chari and Rajagopalan [30], the colloidal suspensions used in this study can be considered dilute up to a concentration of approximately 10 wt%. For the colloidal suspensions with less than 10 wt% alumina the particle-particle interactions in the bulk solution and in the interfacial region can be neglected [30]. Therefore, it is believed that interactions observed in our experiments with 0.05 wt% solids will be similar to interactions that occur in slurries with up to 10 wt% solids. However, no attempts have been made to measure colloidal behavior with a higher concentration of solids and further investigation is needed to verify this.

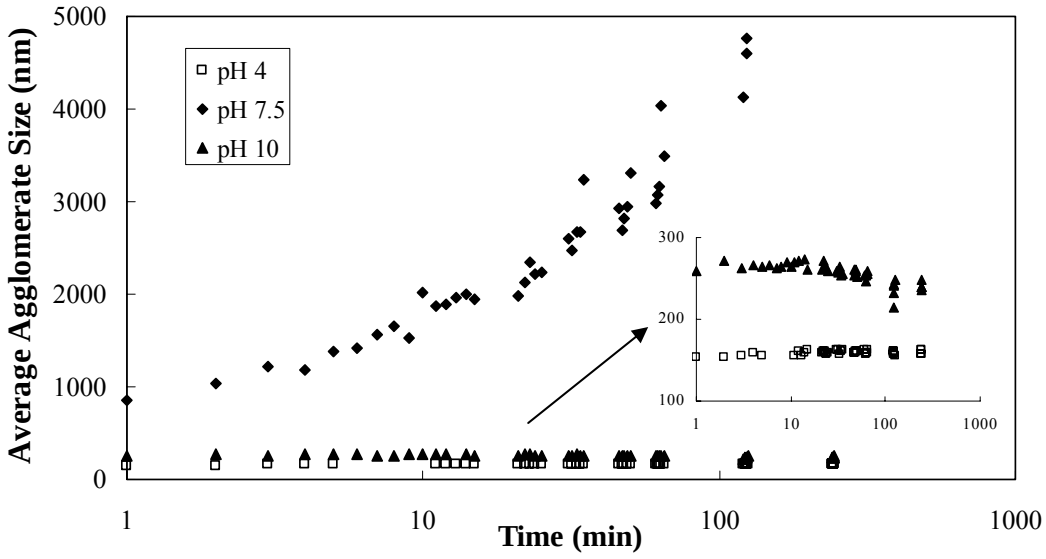

Figure 3.1 Average agglomerate size vs. time for alumina in a 1mM KNO_3 solution at various pH values.

Table 3.1 Concentration of additives used in the alumina slurry.

a) 1 mM KNO_3
b) 1 mM KNO_3, 0.1 M Glycine
c) 1 mM KNO_3, 0.1 M Glycine, 0.1 wt% H_2O_2
d) 1 mM KNO_3, 0.1 M Glycine, 2.0 wt% H_2O_2
e) 1 mM KNO_3, 0.1 M Glycine, 0.1 wt% H_2O_2, 0.01 wt% BTA, 0.1 mM SDS
f) 1 mM KNO_3, 0.01 M EDTA, 0.1 wt% H_2O_2, 0.01 wt% BTA, 0.1 mM SDS

3.6 Results and Discussion

The zeta potential measurements for the alumina with and without 0.12 mM copper nanoparticles are compared in Figure 3.2. The IEP of the alumina in the presence of copper (pH~6.7) is just slightly higher than the IEP without copper (pH~6.5). The IEP of α-alumina has been published as 9.2 in an aqueous dispersion [2]. The IEP has been observed to vary between 5 and 9.5 depending on the impurities in the sample and the extent of hydration. Salts such as SO_4^{2-}, Cl^-, $H_2PO_4^-$, and NO_3^- can lower the IEP significantly depending on concentration [25]. The presence of 1 mM KNO_3 in solution may have lowered the IEP of the measured Cabot α-alumina in Figure 3.2 compared to that in the literature [2]. Figure 3.2 also shows the magnitude of the zeta potential, which at pH values greater than 8 is slightly lower (8-12 mV) in the presence of copper.

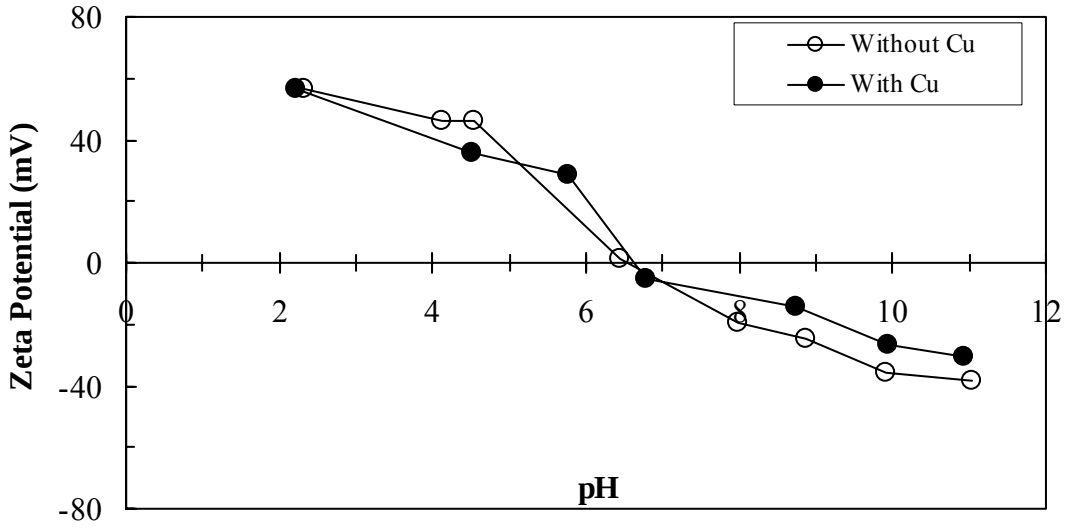

Figure 3.2 Zeta potential versus pH for alumina in 1 mM KNO_3 solution with and without 0.12 mM copper.

In addition to the zeta potential of the alumina, the effective particle size distribution as a function of pH was also investigated. Studies have shown that the alumina agglomerate size distribution is normally distributed only under certain conditions, and most often the alumina has a bimodal or even trimodal distribution [21, 24]. Figure 3.3 shows the agglomerate size distribution of alumina in a 1 mM KNO_3 solution for various pH values. The size distributions are bimodal for all pH values without copper, except at pH 2.33 which is trimodal. For pH values less than the IEP (~6.5) the majority of the agglomerates are of a smaller size range, while at pH values near and above the IEP the majority of the agglomerates are a larger size range. Therefore, some agglomeration occurs at all pH values without additives in the solution. Table 3.2 shows the percentage of agglomerates in the two peaks, and the average agglomerate size and standard deviation for each of the peaks in the bimodal distributions with varying pH. Below a pH value of 6, the majority of the particles

suspended in the solution are less than 200 nm, and a small percentage (<20%) of the particles are agglomerated. The agglomerate size decreases as the pH increases, at pH values <6. Between pH values 6 to 9, the majority of the particles are agglomerated and >1.3 μm. Above pH 9.9, the agglomerates are all less than 800 nm.

The addition of copper into the solution did affect the effective particle size distribution. As also shown in Table 3.2, all peaks were bimodal, except at pH 8.8 which had a single peak. All agglomerates in the distributions were <850 nm at pH values less than 6. At a pH of 10, the majority of the agglomerates were >1.6 μm, compared to the ~722 nm without copper at the same pH. At pH 6.8, 11% of the agglomerates were >9.0 μm. The agglomerate size at pH 2 is much smaller with copper (812 nm) than without copper (5.0 μm), and the agglomerate size at pH >10.8 is 4.6 μm with copper whereas without copper the majority of the particles are ~200 nm. In both cases there were pH values (pH 11.0 without Cu and pH 4.5 with Cu) where a small percentage (<10%) of the particles was significantly smaller (<75 nm) than the median aggregate diameter of 150 nm [24]. This means that some of the aggregates are breaking up prior to measurement, possibly due to the ultrasonication treatment.

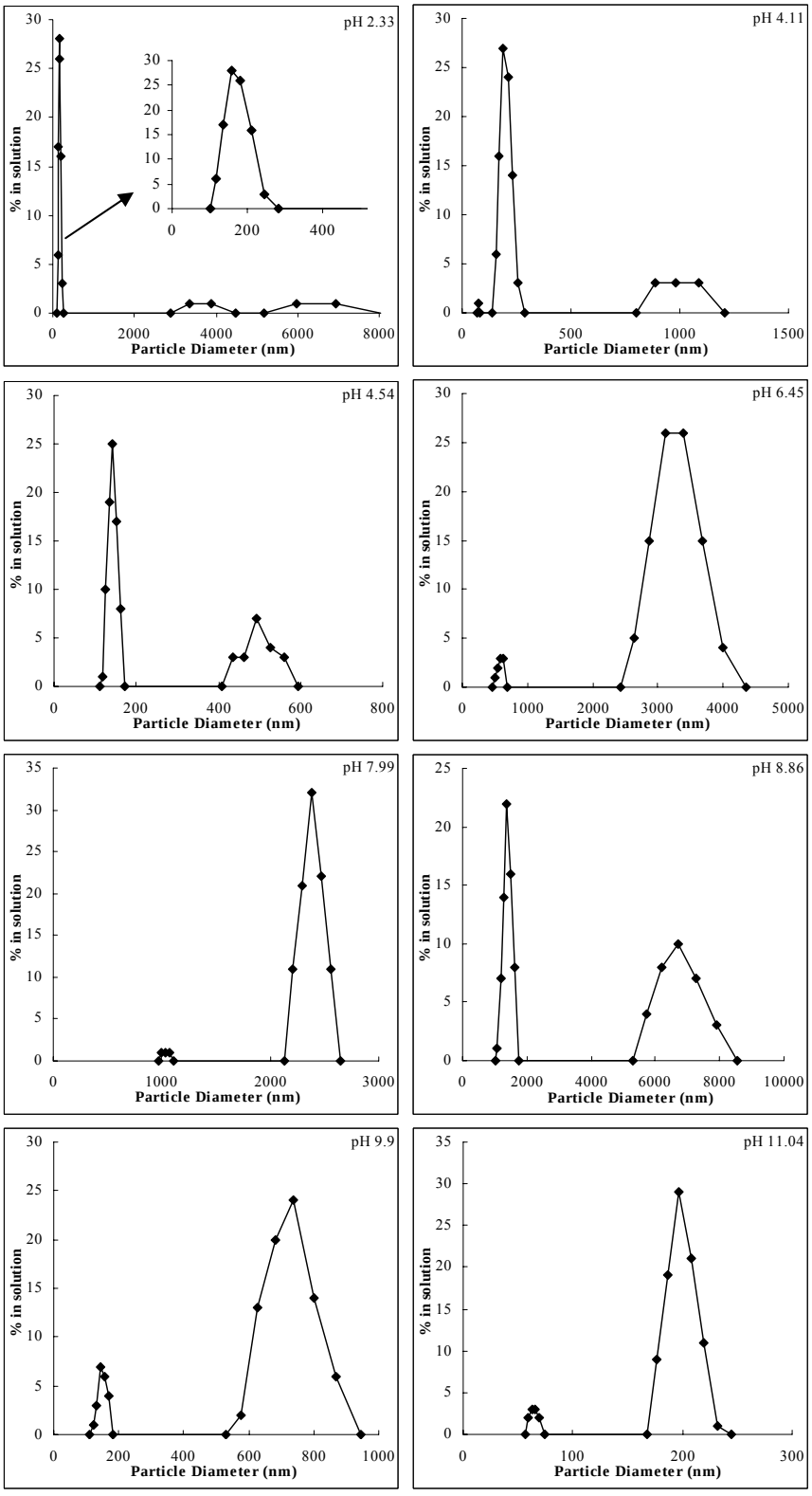

Figure 3.3 Agglomerate distributions of alumina in a 1 mM KNO_3 solution for various pH values.

Table 3.2 Percentage of agglomerates, average agglomerate size, and standard deviation for the bimodal distributions of the alumina in solution with various additives and at different pH values.

Solutions*	Without Copper							With Copper						
		Small Particles			Large Particles				Small Particles			Large Particles		
	pH	%	Ave. (nm)	σ (nm)	%	Ave. (nm)	σ (nm)	pH	%	Ave. (nm)	σ (nm)	%	Ave. (nm)	σ (nm)
a	2.3	96	169	30	4	5034	1476	2.2	86	161	14	14	812	59
	4.1	91	197	28	9	985	82	4.5	3	47	3	97	233	21
	4.5	80	142	11	20	497	38	5.8	38	117	7	62	313	18
	6.5	9	578	47	91	3252	334	6.8	89	1695	126	11	9376	528
	8.0	3	1037	31	97	2380	100	8.8	100	2161	17			
	8.9	68	1388	132	32	6708	616	10.0	10	297	22	90	1636	147
	9.9	21	148	13	79	722	73	10.9	95	181	33	5	4627	790
	11.0	10	64	4	90	199	13							
b	2.3	95	312	77	5	8098	1291	2.0	23	223	48	77	697	162
	4.0	100	1319	3				4.0	15	240	22	85	1000	90
	6.9	100	2003	19				6.2	100	1915	550			
	8.8	100	2054	20				8.0	100	1879	7			
	9.6	38	1033	93	62	6333	631	9.5	5	346	30	95	2083	219
								10.7	34	961	53	66	2224	136
c	2.3	100	334	3				2.6	6	272	19	94	1740	186
	4.8	100	691	3				5.0	51	1132	69	49	3261	224
	7.0	100	779	5				6.9	17	668	43	83	2875	444
	9.0	100	1700	6				9.0	32	819	42	68	2186	124
	11.2	13	662	36	87	1555	79	10.9	73	1352	221	25	3517	634
d	2.8	59	131	6	41	296	14	2.6	100	163	10			
	4.2	4	58	2	96	193	13	3.8	100	162	1			
	5.3	88	154	16	12	869	95	5.0	100	165	1			
	6.9	100	1834	15				7.0	100	1409	5			
	8.9	100	1754	154				9.1	100	1501	5			
	10.3	100	1240	12				11.2	24	614	41	76	2303	170
e	2.4	76	560	69	24	8976	821	2.8	100	260	2			
	4.8	78	846	87	22	9123	682	4.0	100	303	3			
	6.8	30	675	96	70	9062	748	5.6	59	464	69	38	1123	162
	9.0	66	1073	96	34	9235	607	7.5	100	1460	16			
	11.2	61	711	84	39	9062	753	8.9	100	912	10			
								11.5	100	552	6			
f	2.4	16	133	16	84	8643	1082	2.4	68	983	362	28	7700	1761
	4.1	30	484	51	70	3646	402	4.1	52	1062	106	48	9232	621
	6.4	17	441	31	83	2088	186	6.5	16	462	614	82	2970	1078
	9.0	55	795	54	45	2662	202	9.0	100	2238	17			
	11.0	34	347	19	66	1022	58	11.0	6	209	14	94	1461	162

*As listed in Table 3.1

During CMP large agglomerates can cause unwanted defects and scratches on the wafer surface. Because small amounts of large agglomerates are often found in CMP slurries, typical CMP processes will incorporate a filtration system to remove these larger particles before the slurry is dispersed onto the polishing pad. The majority of the commercially available filtration units are able to effectively remove 80% of all

agglomerates >2 μm [31]. Therefore, these large agglomerates are not a concern during CMP if filtration is used. Figure 3.4 shows a comparison of the agglomerate size of the alumina both with and without copper before and after filtration of the large agglomerates (>2.3 μm). The small and large agglomerate sizes are shown separately for the pH values with bimodal distributions. The error bars in Figures 3.4 and 3.5 indicate the standard deviation of the particle size distribution. The agglomerate size of the small distributions reflects the magnitude of the zeta potential such that at larger absolute zeta potentials, the agglomerate sizes are smaller. Between the pH values of 2 and 6, the small alumina effective particle sizes are similar both with and without copper (~150 nm), but there are larger agglomerates without copper (~900 nm) than with copper (~300 nm). This may be due to an increase in repulsive forces between the copper and alumina. According to the potential-pH diagram for the copper-water system between pH values of 2 and 4 copper can exist as either a solid substance, Cu, or dissolved into solution as Cu^{2+} or Cu^{+} [32].

The solution was a very light reddish orange color, indicating that the copper is either dissolved as Cu^{+} or remains in solid form as Cu [32]. With some of the copper particles dissolving to Cu^{+}, the repulsive forces between the positively charged alumina particles and the Cu^{+} ions may have caused a decrease in the agglomeration of the alumina. Between pH values 7 and 10, the smaller agglomerate size of the alumina with copper was larger by ~200-1000 nm than without copper. This may be due to attractive interactions between the copper and the alumina particles. Between the pH values of 7 and 10 copper in water will oxidize to either cupric oxide (CuO) or cuprous oxide (Cu_2O) [32]. The black color of the solution observed indicated that CuO was

mainly formed [32]. The IEP of CuO is pH~9.5 [25], whereas the measured IEP of the Cabot alumina was pH~6.5. Between the pH values of 6.5 and 9.5 the alumina is negatively charged, while the CuO is positively charged [25]. Even though there is a small amount of CuO in solution, the CuO and alumina may agglomerate, thereby increasing the agglomerate size. If it is assumed that the average alumina aggregate size is 500 nm and the average CuO particle size is 120 nm between the pH values of 6.5 and 9.5, the ratio of alumina particles to CuO particles is ~3:1. At pH~10, which is very near the IEP of CuO, the size of the small alumina agglomerates without copper was 148 nm, and with copper it was 297 nm. This increase in agglomerate size with the addition of Cu may be due to a CuO particle adhering to the alumina aggregate and causing the ~150 nm increase in the agglomerate size. As the pH increases to ~11 the majority of the alumina agglomerates without copper are 199 nm while with copper slightly decrease to 181 nm which may be due to the increase in repulsive charges at this pH between the negatively charged CuO and alumina.

The first slurry additive studied was glycine, which has been found to act as a stabilizing agent for an alumina dispersion [21]. Figure 3.5 compares the zeta potential and agglomerate size of the alumina in a 0.1 M glycine solution with and without copper. The addition of glycine increased the IEP of the alumina to ~9 in the presence of copper. Without the addition of copper, glycine had no effect on the IEP (pH~6.5), or the magnitude of the zeta potential which was >25 mV at pH values <7 and 0-20 mV at pH values >7. The agglomerate sizes were similar both with and without copper (~2.0 μm at pH values between 6 and 9, and <1.5 μm for pH values <6).

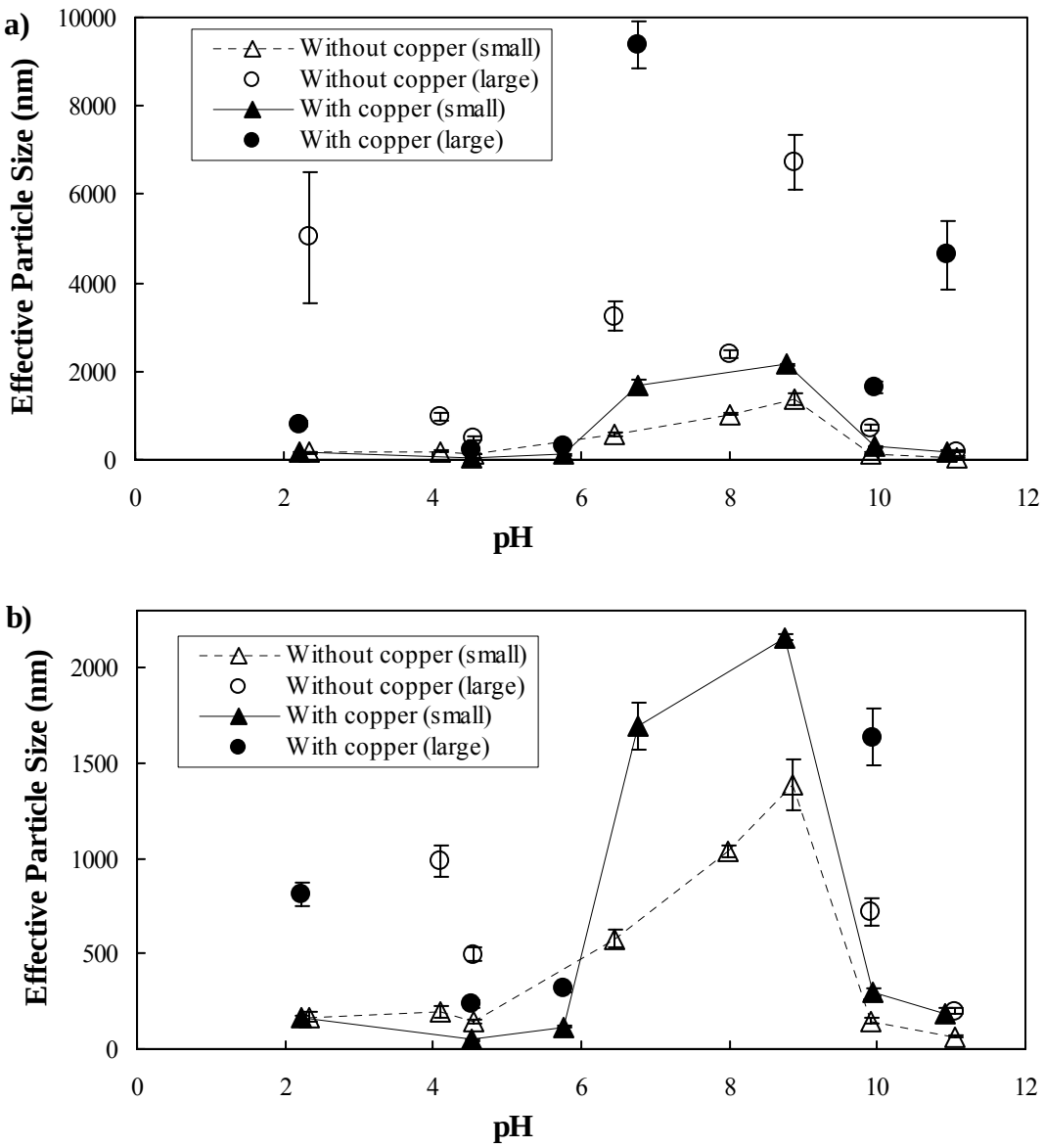

Figure 3.4 Agglomerate size versus pH for alumina in a 1 mM KNO_3 solution with and without 0.12 mM copper a) for all agglomerates and b) after filtration of large agglomerates (error bars indicate standard deviation of the agglomerate size distribution).

Glycine addition caused the agglomerate size distributions to become more unimodal between pH values of 6 and 9 both with and without copper as shown in Table 3.2. Again, without copper there are large agglomerates (>8.0 μm) at a pH of ~2,

whereas with copper addition these agglomerates are <700 nm. This may be due to an increase in the repulsive forces in the presence of copper. Aksu and Doyle reported that glycine exists in aqueous solutions in three different forms, $^{+}H_3NCH_2COOH$ (cation), $^{+}H_3NCH_2COO^{-}$ (zwitterion), and $H_2NCH_2COO^{-}$ (anion), and in the absence of other species the cation predominates at pH values less than 2.35 and the anion predominates at pH values greater than 9.78 [20]. Glycine forms soluble complexes with both cupric and cuprous ions [20]. Aksu et al. constructed a potential-pH diagram for the Cu-H_2O-glycine system with copper and glycine concentrations of 10^{-4} M and 0.1 M, respectively. At pH 2 the copper exists as either a solid, Cu, or in solution as $Cu(H_3NCH_2COO)^{2+}$ [20]. The positively charged Cu-glycine complex in the solution may increase the repulsion between the positively charged alumina agglomerates and cause less agglomeration to occur. Similarly, at pH 4 the alumina is more agglomerated without copper (1.3 μm) than with copper (1.0 μm) possibly due to the increase in repulsion from the positively charged $Cu(H_2NCH_2COO)^{+}$ species. Between the pH values of 6 and 9, the agglomerate size of the alumina is ~2.0 μm both with and without copper and the agglomerate size distribution is unimodal. The glycine forms a neutrally charged complex with the copper, $Cu(H_2NCH_2OO)_2$, between pH 6 and 9 which eliminates the interactions between the copper and the alumina and stabilizes the distribution. At pH values greater than 9.5 the alumina is again more agglomerated without copper (6.0 μm) than with copper (2.0 μm). At these high pH values the glycine can complex with the copper to form a negatively charged ion, $Cu(H_2NCH_2COO)_2^{-}$, that may increase the repulsive forces between the negatively charged alumina agglomerates and decrease the agglomeration.

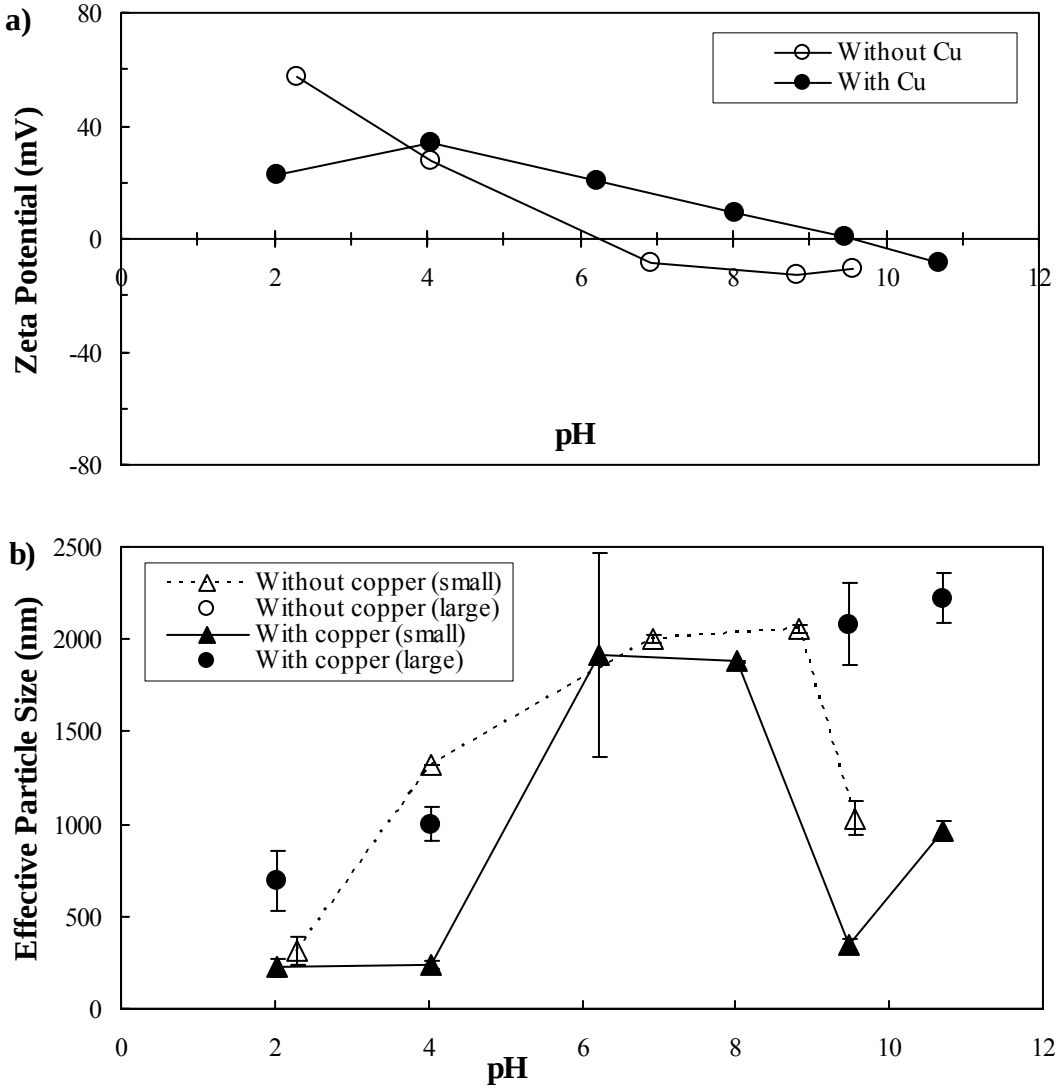

Figure 3.5 a) Zeta potential and b) agglomerate size versus pH for alumina in 0.1 M glycine, and 1 mM KNO_3 solution with and without 0.12 mM copper (error bars indicate standard deviation of the agglomerate size distribution).

Hydrogen peroxide is used as an oxidizing agent in copper CMP slurries. Typical concentrations of H_2O_2 in the slurry range from 0.1-5.0 wt% [21]. Figure 3.6 shows the zeta potential measurements for the alumina agglomerate in 0.1 wt% H_2O_2 and 0.1 M glycine in 1 mM KNO_3 solution both with and without copper nanoparticles. The addition of 0.1 wt% H_2O_2 to the slurry caused a >5 mV decrease in the zeta

potential for all pH values with copper addition. The agglomerate size decreased with the 0.1 wt% H_2O_2 addition without copper, and increased the particle agglomeration for all pH values with copper as shown in Table 3.2. The lower magnitude of the zeta potential with Cu and H_2O_2 caused the increase in alumina agglomeration. Without copper the agglomerates have a unimodal distribution for all pH values except at a pH of ~11. With the addition of copper the distribution becomes bimodal for all pH values, with agglomerated particles greater than 1.7 μm. It is unclear why the magnitude of the zeta potential decreased, causing an increase in agglomeration when 0.1 wt% H_2O_2 is added to the Cu-H_2O-glycine system. It has been shown that the addition of H_2O_2 to the Cu-H_2O-glycine system will significantly increase the dissolution rate of copper [33-35]. Xu et al. believe that the most likely reactions occurring in the Cu-H_2O-H_2O_2-glycine system are [35]

$$Cu \rightarrow Cu^{2+} + 2e^- \quad \text{(oxidation reaction)} \quad [3.2]$$

$$Cu^{2+} + 2(H_2NCH_2COOH) \rightarrow Cu(H_2NCH_2COOH)_2^{2+} \quad \text{(copper complexing)} \quad [3.3]$$

$$H_2O_2 + 2e- \rightarrow 2OH^- \quad \text{(reduction reaction)} \quad [3.4]$$

$$Cu^{2+} + 2OH^- \rightarrow Cu(OH)_2 \quad \text{(precipitation formation)} \quad [3.5]$$

The copper may exist in the solution as either a hydrated cupric oxide, $Cu(OH)_2$, or in a soluble complex with glycine [35]. Hydrated cupric oxide has a reported IEP between 7.6-9.4 [25], and therefore will be similarly charged to the alumina. As was shown for the Cu-H_2O-glycine system, the Cu-glycine complex will be positively charged at pH values <4, neutrally charged at pH values 6-9, and negatively charged for pH values >9 [33]. The presence of both the $Cu(OH)_2$ and the Cu-glycine complex in solution with the alumina should cause an increase in repulsion between the alumina agglomerates for

all pH values and less agglomeration would be observed. This is not the case for the system with 0.1 wt% H_2O_2 and further investigation is required to understand this. However, when the H_2O_2 concentration is increased to 2.0 wt% in the Cu-H_2O-glycine system, less agglomeration of the alumina particles is seen which is consistent with the literature [33-35].

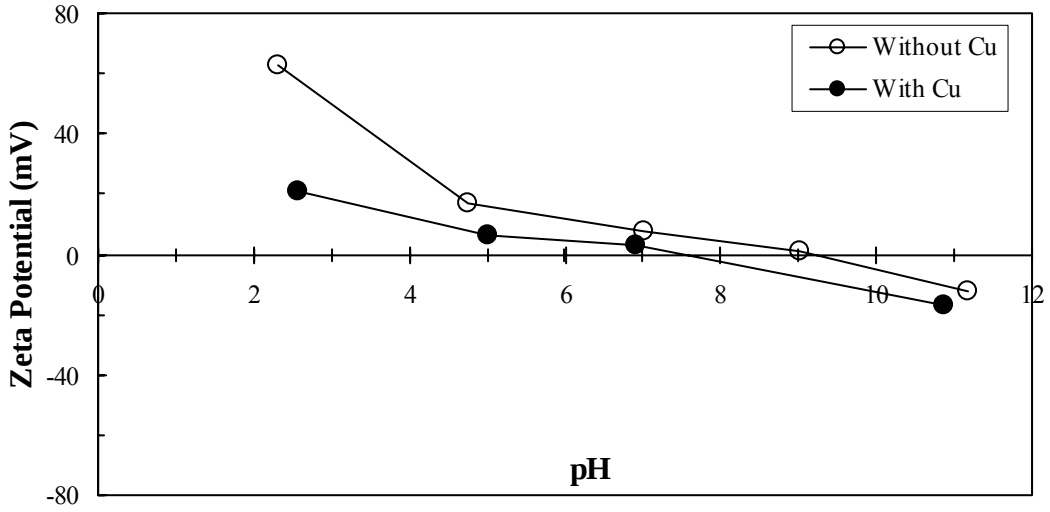

Figure 3.6 Zeta potential versus pH for alumina in 0.1 M glycine, 0.1 wt% H_2O_2, and 1 mM KNO_3 solution with and without 0.12 mM copper.

Table 3.2 shows the agglomerate size measurements for a 0.1 M glycine, 2.0 wt% H_2O_2 in a 1 mM KNO_3 solution both with and without copper. For pH values less than 5 the alumina agglomerate size without Cu in solution is 131-296 nm with bimodal distributions. With Cu the agglomerates are 162-165 nm and have unimodal distributions. At pH values between 6.9 and 9.1 the effective alumina agglomerate size is 1.7-1.9 μm without copper and 1.4-1.5 μm with copper. The alumina agglomerates have a unimodal distribution for all pH values with copper except at a pH of 11. The alumina exhibits less agglomeration in the presence of copper than without copper for all pH values. The zeta potential measurements could not be made at the higher H_2O_2 concentration because of electrolysis and bubbling of oxygen on the electrode.

Seal et al. studied the effect of hydrogen peroxide and glycine on copper CMP and observed an increase in MRR (~350 nm/min) as H_2O_2 concentration increased from 0.1 to 2 wt% [12]. It was suggested by Seal et al. that the MRR increase was due to Cu-glycine complex formation that is easily dissolved into the solution [12]. However, the increase may also be due to the effect that these additives have on the alumina abrasive size distribution. At pH 2.6 the alumina agglomerate size distribution in 0.1 wt% H_2O_2, 0.1 M glycine and 1 mM KNO_3 in the presence of copper was bimodal with 94% of the agglomerates being 1.74 ± 0.2 μm in diameter, whereas the agglomerate sizes when H_2O_2 was increased to 2.0 wt% had a unimodal distribution with agglomerates 163 ± 10 nm in diameter. According to the Luo and Dornfeld CMP model, slurries containing a smaller size distribution of abrasives will produce higher MRR because there are more active abrasives embedded into the polishing pad and actively removing material from the wafer surface [29].

A combination of the slurry additives was also studied which contained glycine, H_2O_2, SDS, and BTA. Figure 3.7 shows the zeta potential measurements for alumina with the combination of slurry additives (0.1 M glycine, 0.1 wt% H_2O_2, 1 mM SDS, and 0.01 wt% BTA) with and without copper. The zeta potential was a negative value for all pH values with this mixture of additives both with and without copper, except at pH 9.0 without copper which had a zeta potential of ~5mV. The negative zeta potential is due to the SDS which is an anionic surfactant that adsorbs onto the alumina [21]. As shown in Table 3.2, the distributions are all bimodal without the addition of copper and the average agglomerate size of the smaller of the two peaks is similar to that typically seen without additives (<900 nm at pH values <7, >1.0 μm at pH values between 7 and 9, and <1.0 μm at pH values >11). The large peak in each of the distributions without copper has an average agglomerate size >8.0 μm. With the addition of copper the distributions become unimodal at all pH values except 5.6 and the average agglomerate sizes are similar to that typically seen without any additives. The combination of these chemical additives in the presence of copper eliminates large agglomerates and has a unimodal distribution. Without the addition of copper these chemical additives cause an increase in the agglomeration of the alumina for all pH values.

Another slurry solution was studied except that EDTA was used instead of glycine as the complexing agent. Figure 3.8 shows the zeta potential measurements with 0.01 M EDTA, 0.01 wt% BTA, 0.001 M SDS, 0.1 wt% H_2O_2 in 1 mM KNO_3 solution with and without copper. The zeta potential measurements are slightly more negative (-2 to -12 mV without copper and -4 to -27 mV with copper) than with the glycine (-10 to 5 mV both with and without copper). As shown in Table 3.2, the

alumina agglomerate size distributions are bimodal for nearly every pH value both with and without copper. The distributions with copper compared to those without copper at each of the pH values are very similar. This suggests that the EDTA eliminates the effects that the copper particles have on the alumina dispersion. This is consistent with literature, in that EDTA is known to complex with positively charged metal ions, effectively preventing further reaction [2]. The distributions remained bimodal with the combination of all of the chemical additives in which EDTA was used as the complexing agent.

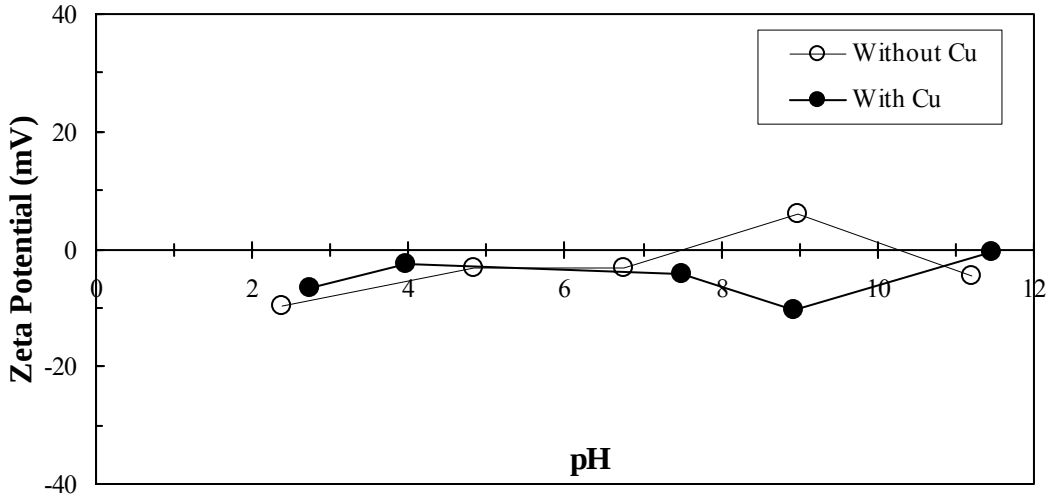

Figure 3.7 Zeta potential versus pH for alumina in 0.1 M glycine, 0.01 wt% BTA, 1 mM SDS, 0.1 wt% H_2O_2, and 1 mM KNO_3 solution with and without 0.12 mM copper.

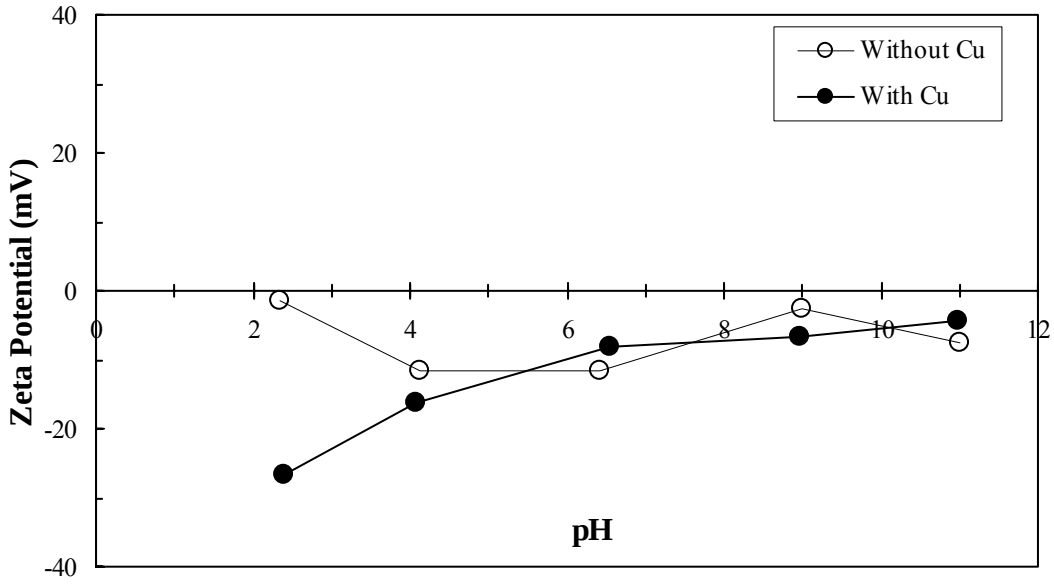

Figure 3.8 Zeta potential versus pH for alumina in 0.01 M EDTA, 0.01 wt% BTA, 1 mM SDS, 0.1 wt% H_2O_2, and 1 mM KNO_3 solution with and without 0.12 mM copper.

3.7 Conclusions

The role of chemical additives as well as the effect of copper particles on the colloidal properties of the alumina abrasives was examined. It was found that the addition of copper nanoparticles into the slurry affects the colloidal properties of the alumina abrasives. Even with a small amount of copper in the slurry solutions, an increase or decrease in agglomeration of the alumina is observed depending on the state of the copper in the solution. In general, when the pH is low and the copper is dissolved as Cu^+, the repulsive forces between the Cu^+ and the positively charged alumina increase and the alumina particles agglomerate less. As the pH increases and the Cu forms CuO, the alumina becomes attracted to the CuO up to pH~10 because they are oppositely charged. At pH values greater than 10 the CuO and alumina are again similarly charged and repel one another, causing a decrease in alumina agglomeration.

According to our particle size data in Table 3.2, an acidic alumina slurry will have some large agglomerates between 500-5000 nm. As copper is removed during CMP and dissolves into the low pH slurry as Cu^{+}, the large alumina agglomerates will decrease in size to 300-800 nm. In contrast, in an alkaline slurry the large alumina agglomerate size is between 700-7000 nm. As copper is removed at high pH it will form CuO and the large alumina agglomerates will increase in size to 2000-9000 nm. As large agglomerates are known to cause defects [2], an acidic slurry should yield fewer defects than an alkaline slurry.

The addition of glycine to the slurry solution was found to stabilize the alumina suspension, as was previously seen [21]. When copper was added the highly soluble Cu-glycine complex can form and the increase in repulsive forces between the Cu-glycine complex and the alumina at pH<4 and pH>9 caused a decrease in agglomeration. Addition of 2.0 wt% H_2O_2 to the Cu-H_2O-glycine system increases the solubility of the Cu-glycine complex and decreases agglomeration. However, it was observed that a smaller amount (0.1 wt%) of H_2O_2 to the Cu-H_2O-glycine system will actually increase the agglomeration and further investigation is needed to determine the effect on agglomeration and state of the copper at this low H_2O_2 concentration.

Although various chemical additives were studied, it was found that the pH of the solution had the largest effect on the zeta potential and agglomerate size distributions, as was seen previously [21]. At pH values less than the IEP the agglomerates were positively charged (except for solutions containing SDS) and the size distributions were narrow. Near the IEP, agglomerate sizes were much larger as well as broadness of the size distribution peaks. The copper addition had the largest

affect on the alumina when there was no complexing agent in the solution. Additionally, further investigation of the time to agglomeration is needed to determine if diffusion limited agglomeration or reaction limited agglomeration is occurring [30], which may also help to explain some of the results.

The slurry chemistries studied in this research were used in CMP experiments on 100 mm Cu wafers to obtain MRR data. This experimental MRR data were then compared to MRR predictions from the Luo and Dornfeld CMP model [29] and will be the subject of a future publication. The agglomerate size distributions of the alumina were used in the Luo and Dornfeld model to calculate MRR. It was found that the agglomerate size distribution of the alumina in the presence of copper better predicted the MRR [24].

3.8 Acknowledgements

This work was sponsored by FLCC Consortium through a UC Discovery grant. The authors gratefully acknowledge all the companies involved in the UC Discovery grant including Advanced Micro Devices, Applied Materials, ASML, Atmel Corporation, Cadence, Canon, Cymer, Cypress, Dupont, Ebara Technologies Inc., Hitachi Global Storage Technologies, Intel Corporation, KLA-Tencor, Mentor Graphics, Nikon Research Corporation of America, Novellus Systems Inc., Panoramic Technology, Photronics, Synopsys, and TEL USA. Additionally, the collaboration of Professors Dornfeld and Doyle and their research groups from University of California, Berkeley is greatly appreciated.

This chapter, in full, is a reprint of the material as it appears in the Journal of the Electrochemical Society, Robin Ihnfeldt and Jan B. Talbot, Vol. 153, Issue 11, pg. G948 (2006). The dissertation author was the primary investigator and author of this paper.

REFERENCES

1. G. Yehiel and R. Kistler, *Electrochemical 198th Society Meeting Abstracts*, **2000-2**, 496 (2000).

2. M.R. Oliver, *Chemical-Mechanical Planarization of Semiconductor Material*, Springer-Verlag, Berlin, Germany (2004).

3. R. J. Hunter, *Introduction to Modern Colloid Science*, Oxford University Press, Oxford, New York (1993).

4. A. Jindal and S.V. Babu, *J. Electrochemical Soc.*, **151** (10), G709-G716 (2004).

5. Y. Ein-Eli, E. Abelev, and D. Starosvetsky, *Electrochimica Acta*, **49**, 1499 (2004).

6. Z. Lu, S. Lee, S.V. Babu, and E. Matijevic, *J. Colloid and Interface Science*, **261**, 55 (2003).

7. P. Bernard, Ph. Kapsa, T. Coude, and J.C. Abry, *Wear*, **259**, 1367 (2005).

8. T. Du, Y. Luo, and V. Desai, *Microelectronic Engineering*, **71**, 90 (2004).

9. T. Du, A. Vijayakumar, and V. Desai, *Electrochimica Acta*, **49**, 4505 (2004).

10. Z. Li, K. Ina, P. Lefevre, I. Koshiyama, and A. Philipossian, *J. Electrochemical Soc.*, **152** (4), B299-G304 (2005).

11. S. Deshpande, S.C. Kuiry, M. Klimov, Y. Obeng, and S. Seal, *J. Electrochemical Soc.*, **151** (11), G788-G794 (2004).

12. S. Seal, S.C. Kuiry, and B. Heinmen, *Thin Solid Films*, **423**, 243 (2003).

13. S. Ramarajan, Y. Li, M. Hariharaputhiran, Y.S. Her, and S.V. Babu, *Electrochemical and Solid-State Letters*, **3** (5), 232-234 (2000).

14. C. Bellman and D. Zeidler, *Tenside Surfactants Detergents*, **39**, S206 (2002).

15. J. Park, S. Lee, and H. Kim, *Mat. Res. Symp. Proc.*, **566**, 176 (2000).

16. A. Sorooshian, R. Ashwani, H.K. Choi, M. Moinpour, A. Oehler, and A. Tregub, *Mat. Res. Soc. Symp. Proc.*, **816**, 125 (2004).

17. D. Lee, N. Kim, and E. Chang, *Material Science and Engineering B*, **118**, 293 (2005).

18. S. Aksu and F.M. Doyle, *J. Electrochemical Soc.*, **149** (6), G352-G361 (2002).

19. S. Aksu and F.M. Doyle, *J. Electrochemical Soc.*, **149** (7), B340-B347 (2002).

20. S. Aksu and F.M. Doyle, *J. Electrochemical Soc.*, **148** (1), B51-B57 (2001).

21. T. Gopal, PhD Thesis, University of California, San Diego (2004).

22. T. Gopal and J. B. Talbot, *J. Electrochemical Soc.*, under revision (2005).

23. T. Du, A. Vijayakumar, and V. Desai, *Mat. Res. Soc. Symp. Proc.*, **816**, 29 (2004).

24. R. Ihnfeldt, MS Thesis, University of California, San Diego (2005).

25. G.A. Parks, "The Isoelectric Points of Solid Oxides, Solid Hydroxides, and Hydroxo Complex Systems", *Chem. Tevs.*, **65**, 177 (1965).

26. Brookhaven Instruments Corporation, ZetaPlus Instruction Manual, Holtsville, NY (1994).

27. Brookhaven Instruments Corporation, 90Plus/BI-MAS Operation Manual, Holtsville, NY (1994).

28. http://w1.cabot-corp.com/controller.jsp?N=23+4294967128+3033&entry=product (accessed June 2006).

29. J. Luo and D. Dornfeld, *Integrated Modeling of Chemical Mechanical Planarization (CMP) for Integrated Circuit Fabrication: from Particle Scale to Feature, Die and Wafer Scales*, Report, University of California, Berkeley (October 2003).

30. M. Elimelech, J. Gregory, X. Jia, and R. Williams, *Particle Deposition & Aggregation,* Butterworth-Heinemann, Oxford, New York (1995).

31. R. K. Singh, *Semiconductor International*, **9**, 64 (2005).

32. M. Pourbaix, *Atlas of Electrochemical Equilibria in Aqueous Solutions*, National Association of Corrosion Engineers, Houston, Texas (1974).

33. S. Tamilmani, W. Huang, S. Raghavan, and R. Small, *J. Electrochemical Soc.*, **149**, G638 (2002).

34. S. Deshpande, S.C. Kuiry, M. Klimov, Y. Obeng, and S. Seal, *J. Electrochemical Soc.*, **151**, G788 (2004).

35. G. Xu, H. Liang, J. Zhao, Y. Li, *J. Electrochemical Soc.*, **151**, G688 (2004).

CHAPTER 4

MODELING OF COPPER CMP USING THE COLLOIDAL BEHAVIOR OF AN ALUMINA SLURRY WITH COPPER NANOPARTICLES

4.1 Abstract

The measured agglomerate size distributions of alumina abrasives in various slurry chemistries and at different pH values were used in a model to predict material removal rates (MRR). The alumina agglomerate size and distribution were measured both with and without the presence of copper nanoparticles in the solution for each slurry chemistry studied. Although, the agglomerate sizes were measured under quiescent conditions, it is determined that the agglomerated abrasive particles remain intact during CMP, hence the measurements can be used in the CMP model. The model predictions using these measurements both with and without copper in solution were compared to experimental copper CMP data. The model was unable to predict the MRR when the slurry did not have any chemical additives because the dispersion was unstable and small fluctuations in the agglomerate size and distribution caused large changes in the predicted MRR. The model predictions were in excellent agreement with experimental MRR for a slurry with 0.1M glycine in alkaline conditions. The model results from the size distribution measurements with copper in solution agreed slightly more with experiment than those without copper.

4.2 Introduction

Chemical mechanical planarization (CMP) is used in integrated circuit manufacturing to remove excess material and provide a globally planarized wafer

surface. Numerous materials, including copper, tantalum, and various oxides, have been polished with different slurries. As copper has become the interconnect material of choice and a complete investigation of the polishing behavior of this material continues to be important, the focus of our research is copper CMP [1]. Our previous experimental work investigated the effects of common slurry additives on the colloidal behavior of alumina suspensions used for copper CMP [2, 3]. The objective of this study was to incorporate the measured agglomerate size distributions found in typical copper CMP slurries into an existing model of Luo and Dornfeld [4, 5] to predict material removal rates (MRR). These predictions were then compared to our experimental copper CMP data [2].

The main components of the CMP process are the wafer, the pad, the conditioning disk, and the slurry. The slurry provides the chemical and mechanical action on the wafer [6], while the pad provides a medium to carry the chemicals and abrasives across the surface of the wafer [1]. A conditioning disk is rotated across the pad surface to roughen it before and during CMP [1]. For these components there are a number of process variables that will affect MRR. These process variables include wafer and pad velocity, down pressure, pad hardness and roughness, wafer hardness, slurry flowrate, chemical additives, the type and size of abrasive particles, and temperature [1]. Previous work has shown that chemical additives in the slurry can affect the agglomeration and thus, size distributions of the abrasive particles [2, 3, 7, 8]. The agglomeration is also affected by the presence of copper in the slurry, which will be present during a CMP process as the copper is removed from the wafer surface [2, 3]. Various studies of copper CMP have shown that changes in the colloidal behavior of the

abrasive agglomerates can affect the MRR [4, 5, 9-13]. Basim et al. found that control of particle-particle interactions is required to ensure slurry stability and low surface defectivity, while particle-substrate interactions must also be tailored to allow for adequate removal rates [11].

Numerous models of CMP have been proposed with the earliest known as Preston's equation:

$$MRR = K_P \cdot P \cdot v, \qquad [4.1]$$

which gives a linear variation of the removal rate with the applied pressure, P, and linear velocity, v [14]. Preston's constant, K_P, is a proportionality constant that accounts for all other physical considerations. Nanz and Camilletti have presented a comprehensive summary of models for CMP prior to 1994, which for the most part do not account for changes in the colloidal effects or surface forces [14]. More recent models have been developed that account for surface changes due to chemistry [15-17], as well as models that also incorporate the effect of colloidal behavior on CMP [4, 5, 10, 18]. Mazaheri and Ahmadi developed a model to describe the MRR which includes the electrostatic repulsion and attraction between the slurry abrasives and the wafer surface. They found that the MRR is significantly larger when the zeta potentials of the surface and the abrasive have opposite polarity and much smaller when the zeta potentials have the same polarity [10].

4.3 Luo and Dornfeld Model

The model of Luo and Dornfeld is a mechanical model based upon the physical principles of CMP [4, 5]. This model incorporates both particle-particle and particle-

surface interactions of the abrasives and the wafer surface through the average abrasive size, the abrasive size distribution, and the wafer surface hardness, in order to predict the MRR [4, 5]. The simplified model equation for the MRR is given by:

$$MRR = \rho_W NV + C_0 \qquad [4.2]$$

where ρ_W is the density of the wafer, N is the number of active abrasives, V is the volume removed by a single abrasive, and C_0 is the MRR due to chemical etching. The removal due to chemical etching is neglected because it is usually small compared to the overall MRR [4, 5].

The model assumes a solid-solid contact mode (rather than a hydrodynamic mode) and the bulk of the material removal is due to a quasi-static abrasion, or removal from the sliding of the wafer surface over the abrasive particle that is embedded in the pad [4, 5]. In considering the pad-wafer interface, the model assumes that the pad is soft and elastically deforms to the wafer surface, and that the abrasive particles are small so that the pad asperities deform around them. A detailed derivation of the Luo and Dornfeld model can be found elsewhere [4, 5]. The model equation for the MRR based on thickness (nm/min) is given by:

$$MRR = \underbrace{A_1\left(\frac{1}{x_{avg}} + \frac{6\sigma}{x_{avg}^2} + \frac{9\sigma^2}{x_{avg}^3}\right)}_{\text{Thickness Removed}}\underbrace{\left[1 - \Phi\left(3 - A_2\frac{\left(x_{avg} + 3\sigma\right)}{\sigma}\right)\right]}_{\text{Probability of Active Abrasives}} \qquad [4.3]$$

where

$$A_1 = \frac{2\sqrt{2}d_s\rho_s m_{s-a} D_{SUM} al}{\rho_a \pi}\frac{E_P}{\left(b_1 H_W\right)^{\frac{3}{2}}}\sqrt{P_0 v}, \qquad [4.4]$$

and

$$A_2 = \frac{1}{4\pi}\left(\frac{4}{3}\right)^{4/3}\left(\frac{1}{H_P}+\frac{2}{H_W}\right)\left(\frac{E_P}{R}\right)^{2/3}\left(\frac{P_0}{D_{SUM}}\right)^{1/3} \qquad [4.5]$$

where x_{avg} is the average abrasive size, σ is the standard deviation of the abrasive size distribution and the remaining parameters in Eqs. 4.3-4.5 are defined in Table 4.1.

The product of the first two terms of the model equation (Eq. 4.3) represents the thickness removed per unit time while the third term represents the probability of active abrasives. Eq. 4.3 shows that this model has a linear dependence on the velocity, v, while the down pressure, P_0, dependence is much more complicated with a square root dependence in the A_1 term and a dependence to the 1/3 power in the probability density function. The third term in Eq. 4.3 must be less than 0.5 because the model assumes a Gaussian distribution and the active abrasive size, x_{act}, must be greater than the average abrasive size, x_{avg}. This term is then limited according to the following criteria:

$$\frac{x_{avg}}{\sigma} < \frac{3(1-A_2)}{A_2} \quad . \qquad [4.6]$$

In the model when the value of the left side of Eq. 4.6 approaches the value of the right side of this equation the MRR predictions become very large and unreasonable.

The Luo and Dornfeld model has been used very successfully to predict MRR for CMP of SiO_2 under many sets of conditions (various P_0, H_P, etc.) [4, 5]. It has even been used with some success to predict tungsten CMP MRR [4, 5]. However, prediction of copper CMP MRR is much more difficult due to the complexity of the copper system in which chemical effects are more significant than in the SiO_2 system. The goal of our research is to incorporate the chemical effects of the slurry into the Luo

and Dornfeld model. The motivation for further development of this model is to improve the understanding of the copper CMP process and also to provide a tool to predict MRR and compare to experimental data.

An important effect of the slurry chemistry for the copper CMP process is the colloidal properties of the abrasives. Our previous work characterized the colloidal behavior through the measurement of zeta potential and agglomerate size distributions of an α-alumina dispersion as a function of slurry chemistry and also in the presence of copper [3]. It was found that the presence of copper can increase or decrease the agglomeration of alumina depending on the chemical additions and pH of solution [3].

4.4 Review of Gopals' Work

Recently, Gopal and Talbot [19] incorporated measured particle aggregate size distribution data into the model of Luo and Dornfeld to predict the trends of MRR for copper CMP and then compared the predictions to experimental polishing rates from the literature. For slurries containing various concentrations of H_2O_2 and glycine, the model predicted the highest MRR for a solution with 2.0wt % H_2O_2 and 0.1M glycine, which are similar to that observed in the literature that yielded high experimental MRR [20].

In this study, agglomerate size distribution measurements (x_{avg} and σ) will be used in the Luo and Dornfeld model to predict MRR. It is assumed that the pad properties do not change with chemical addition and therefore, the only terms that will be affected by addition of chemical additives to the slurry are x_{avg}, σ, and H_W. However, for the purpose of this study, H_W will be assumed constant using the value for

bulk metallic Cu of 2.3 GPa [21]. Then the Luo and Dornfeld model predictions are compared to our experimental copper MRR data from CMP of silicon wafers sputter deposited with 1 μm copper on 300 Å tantalum using the same slurry chemistries as a function of pH [2]. It should be noted that the experimental copper CMP data used in this study is limited to only one set of polishing conditions. Further comparison of the model to experimental copper CMP data over a wider range of conditions (various P_0, H_P, v, etc.) is needed to better validate this model for the copper CMP process. However, the comparisons in this study provide a better understanding of the copper CMP process. Additionally, future work will incorporate the effect of chemical additives on the wafer surface hardness.

4.5 Experimental

4.5.1 Agglomerate Size Distributions

The procedure for measuring the agglomerate size distribution is described elsewhere [2, 3]. The measurements were performed using alumina (from a 40wt% α-alumina in DI water slurry manufactured by Cabot Corporation) and the concentrations of additives as listed in Table 4.2. The alumina powder is reported to have a primary spherical particle size of 20 nm diameter, but forms globular aggregates with a median aggregate diameter of 150 nm [22]. Table 4.3 lists the agglomerate size and distribution of each of the slurry chemistries that were studied. For the distributions that were bimodal or trimodal, the agglomerate size and distribution is shown for each distribution along with the percentage of the agglomerates in each distribution. Experiments were performed both with and without the presence of copper

nanoparticles (<100 nm in diameter, from Aldrich). A diluted concentration of ~0.05wt% of alumina in the samples was needed to measure the agglomerate size distributions. In order to maintain a similar ratio of copper to alumina as during a typical CMP process, a concentration of 0.12mM Cu was used [2, 3]. The effects of the chemical additives on the agglomerate size and modality are discussed elsewhere, as well as a comparison of with and without copper [3].

4.5.2 Copper Chemical Mechanical Polishing

Polishing experiments were performed on a Toyoda Machine Works, Model SP46, which is a basic rotary CMP machine. An IC1000 circular polishing pad (22 inch diameter) from Rohm and Haas Electronic Materials CMP Inc. was used to polish 100 mm silicon wafers sputter deposited with 1 μm copper on 300 Å tantalum from International Wafer Service Inc. Wafers were weighed using a Sartorius scale (model 1712 MP8) before and after polishing to obtain MRR [2], which had a measurement error of ± 0.5mg. Therefore, the uncertainty for the MRR was calculated as ± 14 nm/min.

For all experiments an α-alumina dispersion (from Cabot Corporation) was used with a dilution ratio of 0.1 [2]. All polishing experiments were performed at 1.0 psi, which was the maximum applied pressure of the polishing machine. The platen rotational speed and the wafer rotational speed were both set at 30 rpm with a 150 ml/min slurry delivery rate. All wafers were polished for 2 minutes (maximum polish time possible due waste restrictions) and then removed from the machine, rinsed with

DI water and dried. Table 4.2 lists the concentration of additives used in the slurry solutions. The pH of the solution was adjusted using KOH or HNO_3.

4.6 Results and Discussion

4.6.1 Forces on Abrasives

The Luo and Dornfeld model assumes that material removal occurs due to the plastic deformation of the wafer surface by a spherical abrasive. In this study the size and standard deviation of the abrasives were measured under quiescent conditions with the addition of chemical additives which typically increase agglomeration. For these measurements to be applicable in the Luo and Dornfeld model, it is assumed that the agglomerated abrasive particles must be strong enough to withstand the shear force of the wafer during CMP, so that they do not break up. Therefore, the shear force, F_S, of the wafer sliding over the agglomerate must be less than the force required to break up the agglomerate, F_B. Figure 4.1 shows the interaction between the wafer, agglomerate, and pad during CMP. The shear force is directly proportional to the normal force, F_N, on the particle and can be calculated using Amonton's law [23, 24]

$$F_S = u_f F_N \qquad [4.7]$$

where μ_f is the coefficient of friction between the wafer surface and the contacting pad asperities tips [23]. The normal force, F_N, is given by the following

$$F_N = P_C A_S \qquad [4.8]$$

where A_S is the surface area of contact between the abrasive and the wafer and is given by

$$A_S = \frac{\pi x_{avg} \Delta_W}{2} \qquad [4.9]$$

and Δ_W is the indentation depth of the abrasive into the wafer which is derived in the Luo and Dornfeld model [4, 5] as

$$\Delta_W = \frac{x_{avg} P_C}{2H_W}. \qquad [4.10]$$

where P_C is the contact pressure as given in the Luo and Dornfeld model as:

$$P_C = \frac{P_0 A_0}{A} = \frac{1}{b_1}\left(\frac{4E_P}{3}\right)^{\frac{2}{3}} P_0^{\frac{1}{3}}. \qquad [4.11]$$

The total contact area between the wafer and the pad, A_0, in Eq. 4.11 is equal to $\pi D^2/4$, where D is the diameter of the wafer [4, 5]. The contact area, A, in Eq. 4.11, between the pad asperities and the wafer surface is given by [4, 5]:

$$A = \pi\left(\frac{3R}{4D_{SUM}}\frac{P_0}{\left(\frac{4E_P}{3}\right)}\right)^{\frac{2}{3}} D_{SUM} A_0 = b_1\left(\frac{P_0}{\left(\frac{4E_P}{3}\right)}\right)^{\frac{2}{3}} A_0 \qquad [4.12]$$

Substituting Eqs. 4.8-4.11 into Eq. 4.7, the shear force on the agglomerate is given by

$$F_S = \frac{\pi}{4}\frac{\mu_f}{H_W} x_{avg}^2 P_C^2. \qquad [4.13]$$

Table 4.1 Values for parameters used in Luo and Dornfeld model (Eq. 4.3) [5].

Parameter	Value
dilution ratio d_s	0.1 [5]
down pressure P_0 (psi)	1
wafer diameter (mm)	100
Young's Modulus for the pad E_P (MPa)	2.3 [5]
number of asperities per unit area of pad D_{SUM} (cm^{-2})	27 [5]
mean asperity area (mm^2)	18500 [5]
asperity height l (mm)	58 [5]
asperity radius R (mm)	6.5 [25, 26]
density ρ_a of abrasive (alumina) (g/cm^3)	3.7 [22]
linear wafer velocity v (m/s)	0.3
hardness H_W of bulk Cu metal (GPa)	2.3 [21]
hardness H_P of IC1000 polishing pad (MPa)	100 [5]
density ρ_s of slurry (g/cm^3)	1.4 [22]
slurry concentration m_{s-a} (%)	40 [22]

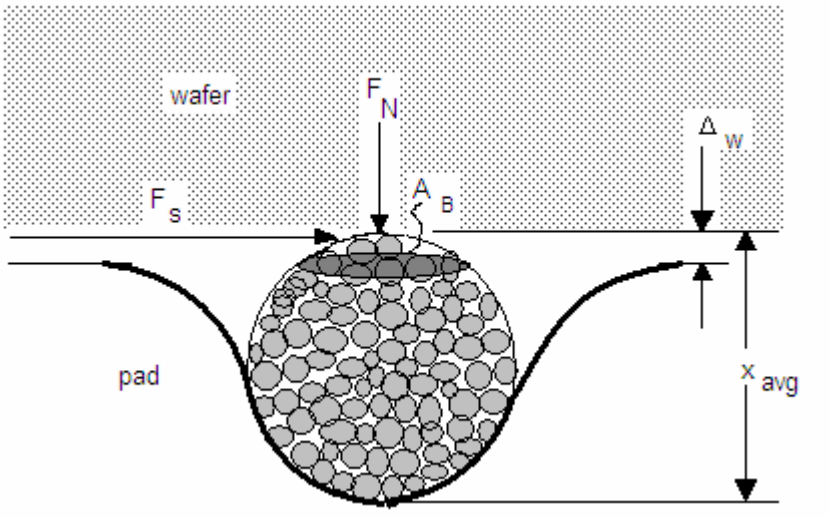

Figure 4.1 Schematic of the wafer/abrasive/pad contact.

Table 4.1 gives the value of each of the parameters used in the model equations, which correspond to the CMP experiments that were performed in this study. The IC1000 pad material has a Young's modulus of E_P~2.3 MPa [5]. Therefore, E* using

Eq. 2.13 was calculated as 3.1 MPa. The number of asperities per unit area of pad, D_{SUM}, is estimated as ~27 cm^{-2}, the mean asperity area, a, is estimated as ~18,500 μm^2, and the asperity height l is ~58 μm [5]. A typical asperity radius R is between 1 and 10 μm and the average asperity radius across the pad can be estimated by the surface roughness of the pad [25], which for a well conditioned IC1000 pad is ~6.5 μm [26].

Table 4.2 Concentration of additives used in the alumina slurry.

a)	1 mM KNO_3
b)	1 mM KNO_3, 0.1 M Glycine
c)	1 mM KNO_3, 0.1 M Glycine, 0.1 wt% H_2O_2
d)	1 mM KNO_3, 0.1 M Glycine, 2.0 wt% H_2O_2
e)	1 mM KNO_3, 0.1 M Glycine, 0.1 wt% H_2O_2, 0.01 wt% BTA, 0.1 mM SDS
f)	1 mM KNO_3, 0.01 M EDTA, 0.1 wt% H_2O_2, 0.01 wt% BTA, 0.1 mM SDS

Table 4.3 Percentage of agglomerates, average agglomerate size, and standard deviation for the multimodal distributions of the alumina in aqueous solution with various additives and at different pH values.

Solutions***		Small Particles			Large Particles			Larger Particles		
	pH	%	Average (nm)	σ (nm)	%	Average (nm)	σ (nm)	%	Average (nm)	σ (nm)
a	2.9	9	66	3	91	192*	12			
	8.3	22	229	24	78	1670*	197			
	11.7	29	141	7	71	381*	23			
a w/ Cu	2.9	48	119	5	52	235*	9			
	8.3	41	270	89	14	1867*	445	45	8417	1114
	11.7	100	3747*	2506						
b	3.1	11	76	3	89	194*	10			
	8.5	36	836	84	52	2223*	242	12	9166	671
	10.0	22	762	49	78	2272*	159			
b w/ Cu	3.1	27	96	4	73	219*	9			
	8.5	39	986	78	61	3746*	319			
	10.0	47	1217	187	53	4761*	820			
c	3.0	2	36	3	98	176*	15			
	8.3	91	1667*	371	9	9300	571			
	10.0	89	1866*	348	11	9217	561			
c w/ Cu	3.0	9	55	3	91	199*	15			
	8.3	70	1432*	97	30	5000	325			
	10.0	5	403	33	95	2382*	241			
d	3.0	9	70	3	91	184*	10			
	8.3	30	732	39	70	2049*	122			
	10.0	75	1574*	142	25	9336	525			
d w/ Cu	3.0	4	52	2	96	167*	11			
	8.3	100	1565**	12						
	10.0	90	1278*	124	10	9247	574			
e	3.0	88	286*	48	12	8830	936			
	8.4	44	1042*	79	56	9222	613			
	10.8	67	959*	103	33	9182	658			
e w/ Cu	3.0	6	113	13	82	341*	74	12	8555	1150
	8.4	67	1148*	94	33	9257	599			
	10.8	47	957*	93	53	9199	651			
f	2.6	9	272	35	44	1330*	279	47	8760	967
	9.0	75	2615*	150	25	9498	398			
	10.9	1	146		99	1516*	178			
f w/ Cu	2.6	33	508*	58	67	8939	844			
	9.0	80	1930*	136	20	9420	481			
	10.9	1	199		88	883*	142	11	8830	981

*Distribution used in Luo and Dornfeld model

**Measured x_{avg} and σ values approach the limit of Eq. 4.6 and are not shown in the MRR prediction in Figures 4.2-4.5

***As listed in Table 4.1, solution with copper contains 0.12 mM copper nanoparticles

For a thin film of copper on a silicon wafer the hardness, H_W, is estimated as ~2.3 GPa [21]. This hardness value is approximately the value of bulk copper, but with the addition of chemical additives to the slurry this value could vary significantly from 0.4 to 2.4 GPa as measured by Jindal and Babu [27]. However, for the purposes of this study the hardness is assumed constant with a value of 2.3 GPa [21]; future work will

measure the chemical effects on nanohardness of copper which will then be used in the model.

The coefficient of friction, μ_f, is dependent upon the relative velocity, v, of the wafer and the pad. When using a rotational type of CMP machine, the platen and the wafer rotate at speeds of Ω_p and Ω_w, respectively. If an effective wafer rotation speed is defined as $\omega = \Omega_p - \Omega_w$ and an effective belt speed is defined as $v = \Omega_p \cdot e$, where e is the offset between the center of the platen and the center of the wafer, the velocity distribution can be compared to a linear machine, which typically has a belt that moves in one direction while the wafer rotates on top [5]. For the CMP experiments of this study, the head and platen speed were both set at 30 rpm and the center offset was ~10 cm. The effective wafer rotation speed is $\omega = 0$, and the effective belt speed is v~0.3 m/s. The coefficient of friction at this relative velocity is estimated as μ_f~0.56 [23]. The contact pressure was calculated from Eq. 4.11 as P_C~6.9 MPa. For an agglomerate size of x_{avg}= 200 nm, the shear force from Eq. 4.13 is F_S~3.6x10^{-10} N.

The force required to break up an agglomerate, F_B, can be calculated using the following equation which was developed to determine the shear strength of a powder [28]:

$$F_B = \mu_S (P_C + C_S) A_B \qquad [4.14]$$

where μ_s is the static coefficient of friction between alumina particles, μ_s~0.68 [28], P_C is the contact pressure (Eq. 4.11), C_S is the cohesive strength of the agglomerate, and A_B is the cross-sectional breaking plane where the particles in the agglomerate would break due to shear sliding [28]. When a powder is just about to slide across a surface plane,

the magnitude of the cohesive and frictional properties of the particles, the manner in which they are assembled, and the prior history of the powder taken together, determine the relationship between the compressive stress, P_C, which presses two powder layers together and the shear strength, F_B, developed on that surface [28]. An estimation for the cohesive strength, C_S (MPa), of an agglomerate filled with a liquid was developed by Rumpf [29]:

$$C_S = a' \frac{(1-\varepsilon)}{\varepsilon} \frac{\alpha}{d_p} \qquad [4.15]$$

where a' is a correction factor and has values between 6-8 [29], ε is the porosity of the agglomerate, which for random loose packing of spheres can be estimated as ε~0.399 [30], α is the surface tension of the liquid, which for water is α = 72 dyn/cm [31], and d_p is the primary particle diameter, which is d_p = 20 nm for this study [22]. The Rumpf model (Eq. 4.15) assumes the agglomerate is fully saturated by liquid and the particles are spherical and monosized [29]. This model was originally verified using agglomerates with primary particle sizes >10 μm. However, recent work by Gopalkrishnan et al. has shown that the Rumpf model is applicable for agglomerates with primary particle diameters between 8-120 nm [32]. The cohesive strength of the agglomerates, C_S, was calculated as 32.5 MPa using the smallest correction factor value of 6. The breaking plane of the agglomerate, A_B, is equivalent to the projected area of contact between the wafer and the abrasive as given in the Luo and Dornfeld model [5] as

$$A_B = \frac{\pi x_{avg}^2 P_C}{2H_W}. \qquad [4.16]$$

Substitution of Eq. 4.16 into Eq. 4.14 gives the required force to break up the agglomerates as

$$F_B = \frac{\pi \mu_S x_{avg}^2}{2H_W} P_C \left(P_C + C_S\right). \quad [4.17]$$

For an agglomerate with x_{avg} = 200 nm, P_C = 6.9 MPa, H_W = 2.3 GPa, and C_S = 32.5 MPa, F_B = 5.0 x 10^{-9} N, which is an order of magnitude larger than F_S and indicates that the agglomerates will not break up due to contact pressure during CMP. A comparison of Eq. 4.13 for F_B versus Eq. 4.17 for F_S shows that F_B would always be larger than F_S as long as the following criteria is meet:

$$\frac{C_S}{P_C} > \frac{\mu_f}{2\mu_S} - 1. \quad [4.18]$$

The left side of Eq. 4.18 is always positive unless the cohesive strength between the particles is zero, in which case the left side of Eq. 4.18 will be zero. However, the coefficients of friction, μ_f and μ_s, are constant in this study and the right side of Eq. 4.18 is a negative value and will always be less than the left side of Eq. 4.18.

In this study the percent pad contact area (A/A_0*100) calculated from the Luo and Dornfeld model is ~0.1%. However, several researchers [11, 33] have shown that the Luo and Dornfeld model underestimates the actual pad contact area, A, which will significantly influence the force exerted on the asperities and the abrasives. Elmufdi and Muldowney optically measured the pad contact area of an IC1000 pad at 1 psi and found it to be ~0.3% [33]. Basim et al. also found the percent contact area of the IC1000 pad to be between 0.25 and 0.54% for down pressure between 1 and 7 psi [11]. Recalculation of the contact pressure, P_C, assuming a 0.3% pad contact area, gives a

value of ~2.3 MPa. Using P_C = 2.3 MPa to recalculate the shear force on the abrasive and the required force to break up the agglomerate gives values of F_S~4.0 x 10^{-11} N and F_B~1.5 x 10^{-9} N, respectively, which also indicates that the agglomerates would not break up during CMP.

Furthermore, an experiment was performed to test the strength of the alumina agglomerates formed in this study. Our previous work measured agglomeration as a function of time after 5 minutes of ultrasonication [3]. It was found that for pH values near the IEP (pH ~7-9), the average agglomerate size increased with time until the agglomerates became very large (>5μm) and began to settle. This occurs within 2 hours after ultrasonication. For pH values outside of this range the agglomerate size reached a steady state value within 5 minutes of ultrasonication. At pH 11.7 the steady state average agglomerate size was measured as 260 nm. To test the strength of the agglomerates, an experiment was performed where the solution pH was adjusted near the IEP (pH 8.3) and the abrasives were allowed to aggregate for 5 minutes. The solution was then raised to pH 11.7, ultrasonicated for 5 minutes and the average agglomerate size was measured as 1.40 μm. The solution was ultrasonicated again for 5 minutes, and the average agglomerate size was remeasured as 1.38 μm. The steady state average agglomerate size of 260 nm at pH 11.7, was much less than the agglomerate size measured after the particles were allowed to aggregate, indicating that ultrasonication is not strong enough to break the agglomerates apart once they are formed. The force that ultrasonication exerts on the agglomerates can be calculated using an equation developed by Zimon [34]

$$F_U = \frac{2\pi^3}{3}\rho_a d^3 \upsilon^2 y \qquad [4.19]$$

where ρ_a is the abrasive density ~3.7 g/cm^3 [22], d is the diameter of the agglomerate ~1.4 μm in this experiment, ν is the vibration frequency, 40 kHz [35], and y is the vibration amplitude, ~120 μm [36]. For the 1.40 μm agglomerates in the experiment, the force during ultrasonication is F_U~4.0 x 10^{-8} N, which is larger than F_S calculated from Eq. 4.13 as 1.8 x 10^{-8} N during CMP. This experiment further indicates that the agglomerated abrasives are strong enough to sustain the shear force exerted during CMP.

The Luo and Dornfeld model assumes that the pad is soft, so that the pad asperities deform around the abrasives and the abrasives are small compared to the pad asperities. The pad asperities are on the order of 10 μm in diameter [26], so the agglomerates must be significantly less than this for the model. An agglomerate that is so large that the pad asperity cannot deform completely around it may have much different shear forces acting on it than those calculated in this paper. From the experiment using ultrasonication to test the strength of the agglomerates, it was shown that agglomerates up to ~1.4 μm will not break up during CMP. However, Table 4.3 shows that there are agglomerates much larger than 1.4 μm. The hydrodynamic shear of the fluid can be used to determine the maximum agglomerate size, D_{max}, that is stable in the fluid during CMP as follows:

$$D_{\max} = 2r\left(\frac{H}{18\pi\pi r\delta^2}\right)^{\frac{1}{2}} \qquad [4.20]$$

where H is the Hamaker constant, r is the primary particle radius, τ is the shear stress, and δ is the separation distance of the particles in the primary medium [37]. This equation was developed by balancing the van der Waals force between two particles with the hydrodynamic force acting to separate two particles [37]. The expression gives D_{max} as a function of the shear stress and the primary particle radius. For an aqueous alumina suspension it was assumed that $H = 4.17 \times 10^{-20}$ J [38], and $\delta = 0.4$ nm [39] with $r = 10$ nm for the Cabot alumina dispersion [22]. The Reynold's number for this system was calculated to be ~25, therefore, it is assumed that the flow is laminar. The shear stress, τ, is given by the following equation:

$$\tau = -\mu \frac{\partial v_x}{\partial y} = \mu \frac{v}{h} \qquad [4.21]$$

where μ is the slurry viscosity and h is the slurry film thickness. For the CMP experiments performed, the estimated values of $h = 160$ μm and μ=0.001 Pa·s [40] were used to calculate the shear stress in the slurry as approximately 2.1 Pa, which is consistent with the literature [40].

The maximum aggregate size, D_{max}, was calculated as ~4.8 μm for the conditions of the CMP experiments performed in this study. This means that alumina agglomerates that are greater than 4.8 μm will break up during CMP by the shear force of the fluid. Therefore, the distributions that had an average agglomerate size greater than 4.8 μm were not used to calculate the MRR.

4.6.2 Comparison of Model Predictions to Experimental MRR

The Luo and Dornfeld model requires the average agglomerate size, x_{avg}, and the standard deviation of the agglomerate size distribution, σ, to determine the MRR. The size and distribution of the alumina agglomerates under certain conditions were observed to be unimodal, bimodal, and sometimes trimodal [2, 3, 7, 8]. For the experiments that had multimodal distributions the agglomerate size and distribution used to predict the MRR was from the larger distribution, and it was assumed that the smaller agglomerates were inactive. However, if this size was greater than D_{max}, the smaller distribution was used and it was assumed that the agglomerates from the larger distribution would break up during CMP into agglomerates of similar size and distribution as the smaller distribution. One of the measured x_{avg} and σ values listed in Table 4.3 approaches the limit of Eq. 4.6 which causes the model to predict unreasonably high MRR and was not used.

Using Eq. 4.3 the MRR were calculated with the parameters in Table 4.1. Using these parameters the value for A_1 from Eq. 4 is 9.11 x 10^6 nm^2/min and the value for A_2 from Eq. 5 is 0.019. It is assumed that A_1 and A_2 remain constant with the addition of chemical additives to the slurry.

Figure 4.2 compares the experimental MRR with the predictions using the Luo and Dornfeld model for the alumina slurry with no chemical additives both with and without copper nanoparticles present. The MRR for this slurry without any additives was very low, less than 4 nm/min, for the three pH values (2.9, 8.3, 11.7) measured. These low MRR values may be due to only mechanical abrasion occurring. According to the potential-pH diagram for the copper-water system [41] at pH 2.9 copper may

exist as soluble ions in the form of Cu^{2+}, Cu^{+}, or as metal. At pH 8.3 and 11.7 the copper should exist as an oxide in the form of CuO or Cu_2O, hydroxide $Cu(OH)_2$, or as metallic Cu. As the MRR is similarly low at all three pH values, it may be then concluded that the copper is metallic Cu. However, some researchers believe that a very thin layer of the copper film may not follow the potential-pH equilibria. Feng et al. suggest that a layer of Cu_2O exists on the copper surface at all pH ranges in the copper-water system and as the pH increases the compactness of the oxide layer increases [42]. This is consistent with our experimental MRR in that Cu_2O is known to be harder than Cu metal, which would give a lower MRR [42]. Our experimental MRR were obtained with a relatively low down pressure (1 psi) and even a very thin layer of the Cu_2O at the low pH value may have been impenetrable by the alumina abrasives. However, the Luo and Dornfeld model is unable to predict this low MRR because it is very sensitive to the particle size and standard deviation [5, 7, 8]. Without the presence of copper, the MRR predictions ranged from 27 to 276 nm/min depending on pH. With the presence of copper the MRR predictions were higher with a range from 30 to 344 nm/min. It was previously shown that the addition of a complexing agent, such as glycine, to the slurry stabilizes the zeta potential and agglomerate size measurements giving better reproducibility [7]. Without the addition of a complexing agent in the slurry the measurements are more difficult to reproduce and therefore may not represent the agglomerate size distribution of the slurry used for the copper CMP experiments. Because the model is sensitive to these measurements it is unable to predict the MRR if the suspension is not stable.

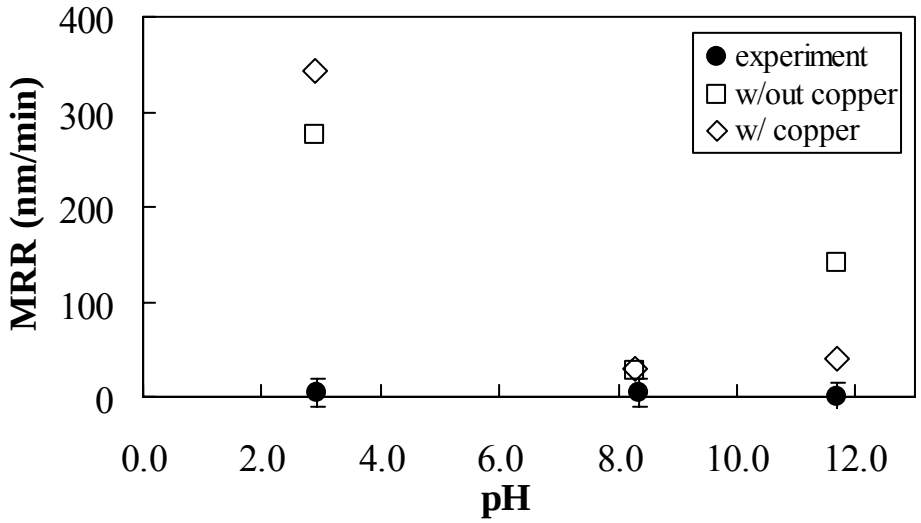

Figure 4.2 Comparison of experimental (closed circle) and model predictions (open symbols) of MRR versus pH for alumina slurry without chemical additives both without and with copper nanoparticles.

Figure 4.3 compares the experimental MRR with the predictions for the alumina slurry with the addition of 0.1 M glycine both with and without copper nanoparticles. The experimental MRR values for this system are low at 2, 9 and 15 nm/min for pH values 3.1, 8.5, and 10.0, respectively. According to the potential-pH diagram constructed by Tamilimani et al. for the copper-water-glycine system with 0.1M glycine and a copper ion activity of 10^{-6} [43], at pH 3.1 the copper may exist as either a dissolved ion in the form of a copper-glycinate complex, $Cu(H_3NCH_2COO)^{2+}$, or as Cu metal. Because the experimental MRR is very small at this pH, most likely there is very little dissolution of the copper surface to form the copper-glycinate complex, and the surface is in the form of Cu metal. At pH 8.5 and 10.0 the copper may exist as a soluble copper-glycinate complex that is neutrally charged, $Cu(NH_2CH_2COO)_2$, or as Cu metal [43]. As the pH of the solution increases, more of the copper surface may form the soluble copper-glycinate species, which may be the reason for the MRR to increase

slightly as the pH increases. The model predictions both without and with copper at pH 3.1 are 314 and 320 nm/min, respectively, which is much higher than the experimental MRR of 2 ± 14 nm/min. This may be due to the use of a constant surface hardness for all pH values. Small increases in the surface hardness of the copper would significantly affect the MRR predictions, which may be an explanation for the predictions being too high for pH 3.1. For pH values 8.5 and 10.0 the predictions for this system agree much better with the experimental data. Without copper the model predicts an MRR of 20 and 22 nm/min at pH values 8.5 and 10.0, respectively. With copper the model predicts an MRR of 12 and 10 nm/min at pH values 8.5 and 10.0, respectively. Figure 4.3 shows that with the addition of glycine to the slurry the MRR is slightly better predicted using the particle size and distribution measurements of the alumina in the presence of copper than without copper.

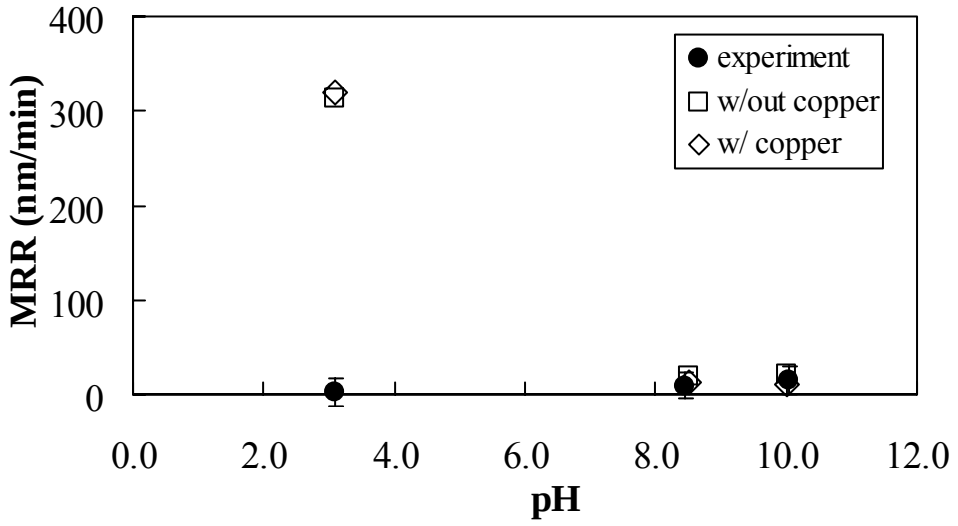

Figure 4.3 Comparison of experimental (closed circle) and model predictions (open symbols) of MRR versus pH for alumina slurry with 0.1M glycine both without and with copper nanoparticles.

Figure 4.4a shows the MRR for the alumina slurry with the addition of 0.1M glycine and 0.1wt% H_2O_2 both with and without copper nanoparticles. At pH 3.0 the experimental MRR was 8 ± 14 nm/min, while the predicted MRR without copper is 262 nm/min and the predicted MRR with copper is 244 nm/min. Again, the high predictions may be due to an incorrect surface hardness value at this pH. The potential-pH equilibria for this system is similar to that of the copper-water-glycine system with the addition of H_2O_2 increasing the redox potential which would cause the copper to more likely form the soluble copper-glycinate complex [43]. This is consistent with the experimental MRR for pH values 8.3 and 10.1 which were much higher, 290 and 350 ± 14 nm/min, than the copper-water-glycine system without H_2O_2. However, the model fails to predict this increase in MRR as the pH increases. The MRR predictions both without and with copper are similar and remain fairly constant for pH values 8.3 and 10.1, which may be due to the surface hardness value remaining constant. It is possible that the formation of the copper-glycinate species may cause a softening of the copper surface that is much more easily removed and dissolved than the metallic Cu surface. However, Figure 4.4a shows that the Luo and Dornfeld model fails to predict the MRR for all pH values in this slurry system.

Figure 4.4b shows the MRR for the alumina slurry with 0.1M glycine and 2.0 wt% H_2O_2 both with and without copper nanoparticles. The experimental MRR ranges from 110 to 290 nm/min. The increase in the experimental MRR for this system with 2.0wt% H_2O_2 compared to the copper-water-glycine system without H_2O_2 may be due to an increase in the dissolution rate of the copper surface and/or a softening of the copper surface due to the formation of different surface species. As stated for Fig. 4.4a,

potential-pH equilibria for this system are the same as the copper-water-glycine system [43] with the H_2O_2 causing an increase in the formation of the soluble copper-glycinate complexes and also increasing the surface oxidation of the copper [43]. Again, as in Fig. 4.4a, for all predictions both with and without copper the model fails to predict the experimental MRR. The predictions without the presence of copper range from 26 to 313 nm/min and do not show the same behavior with pH as the experimental MRR. The model prediction with the presence of copper is outside of the limit of Eq. 4.6 at pH 8.3. At pH 3.0 and 10.0 the MRR predictions with copper are 303 and 35 nm/min, respectively. The failure of the Luo and Dornfeld model to predict the results in this case may be due to the unaccounted changes in the copper film hardness with pH. The model also assumes the material removal due to chemical etching is negligible, but this assumption may not be valid for this slurry chemistry.

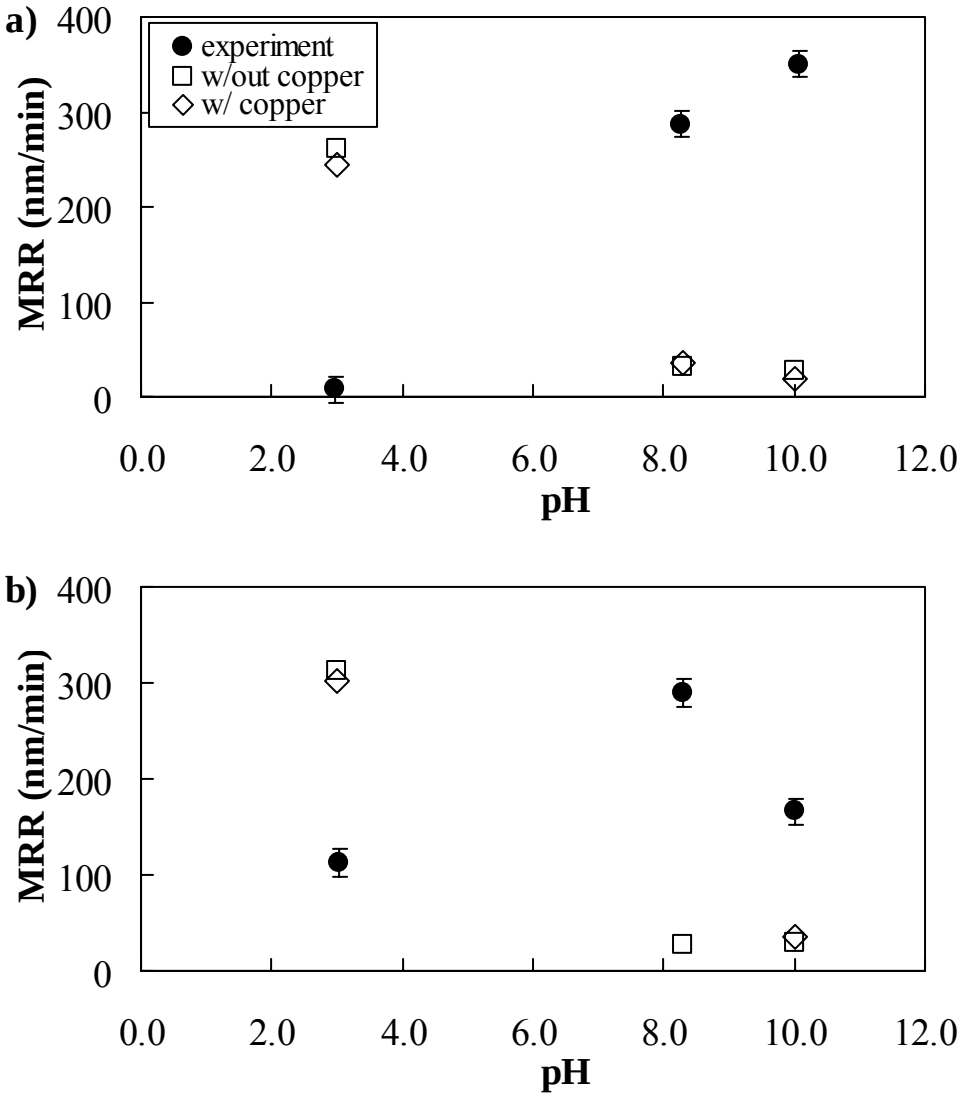

Figure 4.4 Comparison of experimental (closed circle) and model predictions (open symbols) of MRR versus pH for alumina slurry with 0.1M glycine and a) 0.1wt% H_2O_2 or b) 2.0wt% H_2O_2, both without and with copper nanoparticles.

Figure 4.5a compares the experimental MRR to the predictions for the alumina dispersion with the addition of 0.1M glycine, 0.01wt% BTA, 0.001M SDS, and 0.1wt% H_2O_2 both with and without copper nanoparticles. The experimental MRR values were low, 0 and 11 nm/min, at pH values 3.0 and 8.4, respectively, and much higher, 242

nm/min, at pH 10.8. In this slurry system, BTA is a corrosion inhibitor which can bind to the copper surface and prevent dissolution. SDS is a surfactant which will affect the alumina agglomeration and distribution, but it should not affect the copper surface. H_2O_2 will increase the formation of soluble complexes as well as increase surface oxidation [43]. According to the potential-pH diagrams for the copper-water-glycine system and the copper-water-BTA system, at pH 3.0 the copper may exist as Cu metal, or dissolve into solution as either Cu^{2+} or a copper-glycinate complex [43]. The experimental MRR is zero (± 14 nm/min), which indicates that the surface is not dissolving and is most likely metallic Cu. At pH 8.4 the copper may exist as a solid in the form of CuO, CuBTA, or Cu metal, or dissolve into solution as a copper-glycinate complex. The MRR is slightly higher at pH 8.4, 11 ± 14 nm/min, which means there could be an increase in the copper surface dissolution or the surface may be softer if in a different form than at the lower pH. At pH 10.8 the potential-pH diagrams show that the copper will exist as a solid in the form of CuO, Cu_2O, $Cu(OH)_2$ or Cu metal, or it will dissolve into solution as a copper-glycinate complex [43]. The experimental MRR at pH 10.8 is much higher, 242 nm/min, than at the lower pH values and this may be due to an increased dissolution rate or a softer surface hardness due to the formation of a different surface structure. Figure 4.5a shows that the Luo and Dornfeld model fails to predict the MRR for all pH values in this slurry system. Without the presence of copper in the slurry the model predicts MRR values ranging from 46 to 166 nm/min for all pH values, which is inconsistent with the experimental MRR. The addition of copper to the slurry did not have much of an effect on the MRR predictions which ranged from 41 to 155 nm/min.

Figure 4.5b compares the experimental MRR to the predictions for the alumina slurry with 0.01M EDTA, 0.01wt% BTA, 0.001M SDS, and 0.1wt% H_2O_2 both with and without copper nanoparticles. At pH 2.6 the experimental MRR is 2 ± 14 nm/min. In this slurry system the EDTA behaves similarly to glycine, in that it forms soluble complexes with copper in certain pH ranges. According to the potential-pH diagram for the copper-water-ethylendiamine system [44] at pH 2.6 the copper may exist as Cu^{2+} or as Cu metal and the potential-pH diagram for the copper-water-BTA [43] system shows that copper should be in the form of either Cu^{2+} or Cu metal. Because the MRR is so low at this pH there is probably very little dissolution and the copper is in the form of Cu metal in the slurry and on the wafer surface. At pH 9.0 the potential-pH diagrams [43, 44] show that the copper may exist as either solids in the form of CuO, CuBTA, or Cu metal, or the copper will dissolve into solution as a copper-EDTA complex. Because the MRR at this pH was also low, 9 ± 14 nm/min, it is believed that the copper is in the form of one of the solids and does not dissolve into solution. Similarly, at pH 10.9 the potential-pH diagrams show copper may exist as a solid in the form of CuO, Cu_2O or Cu metal, or dissolved into solution as a copper-EDTA complex. The MRR at pH 10.9 was 8 ± 14 nm/min, which is approximately the same as the MRR at pH 9.0 and indicates that the copper surfaces may be similar. This means that the surface may be either CuO, $Cu(OH)_2$ or Cu metal. At pH 2.6 the model predicts 39 nm/min without copper, while the prediction with copper is higher, 88 nm/min. The predictions at pH 9.0 were fairly close to experimental MRR both without and with copper, 21 and 26 nm/min, respectively. At pH 10.9 the prediction without copper, 29 nm/min, was closer to experiment than the prediction with copper, 53 nm/min.

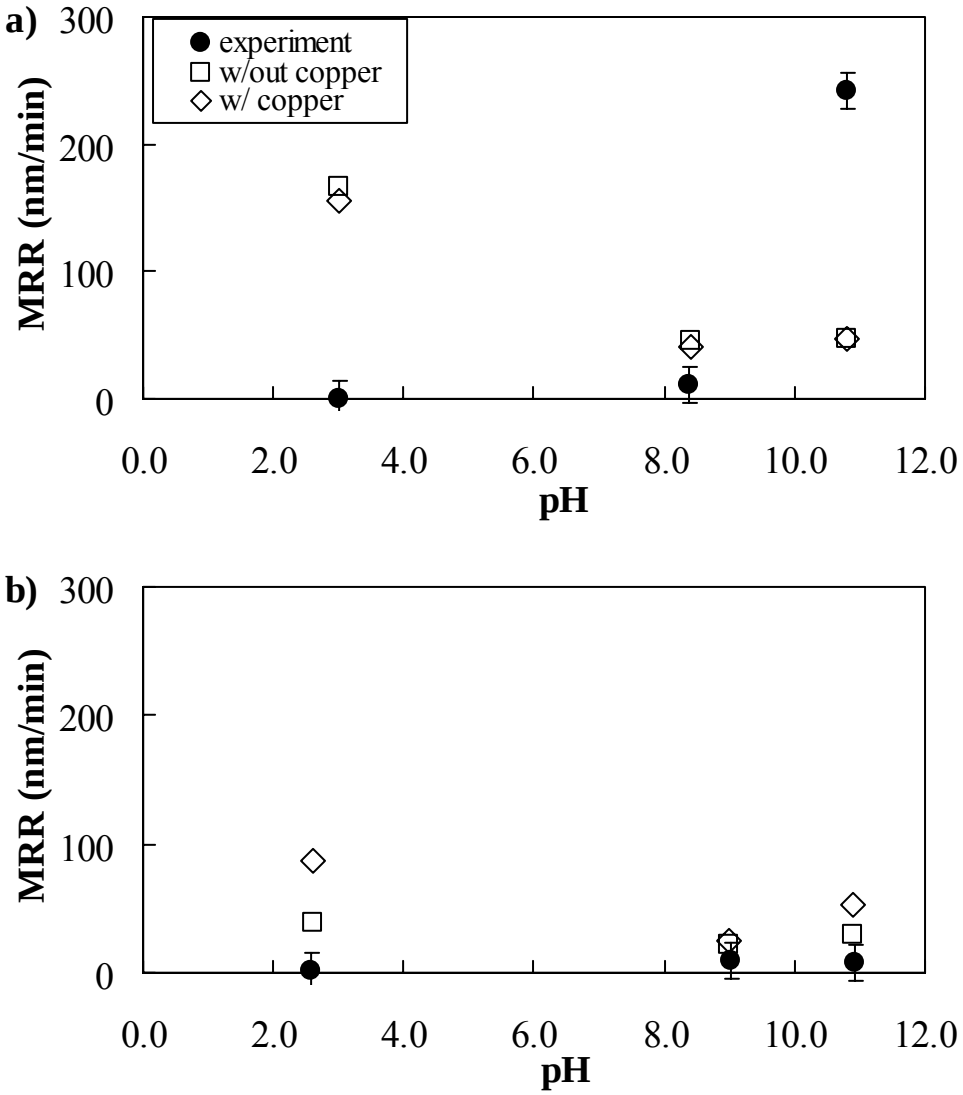

Figure 4.5 Comparison of experimental (closed circle) and model predictions (open symbols) of MRR versus pH for alumina slurry with 0.01wt% BTA, 0.001M SDS, 0.1wt% H_2O_2, and a) 0.1M glycine or b) 0.01M EDTA, both without and with copper nanoparticles.

Figures 4.2-4.5 show that the Luo and Dornfeld model was unable to predict the experimental MRR for several conditions. There are several reasons that may have caused the model to fail. One reason most likely is the constant copper surface hardness used instead of values which change with slurry chemistry. It is well known that copper

oxides/hydroxides may have a different surface hardness (~0.4-2.4 GPa) [27] than bulk Cu metal (2.3 GPa) [21], and changes in pH can affect the compactness of the copper surface leading to changes in the surface hardness [27]. Also, the wafers used in this study had an underlying tantalum layer (bulk hardness~1.5-4.5 GPa [27]) which may affect the copper surface hardness depending on the thickness of the remaining copper layer after chemical etching [45].

Another reason for the model failure is that the model neglects material removal due to chemical etching which may not necessarily be valid for some of the chemistries studied. Additionally, to explain the results of the experiments in this study, the potential-pH diagrams for copper in each of the chemistries from the literature [41, 43, 44, 46] were used. It should be noted that these diagrams only provide information on the thermodynamic equilibrium of the system [46] and kinetics of the reactions was not considered.

4.7 Conclusions

The Luo and Dornfeld model has been used very successfully to predict MRR for SiO_2 CMP. However, this is the first time this model has been applied to the copper CMP process to directly compare with experimental CMP data. Previous studies of the Luo and Dornfeld model have either neglected agglomeration of the abrasives by assuming the shear force on the abrasives was large enough to break apart the agglomerates [4, 5] (x_{avg} is equal to the primary particle diameter), or have assumed the shear force was small so that measured agglomerate sizes could be used [19]. In this study, a method was developed to determine the shear force on the abrasives during

CMP which is compared to the force required to break apart the agglomerates. For the CMP conditions of this study, it was found that the agglomerated abrasive particles do not break apart during CMP, hence the agglomerate size measurements can be used in the CMP model.

The comparisons between experimental MRR and the Luo and Dornfeld model MRR predictions show that the model only agrees under certain conditions. When there is no complexing agent in the slurry and the slurry suspension is unstable and difficult to reproduce, the model is unable to predict the MRR. Small discrepancies in the measured agglomerate distribution may cause large differences in the predicted MRR. When a complexing agent such as glycine is added to stabilize the slurry, the model predictions are in better agreement with the experimental MRR. It was shown that for the slurry containing 0.1M glycine the model predictions using the measured agglomerate size and distribution of the alumina in the presence of copper were closer to the experimental MRR than the measurements done without copper. However, for most of the other slurry systems the model predictions using the measured agglomerate size and distribution of the alumina in the presence of copper were fairly similar to the predictions made using the measurements without copper.

While the results of this study show that the Luo and Dornfeld model was unable to predict the experimental MRR for many cases, there are several reasons that may have caused the model to fail. The model predictions in this study used a constant copper surface hardness, that of bulk Cu metal, for all chemistries at all pH values. In our current research the nanohardness of the copper surface after exposure to the slurry chemicals is being measured. The incorporation of this measured hardness into the

model improves the agreement between the predictions and experimental MRR and will be discussed in a future publication. The Luo and Dornfeld model also neglects material removal due to chemical etching. Investigation of the copper etch rates during exposure to these slurries is being studied to understand the material removal mechanism. The dissolution rate of the copper surface may be significant under some conditions and will also be included in the model in a future work. Additionally, there was a case where the Luo and Dornfeld model prediction was invalid because the measured x_{avg} and σ values were close to or outside of the limit of Eq. 4.6. This caused the predicted MRR to be unreasonably high because the calculated value for the probability of active abrasives is too large. Future improvement of the model will limit the probability of active abrasives to a physically reasonable range.

4.8 Acknowledgements

This work was sponsored by FLCC Consortium through a UC Discovery grant. The authors gratefully acknowledge all the companies involved in the UC Discovery grant: Advanced Micro Devices, Applied Materials, ASML, Atmel Corporation, Cadence, Canon, Cymer, Cypress, Dupont, Ebara Technologies Inc., Hitachi Global Storage Technologies, Intel Corporation, KLA-Tencor, Mentor Graphics, Nikon Research Corporation of America, Novellus Systems Inc., Panoramic Technology, Photronics, Synopsys, and TEL USA, Additionally, the collaboration of Professors Dornfeld and Doyle and their research groups from the University of California, Berkeley is greatly appreciated.

This chapter is a reprint of the material as it appears in the Journal of the Electrochemical Society, Robin Ihnfeldt and Jan B. Talbot, Vol. 154, Issue 12, pg. H1018 (2007), with some additional information. The dissertation author was the primary investigator and author of this paper.

REFERENCES

1. M. R. Oliver, *Chemical-Mechanical Planarization of Semiconductor Material*, Springer-Verlag, Berlin, Germany (2004).

2. R. Ihnfeldt, Masters Thesis, University of California, San Diego (2005).

3. R. Ihnfeldt and J. B. Talbot, *J. Electrochemical Soc.*, **153**, G948 (2006).

4. J. Luo and D. Dornfeld, *IEEE Trans. Semi. Manuf.*, **14**, 112 (2001).

5. J. Luo and D. Dornfeld, *Integrated Modeling of Chemical Mechanical Planarization (CMP) for Integrated Circuit Fabrication: from Particle Scale to Feature, Die and Wafer Scales*, Report, University of California, Berkeley (October 2003).

6. T. Dellin, C. Henderson, M. Strizich, and D. Barton, *21st Century Semiconductor Technology Handbook*, Training Solutions Inc. Albuquerque, New Mexico (2001).

7. T. Gopal, PhD Thesis, University of California, San Diego (2004).

8. T. Gopal and J. B. Talbot, *J. Electrochemical Soc.*, 153, G622 (2006).

9. Z. Li, K. Ina, P. Lefevre, I. Koshiyama, and A. Philipossian, *J. Electrochemical Soc.*, **152** (4), G299 (2005).

10. A. R. Mazaheri and G. Ahmadi, *J. Electrochemical Soc.*, **150** (4), G233 (2003).

11. G. B. Basim, I. U. Vakarelski, and B. M. Moudgil, *J. Colloid and Interface Sci.*, **263,** 506 (2003).

12. K. Osseo-Asare, *J. Electrochemical Soc.*, **149** (12), G651 (2002).

13. G. B. Basim and B. M. Moudgil, *J. Colloid and Interface Sci.*, **256**, 137 (2002).

14. G. Nanz and L. E. Camilletti, *IEEE Trans. on Semicond. Manuf.*, **8**, 4 (1995).

15. E. Paul, F. Kaufman, V. Brusic, J. Zhang, F. Sun, and R. Vacassy, *J. Electrochemical Soc.*, **152** (4), G322 (2005).

16. L. Zhang and R. S. Subramanian, *Thin Solid Films*, **397,** 143 (2001).

17. D. G. Thakurta, D. W. Schwendeman, R. J. Gutmann, S. Shankar, L. Jiang, and W. N. Gill, *Thin Solid Films*, **414**, 78 (2002).

18. P. H. Chen, B. W. Huang, and H. Shih, *Thin Solid Films*, **476**, 130 (2005).

19. T. Gopal and J. B. Talbot, *J. Electrochemical Soc.*, **154 (6)**, H507-H511 (2007).

20. S. Seal, S. C. Kuiry, and B. Heinmen, *Thin Solid Films*, **423**, 243 (2003).

21. S. Chang, T. Chang, and Y. Lee, *J. Electrochemical Soc.*, **152** (10), C657 (2005).

22. http://w1.cabotcorp.com/controller.jsp.?N=23+4294967128+3033&entry=product (accessed June 2006).

23. J. Seok, C.P. Sukam, A.T. Kim, J.A. Tichy, and T.S. Cale, *Wear*, **257**, 496 (2004).

24. S. Tsai, L. Chen, L. Sun, R. Mavliev, W. Hsu, L. Xia, and R. Morad, *IEEE*, **7803**, 7216 (2002).

25. J. Seok, C.P. Sukam, A.T. Kim, J.A. Tichy, and T.S. Cale, *Wear*, **254**, 307 (2003).

26. H. Lu, B. Fookes, Y. Obeng, S. Machinski, and K.A. Richardson, *Materials Characterization*, **49**, 35 (2002).

27. A. Jindal and S. V. Babu, *J. Electrochemical Soc.*, **151** (10), G709 (2004).

28. R. L. Brown and J. C. Richards, *Principles of Powder Mechanics*, Pergamon Press, Elmsford, New York (1970).

29. W. Pietsch, *Agglomeration Proc.*, Wiley-VCH Verlag GmbH, Weinheim (2002).

30. J. K. Beddow and T. P. Meloy, *Advanced Particulate Morphology*, CRC Press, Boca Raton, Florida (1980).

31. N. R. Pallas and Y. Harrison, *Colloids and Surfaces*, **43**, 169 (1990).

32. P. Gopalkrishnan, I. Manas-Zloczower, and D. L. Feke, *Chem. Eng. Sci.*, **62**, 3740 (2007).

33. C. Elmufdi and G. Muldowney, *Mater. Res. Soc. Symp. Proc.*, **914**, F12 (2006).

34. A. D. Zimon, *Adhesion of Dust and Powder*, 2nd ed. Consultants Bureau, Plenum Publishing, New York, 1982.

35. Branson Ultrasonics Corp., Ultrasonic Cleaners Operator's Manual, Danbury, CT (2007).

36. M. Shane, PhD Thesis, University of California, San Diego (1994).

37. M. Elimelech, J. Gregory, X. Jia, and R. Williams, *Particle Deposition and Aggregation*, Butterworth-Heinemann, Oxford, Great Britian (1995).

38. I. D. Morrison and S. Ross, *Colloidal Dispersions: Suspensions, Emulsions, and Foams,* Wiley-Interscience, New York (2002).

39. M. A. Hubbe, *Colloids and Surfaces*, **25**, 311 (1987).

40. C. Cho, S. Park, and Y. Ahn, *Thin Solid Films*, **389**, 254 (2001).

41. M. Pourbaix, *Atlas of Electrochemical Equilibria in Aqueous Solutions*, National Association of Corrosion Engineers, Houston, Texas (1974).

42. Y. Feng, K. Siow, W. Teo, K. Tan, and A. Hsieh, *Corrosion,* **53**, 389, (1997).

43. S. Tamilmani, W. Huang, S. Raghaven, and R. Small, *J. Electrochemical Soc.*, **149** (12), G638 (2002).

44. S. Aksu and F. M. Doyle, *J. Electrochemical Soc.*, **149** (7), B340 (2002).

45. N. Ye and K. Komvopoulos, *J. Tribology*, **125** 685 (2003).

46. S. Aksu and F. M. Doyle, *J. Electrochemical Soc.*, **148** (1), B51 (2001).

CHAPTER 5

EFFECT OF CMP SLURRY CHEMISTRY ON COPPER NANOHARDNESS

5.1 Abstract

Nanohardness and etch rates of copper films sputter-deposited onto a 30 nm tantalum coating on silicon wafers were measured after exposure to aqueous solutions containing various common CMP slurry additives at different pH values. In most cases, the measured hardness values were consistent with the formation of surface films as indicated by the equilibrium potential-pH diagrams. In general, when the pH is low (<4), hardness values are that of Cu metal or slightly higher. As the pH increases to ~8, the hardness decreases to less than Cu metal as hydroxides form or to higher values than Cu metal as oxides form. Exposure to solutions with glycine or EDTA caused hardness values to be less than Cu metal, possibly as areas of the surface become porous. Exposure to H_2O_2 causing harder films in some areas and very porous soft films in other areas on the same surface as passivation and dissolution of the surface occurs.

5.2 Introduction

Copper has become the interconnect material of choice for integrated circuits due to its low electrical resistivity and high thermal conductivity [1]. Copper metallization is mainly performed by electroplating of the single or dual damascene process with a suitable diffusion barrier layer (*e.g.*, tantalum) followed by chemical mechanical planarization (CMP), which is needed to remove excess material and provide a globally planarized wafer surface [2]. The CMP process uses a slurry

containing abrasive particles and chemical additives that account for both the chemical and mechanical action of material removal on the wafer surface [3]. Material removal rate (MRR) is significantly affected by the addition of chemical additives to the slurries [2]. These additives control the state of the copper (CuO, Cu^{2+}, Cu_2O etc.) in the slurry and on the surface of the wafer and need to be optimized so that both the interactions with the wafer surface and the effects on the abrasive particles in the slurry will provide an adequate MRR and planarized surface with minimal defects. Our previous experimental work investigated the effects of common slurry additives on the colloidal behavior of alumina suspensions used for copper CMP [4, 5]. We used this data in the Luo and Dornfeld model of CMP [6, 7] in order to understand and predict copper CMP [8, 9]. In this study, the effects of the common slurry additives on the nanohardness and etch rates of the copper surface were investigated in an effort to better understand the CMP process, but also to be used in our modeling work.

Hardness is a material property which characterizes the resistance of the material to plastic flow due to indentation and sliding wear [10]. Advances in atomic force microscopes have allowed much smaller scale indentations to be made where the applied normal loads are on the order of μN and the indentation of nanometers, thus, allowing measurement of thin films and single crystals [10, 11]. For thin films there are a number of challenges that arise in determining hardness. The hardness depends on the depth of penetration as the films are constrained by their substrates, and the measurement also becomes much more sensitive to the mode of deformation. If the applied normal load is too small (with a small indentation depth), the material deforms elastically and the material hardness cannot be obtained. If elastic-plastic deformation

occurs during indentation, the hardness will decrease as the mean contact pressure increases, and a method, such as that developed by Ye and Komvopolus [10], must be used to determine hardness. If fully-developed plastic deformation occurs, the hardness value is unique and will not vary with load for a homogenous material. However, for layered media, such as that used in this study, the measured hardness may also be affected by the underlying substrate when the indentation depth is too large.

Criteria for determining the maximum indentation depth to avoid substrate effects and minimum indentation depth to ensure fully developed plastic deformation have been developed by Ye and Komvopolus [10]. The maximum indentation depth, δ_{max} can be determined as follows for a copper film on a tantalum barrier layer as used in our studies:

$$\left(\frac{\delta_{\max}}{h}\right)^2 = \ln\left(\xi\frac{H_{Cu}}{H_{Ta}}+1\right)\frac{\sigma_{Y,Ta}/E_{Ta}}{\sigma_{Y,Cu}/E_{Cu}} \qquad [5.1]$$

where h is the copper layer thickness, H is nanohardness , ξ is a tolerance parameter <<1, E is the elastic modulus and σ is the yield strength. The minimum indentation depth can be calculated using the following equation:

$$\frac{\delta_{\min}}{R} \geq \frac{2}{1+0.5\left(E^*/\sigma_{Y,Cu}\right)^{0.94}} \qquad [5.2]$$

where R is the radius of a rigid spherical indentor and E* is given by

$$E^* = \frac{1}{\frac{1-\upsilon_{Cu}^2}{E_{Cu}}+\frac{1-\upsilon_{tip}^2}{E_{tip}}} \qquad [5.3]$$

where ν is Poisson's ratio and E_{tip} is the elastic modulus of the indentor.

There have been several studies of nanohardness of copper surfaces [1, 2, 12-18]. Nanohardness of bulk copper samples was measured by Chang et al. and found to have values of ~2.3 GPa [1]. Soifer et al. studied the nanohardness of bulk copper samples after annealing and found that the hardness was ~1.5 GPa, but increased to ~2.2 GPa near grain boundaries [18]. Beegan et al. used nano-indentation to determine the hardness of a thin copper film (thicknesses of 950 and 1400 nm) of 2.5 ± 0.3 GPa [16].

Equilibrium studies by Aksu and Doyle showed that the nature and properties of the copper surface layer vary with changes in the chemistry and pH of a CMP slurry [19-22]. Copper forms a variety of oxides and hydroxides depending on the pH, the potential at the Cu/slurry interface, and the kinetics of the surface reactions [21]. Several studies have characterized the copper films (oxide, hydroxide, complexes etc.) that are formed in some CMP slurries using techniques such as X-ray photoelectron spectroscopy (XPS) [23-26] or studying potentiodynamic profiles [26, 27]. Jindal and Babu showed that changes in the pH of the slurry affect the structure and compactness of the layer that is formed, thus, affecting the nanohardness of this layer [2].

The CMP model developed by Luo and Dornfeld [6, 7], as well as the model developed by Wang et al. [28], requires the hardness of the material surface in order to predict MRR. The CMP model of Luo and Dornfeld indicates that small changes in the hardness of the surface film can cause significant changes in the MRR [6, 7]. The model proposes that the mechanism of material removal during CMP is due to quasi-static indentation of the abrasive into the wafer surface [6, 7]. According to this model, the indentation of the abrasive into the surface is less than 1 nm for typical abrasive particles of ~200 nm in diameter [6, 7]. The measurements in this study were made at

larger indentation depths greater (>5 nm) than that of the abrasive particle. Also, these measurements are done under quiescent conditions without particles, whereas during CMP the wafer is exposed to flowing slurry. However, the measurements in this study provide some insight to the types of films that may form on the surface during CMP and show the range of hardness values that may be possible. The objective of this paper is to systematically study the effects of the slurry chemistry on the copper surface nanohardness and etch rates in order to improve the understanding of the removal mechanisms occurring during copper CMP. Future work will incorporate these experimental copper surface nanohardness and chemical etch rates into a model of CMP.

5.3 Experimental

5.3.1 Nanohardness Measurements

Copper films (1000 nm) sputter-deposited onto a 30 nm tantalum coating on silicon wafer pieces (~1 cm^2) were immersed in 100 mL of solution (without abrasives) at different pH values. Table 5.1 lists the concentration of additives used in the slurry solutions; these compositions have been used in our previous colloidal and CMP experiments [4, 5, 8, 9]. The pH of the solution was adjusted using KOH or HNO_3. An exposure time of 10 min was chosen to be consistent with slurry exposure time of a typical industrial copper CMP process, which is approximately 5-10 minutes [3]. The pieces were then removed and dried by forced air for ~30 sec and immediately measured.

Table 5.1 Concentration of additives used in the alumina slurry.

a) 1 mM KNO_3
b) 1 mM KNO_3, 0.1 M glycine
c) 1 mM KNO_3, 0.1 M glycine, 0.1 wt% H_2O_2
d) 1 mM KNO_3, 0.1 M glycine, 2.0 wt% H_2O_2
e) 1 mM KNO_3, 0.1 M glycine, 0.1 wt% H_2O_2, 0.01 wt% BTA, 0.1 mM SDS
f) 1 mM KNO_3, 0.01 M EDTA, 0.1 wt% H_2O_2, 0.01 wt% BTA, 0.1 mM SDS

A nanomechanical test instrument (Hysitron, Inc.) was used to measure the nanohardness of the copper film after exposure to typical CMP slurry chemicals. The method for measuring nanohardness was similar to that of Jindal and Babu [2]. Hardness of the surface film was measured with various maximum applied loads between 50-3000 μN (with a resolution of <1 nN [29]). The hardness is the maximum applied load divided by the projected contact area [30]. For the Berkovich diamond tip indenter, the projected contact area A (μm^2) = $24.5h_c^2$, where h_c is the indentation depth (nm). Measurement of indentation depth h_c is accurate to ±0.0002 nm [29]. The projected contact area of our measurements was ~0.014 μm^2. The nanohardness instrumental error was ±0.003 GPa.

The nanohardness of two bulk cuprite samples (from Inspiration Pit Mine, Santa Rita, New Mexico) was measured. The cuprite samples were mounted onto silicon wafer pieces and indentations were made with applied loads between 1000-3000 μN; this higher load was chosen to ensure fully-developed plastic deformation for these bulk samples. These samples were also analyzed for elemental composition by an Environmental Scanning Electron Microscope (ESEM) with Energy Dispersive X-ray (EDX) using a Quanta 600 from FEI Company.

5.3.2 Etch Rate Measurements

The etch rates were measured using the copper films as described immersed in 100 mL of solution (without abrasives) as listed in Table 5.1 for 10 min. The wafer pieces were weighed using a Sartorius balance (model 1712 MP8) before and after immersion with ±0.1 mg accuracy. The error for the etch rate was ±4 nm/min.

5.4 Results and Discussion

5.4.1 Nanohardness Before Exposure

Since a layered film was used in this study, the maximum and minimum indentation depths were determined using the hardness and material property values from the literature listed in Tables 5.2 and 5.3, respectively. For a 1000 nm copper film on a 30 nm Ta coating as shown in Figure 5.1, the maximum indentation depth δ_{max} calculated from Eq. 5.1 is 260 nm. However, the tantalum layer is very thin and even though it is harder than Cu metal as shown in Table 5.2, the silicon substrate is significantly harder and may have more influence on the measurements. Using values for silicon in Tables 5.2 and 5.3 instead of tantalum in Eq. 5.1 gives δ_{max} =132 nm, which is consistent with the general criteria, $\delta_{max} \sim 0.1h$ [11]. The minimum indentation depth using the values in Table 5.3 is calculated as ~0.7 nm, which is much less than the indentation depths (>5 nm) used in this study.

Table 5.2 Hardness values

Hardness technique	Material	Value
Nanohardness (GPa)	Cu	2.5 ± 0.3 [1, 16]
	Ta	3.3 ± 1.5 [2]
	Si	12 ± 2 [31]
	Cu_2O	17 ± 5 *
Moh's hardness [32]	$Cu(OH_)_2$	2.0-2.5
	Cu metal	3
	CuO	3.5
	Cu_2O	4
	Ta	6.5
	Si	6.5
Brinell hardness [32]	Cu	35-40
	Ta	70
	Si	240
Vicker's hardness [32]	Cu_2O	206
	Si	254

*as measured in this study

Table 5.3 Values for material properties.

Property	Material	Value
elastic modulus (GPa)	Cu	110 [33]
	Si	112.4 [33]
	Ta	186 [33]
	diamond tip	1050 [34]
yield strength (MPa)	Cu	80 [35]
	Ta	269 [36]
	Si	1500 [37]
Poisson's ratio	diamond tip	0.07 [34]
	Cu	0.343 [11]
radius of rigid spherical indentor, R (nm)	diamond tip	150 [38]

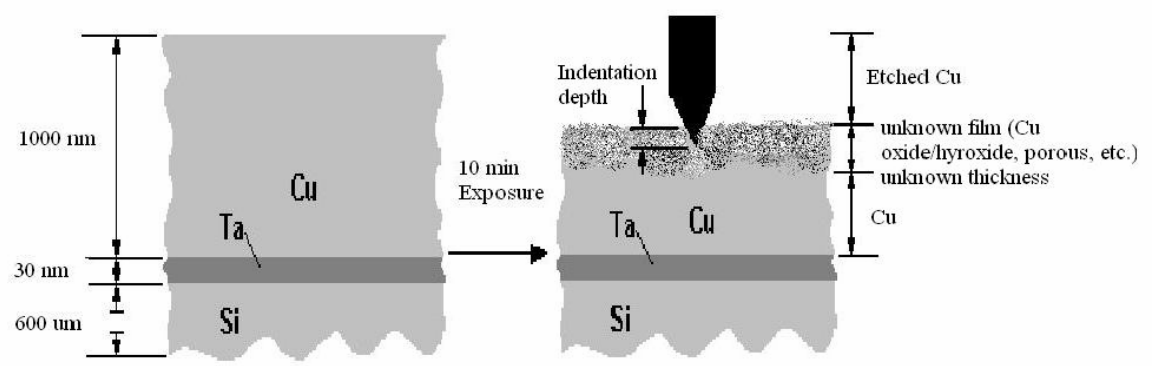

Figure 5.1 Schematic of the silicon wafer pieces sputter deposited with Ta and copper before and after 10 min exposure to various slurry solutions.

Exposure of the copper surface to the various solutions may change the copper surface state and decrease the thickness of the layer due to chemical etching, as illustrated in Fig. 5.1. However, as the properties of the surface film are unknown, the minimum and maximum indentation depth for each sample after exposure to the various solutions cannot be calculated. The hardness measurements in this study were performed with an indentation depth >5 nm, which for most cases is larger than the minimum indentation depth even with possible changes in the copper surface. Because a wide range of applied loads were used in this study (50-3000 μN) some of the hardness measurements had indentation depths greater than the maximum indentation depth even considering exposure to the various solutions. Therefore, only hardness measurements with indentation depths <120 nm, which are unaffected by the underlying materials, were considered.

To determine the error of the hardness measurements associated with the variation in the material of our samples, the nanohardness of a sample was measured without exposure to solution. Figure 5.2 shows both nanohardness as a function of indentation depth and the indentation depth versus applied loads from 50-3000 μN. The

nanohardness near the surface of the wafer (<20 nm indentation depth) is ~9 GPa, which is much greater than that of Cu metal and indicates the formation of copper oxide. As the indentation depth increases to 30 nm the hardness is that of Cu metal. The error associated with the variation in the copper sample was calculated using the measurements with applied loads between 200-1500 μN; this range was chosen to ensure that the indentation depth was deep enough to penetrate any possible thin passivation layer on the surface which may have formed due to exposure to the atmosphere, without having the underlying material affect the measurements. In this range of indentation depths, the hardness measurements of the Cu film were between 2.2-2.8 GPa, which is consistent with literature values [1, 2, 16]. Assuming the material is homogeneous for this range of indentation depth, the error is calculated as ±0.3 GPa.

In Figure 5.2, the hardness measurement near the surface of ~9 GPa indicates the formation of a copper oxide. Several researchers have shown that copper reacts in oxygen-containing environments to form a weak passivation layer [23, 26, 39]. Feng et al. suggest that the passivation layer consists entirely of cuprous oxide (Cu_2O) [39], while Du et al. believe that this layer may have a duplex structure made up of cupric hydroxide/cupric oxide ($Cu(OH)_2$/CuO) followed by a Cu_2O layer [23]. As shown in Table 5.2, the mohs hardness decreases from Cu_2O > CuO > Cu > $Cu(OH)_2$ [32, 40]. The measured hardness value of ~9 GPa near the surface suggests the formation of either CuO or Cu_2O. Figure 5.2b shows that the indentation depth increases nearly linearly as the load increases, indicating that the film is spatially uniform across the surface.

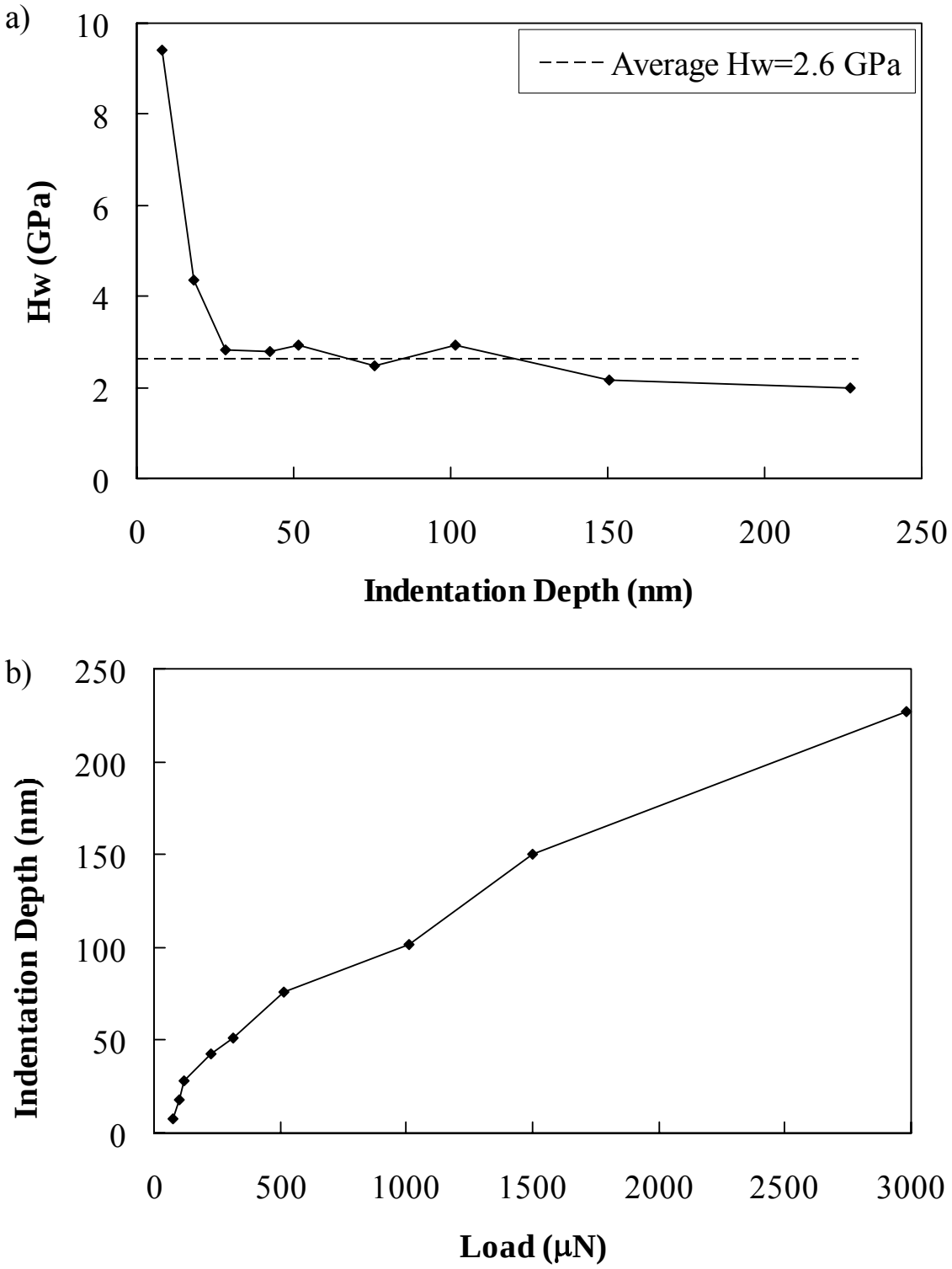

Figure 5.2 a) Nanohardness versus indentation depth and b) indentation depth versus load for the copper film.

Exposure of the copper surface to the various chemistries may cause formation of different films on the surface, such as CuO, Cu_2O, $Cu(OH)_2$ etc. Values for the nanohardness of bulk samples of these substances could not be found in the literature. Tenorite (CuO) only occurs in nature in micron-sized crystals and, therefore, is difficult to obtain [40]. Cuprite (Cu_2O) is a ruby-red crystal which is more abundant and can be found in nature in ~1-3mm sized samples [40]. The nanohardness of two cuprite samples was measured. Sample 1 had hardness values from 8.8 - 21 GPa, with an average value of 17.5 GPa. Sample 2 had hardness values from 5.2 - 29 GPa, with an average hardness value of 17.0 GPa. From EDX analysis the cuprite samples are ~89wt% Cu_2O, with excess oxygen (~6wt%) and impurities of carbon (~4.7wt%), silicon (<0.3wt%), and zinc (<0.06wt%). Comparing the mohs and Vickers hardnesses of Cu_2O to silicon (in Table 5.2), the nanohardness of Cu_2O is expected to be lower than that of silicon [31]. However, the varied measurement techniques often give different results [11]. Furthermore, impurities may increase the hardness of the cuprite samples, as well as indentations near the grain boundaries [17], which is not typically a concern for the macroindentation techniques.

5.4.2 Equilibrium Diagrams

Equilibrium potential-pH diagrams indicate the possible states of the copper at various pH values versus potential for a specified system and are used in this study to aid in explanation of the hardness measurements. Each slurry system requires a different potential-pH diagram. For the copper-water system, a potential-pH diagram constructed by Pourbaix shows that the possible states of copper at various pH values

are dependent upon the copper concentrations which range from 10^{-6} M and 1 M [41]. The concentration of copper during CMP in the bulk solution is transient and will increase with polishing time as the copper is removed from the surface. Our previous work has shown that the average concentration of copper in the bulk solution is ~0.12 mM for typical copper CMP removal rates, assuming a constant fresh supply of slurry to the wafer surface [5]. However, the concentration of copper at the solid-liquid interface between the copper surface and the slurry could be much higher than the concentration of copper in the bulk solution. Tan et al. have shown that the diffusion boundary layer thickness above an etching sample of GaSb is ~140 μm in stagnant liquid [42]. Using the smallest sample area of 312 mm^2 with the highest etch rate of 1.9 mg (for solution d), and assuming all the Cu is in the boundary layer above the sample, the concentration of Cu is ~0.7 M.

Glycine is a complexing agent that is typically used in copper CMP slurries because it forms soluble complexes with both cupric and cuprous ions [19]. The principal copper-glycinate complexes are $Cu(H_3NCH_2COO)^{2+}$, $Cu(H_2NCH_2COO)^{+}$, $Cu(H_2NCH_2COO)_2$, and $Cu(H_2NCH_2COO)_2^{-}$, and are referred to as $CuHL^{2+}$, CuL^{+}, CuL_2, and CuL_2^{-}, respectively. Potential-pH diagrams for the copper-glycine-water system are given by Tamilimani et al. for a 0.1 M glycine concentration and copper concentrations from 10^{-6} M and 10^{-4} M [43]. Aksu and Doyle have also constructed several potential-pH diagrams for glycine concentration from 10^{-4} M and 10^{-1} M and copper concentration from 10^{-6} and 10^{-4} M [20]. For the experiments done in this study the concentration of glycine in the solution is 0.1 M. A potential-pH diagram has been constructed by Patri et al. with a higher concentration of copper (10^{-2} M) and a glycine

concentration of 0.13 M [44]. However, potential-pH diagrams for higher concentrations of copper could not be found. Using the equilibrium equations given in Aksu and Doyle [20], potential-pH diagrams were constructed for copper concentrations of 10^{-4} M, 10^{-2} M and 1 M with a glycine concentration of 0.1 M as shown in Figure 5.3. Figure 5.3c shows that at a copper concentration of 1 M, Cu_2O is possible in solutions with pH>3.5. The thin area of the Cu_2O phase in Figure 5.3c between pH ~3.5 and ~10.0 appears at copper concentrations >0.038 M. It should also be noted that equilibrium phases in Figure 5.3 have not been verified experimentally.

For solution e containing a combination of additives, the potential-pH diagrams from Figure 5.3 will be used in conjunction with the potential-pH diagram for the copper-water-BTA system [43]. In this system, BTA is a corrosion inhibitor which can bind to the copper surface and prevent dissolution [27]. Sodium-dodecyl-sulfate (SDS) is a surfactant which will affect the alumina abrasives in the slurry, but it should not affect the copper surface [45]. For solution f the potential-pH diagrams constructed by Aksu and Doyle for the copper-water-ethylendiamine system [22] will be used in conjunction with the copper-water-BTA diagrams [43]. In this system EDTA behaves similarly to glycine, in that it forms soluble complexes with copper in certain pH ranges.

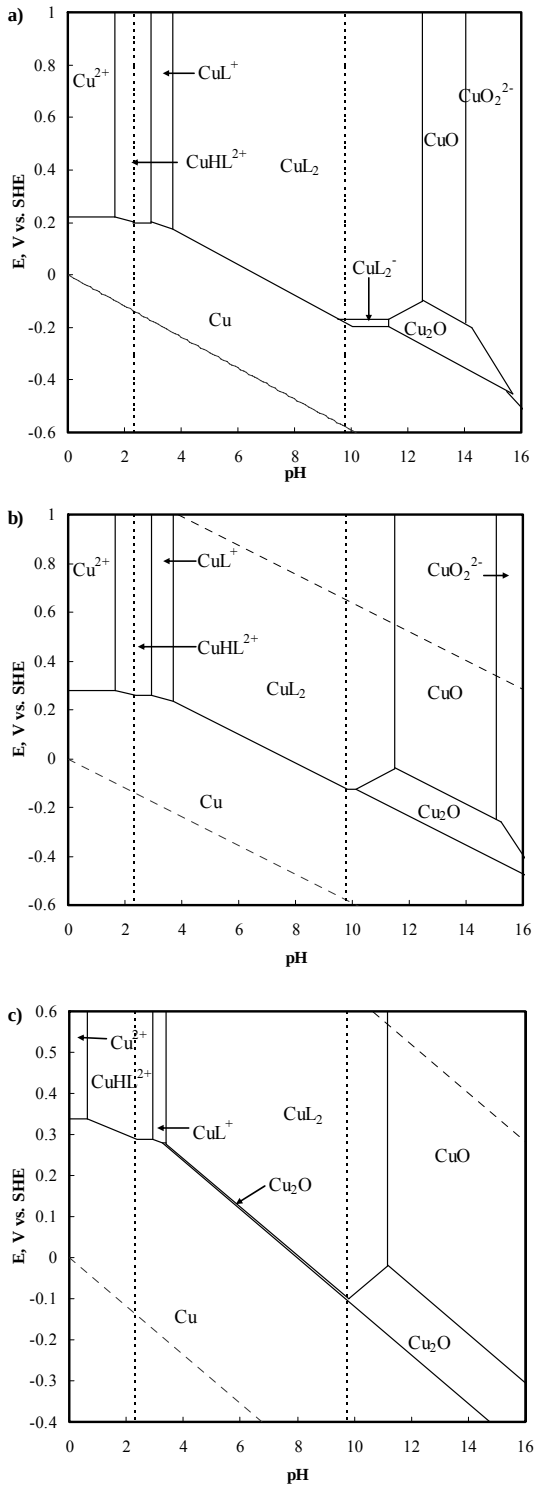

Figure 5.3 Potential-pH diagram for the copper-water-glycine system at a total glycine activity of 0.1 M and a total dissolved copper activity of a) 10^{-4} M b) 10^{-2} M and c) 1 M at 25^0C and 1 atm.

5.4.3 Etch Rate Measurements

Table 5.4 lists the measured chemical etch rates for the copper film after exposure to aqueous solutions with various additives and at different pH values. The measured etch rates show the chemical reactivity of the slurry and are necessary to understand the changes in the composition of the copper surface during exposure. For the solutions with no additives the etch rates were very low (<3.0 nm/min) for all pH values. This indicates that there is very little dissolution of the surface for this solution and it is unlikely that the surface film will be porous or pitted.

For the solution containing 0.1 M glycine the etch rates are low (from 0-2 nm/min) for pH 3.1 and 10.0, indicating very little dissolution of the surface. However, at pH 8.5 the etch rate is slightly higher, 7.6 nm/min, which may be due to increased formation of the Cu-glycine complex which is consistent with the potential-pH diagram in Figure 5.3. The etch rates for the solutions containing both glycine and H_2O_2 are much higher (14– 56 nm/min) at all pH values, than for the other slurries, indicating that these slurries are much more chemically reactive and the surface films may be very porous due to dissolution.

For solution e containing a combination of additives, the etch rates were low, <1.6 nm/min, for pH 3 and 8.4, and slightly higher, 8.6 nm/min, at pH 10.8. For solution f containing a combination of additives with EDTA as the complexing agent, there was no dissolution of the copper surface.

Table 5.4 Measured chemical etch rates and nanohardness at various indentation depth for the copper film after exposure to aqueous solutions with various additives and at different pH values.

Additives[1]	pH	Etch rate (nm/min) (±4nm/min)	Indentation Depth (nm)	Hardness Values (±0.3GPa)	Indentation Depth (nm)	Hardness Values (±0.3GPa)
a	2.9	0.7	14-60	1.6-4.6	112	2.5
	8.3	0.0	13-40	1.8-5.7	60-117	2.3-2.7
	11.7	2.6	10-22	2.0-7.3	60-74	2.3-2.6
b	3.1	1.2	24-40	1.0-3.5	72	2.6
	8.5	7.6	18-32	1.6-5.2	54-70	2.7-2.8
	10.0	0.0	5-62	3.5-16	107	2.7
c	3.0	45	18-45	1.0-4.4	65-100	3.1-3.2
	8.3	33	16-45	2.1-5.6	78	2.3
	10.1	14	13-68	0.34-4.7	102	2.9
d	3.0	38	13-41	2.8-8.2	50-96	3.0-3.3
	8.3	56	18-40	3.8-5.5	70-500	0.04-0.48*
	10.0	33	7-55	4.2-18	115	2.3
e	3.0	1.6	22-50	1.2-3.3	71	2.7
	8.4	0.0	15-40	1.7-5.3	72-110	2.5-2.7
	10.8	8.6	24-40	2.0-3.0	42-88	3.7-4.0*
f	2.6	0.0	7-50	0.9-11	60	3.7*
	9.0	0.0	13-50	2.5-8.0	76	2.5
	10.9	0.0	6-36	2.1-13	53-110	2.5-2.9

[1]As listed in Table 5.1
*Values are different than Cu metal

5.4.4 Nanohardness After Exposure

Table 5.4 lists the range of hardness values for a specified indentation depth range for copper film after exposure to each of the solutions. In Table 5.4 both hardness values very near the surface (<70 nm indentation depth) and from ~70-100 nm indentation depth are reported. Inspection of the measurements in Table 5.4 shows that these hardness measurements do not correlate with pH, etch rate, or chemical additives. This suggests that the each hardness value is very sensitive to the chemistry of the solution and therefore, no simple explanations can be given for the effects. For each of the samples the surface phenomena are different and the following discussion will attempt to explain the nanohardness behavior separately for each of the samples. For

the indentation depths >70 nm the nanohardness is that of Cu metal for all samples, except for three as indicated in Table 5.4, which will also be discussed.

5.4.5 Effect of pH on Hardness

Figure 5.4a shows the nanohardness versus indentation depth of samples after exposure to aqueous solutions at pH 2.9, 8.3 and 11.7. The range of the hardness values for a specified indentation depth range is also listed in Table IV for each of the solutions. After exposure to the pH 2.9 solution the nanohardness within a 60 nm indentation depth ranges from 1.6 to 4.6 GPa. The hardness values near the surface indicate that the surface film is slightly softer than Cu metal in some places and slightly harder than Cu metal in other places; the etch rate suggests very little dissolution of the surface. Figure 5.4b shows the indentation depth versus load for the copper film after exposure to aqueous solution at various pH values. As shown in Fig. 5.4b the indentation depth does not always increase as the load increases near the surface. This suggests that the surfaces of the samples are not spatially uniform and different types of films (oxides, hydroxides, complexes, etc.) may be forming in different areas and/or dissolution of the surface in some areas could decrease the compactness of the surface layer. According to the potential-pH diagram for the copper-water system [41] the possible states of the copper at pH 2.9 are the solids in the form of Cu metal or Cu_2O, or dissolved as Cu^{+}, or Cu^{2+}. The formation of $CuO/Cu(OH)_2$ is inconsistent with the potential-pH diagram, however, it is possible that CuO or $Cu(OH)_2$ may form on the surface as a reaction step in the formation of Cu_2O. Other researches have also

observed the formation of a thin layer of oxide/hydroxide on the surface of the copper in acidic conditions [26].

Hardness was also measured for the copper film after exposure to aqueous solution at pH 8.3, as shown in Figure 5.4. The nanohardness measurements near the surface were between 3.4 - 5.7 GPa within a 25 nm indentation depth, with one measurement of 1.8 GPa at an indentation depth of 20 nm. The hardness measurements near the surface are higher than that of Cu metal (except for one measurement at an indentation depth of 20 nm) suggesting the formation of a copper oxide. The possible states of copper according to potential-pH diagram [41] at pH 8.3 are the solids in the form of Cu metal, Cu_2O, CuO, or $Cu(OH)_2$, which is consistent with no dissolution of the copper surface in this solution. The hardness values of 3.4-5.7 at the surface could be that of CuO. According to the potential-pH diagram, $Cu(OH)_2$ is possible at the same pH and potential as CuO, however, $Cu(OH)_2$ is less stable than CuO [41]. The hardness value of 1.8 GPa at 20 nm indentation depth may be indicative of the formation of $Cu(OH)_2$ in some places on the surface, while the formation of CuO is dominant, as given by the majority of the hardness values measured.

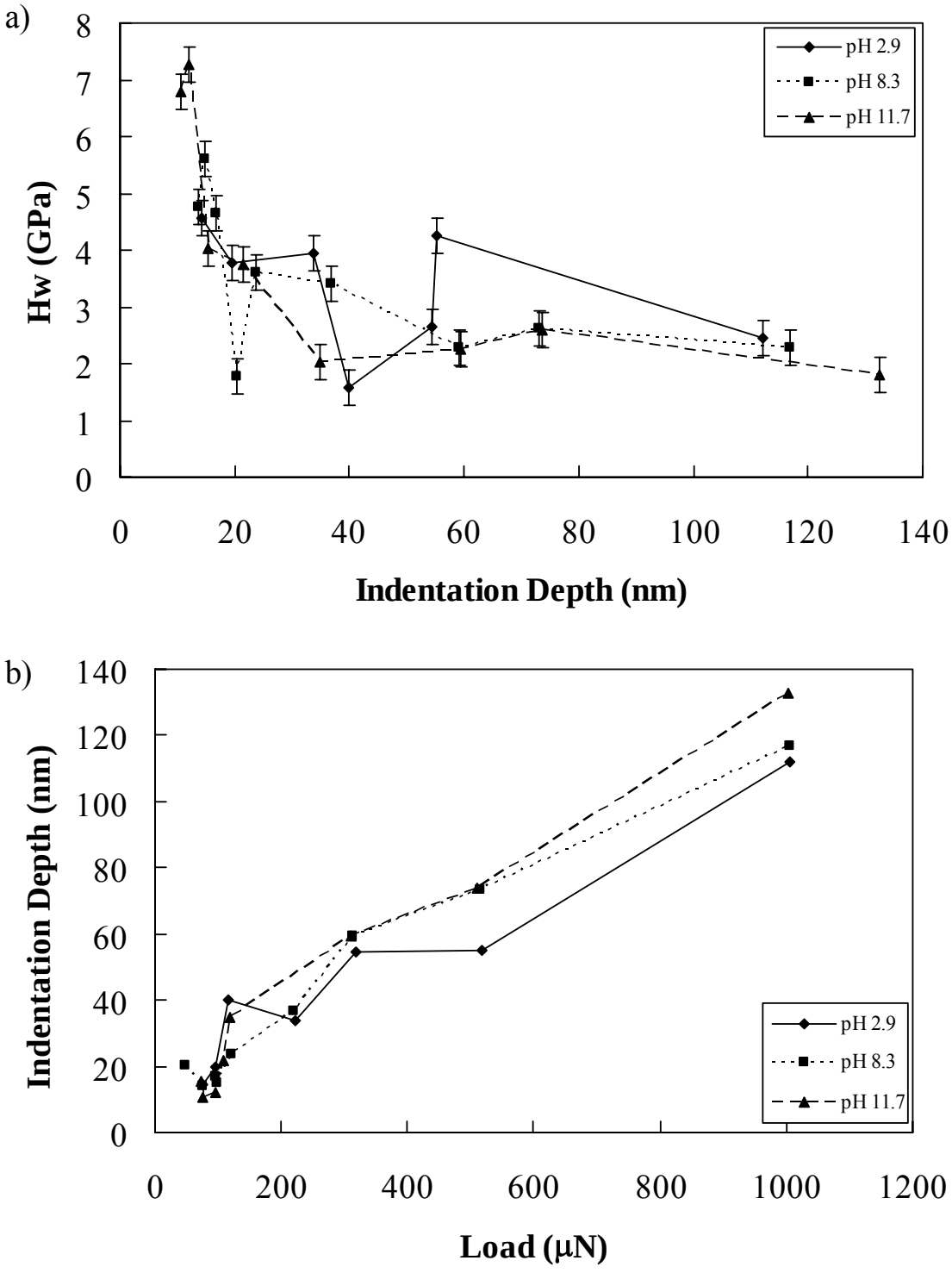

Figure 5.4 a) Nanohardness versus indentation depth and b) indentation depth versus load for the copper film after exposure to aqueous solution at various pH values (error bars indicate ±0.3 GPa variation).

The nanohardness versus indentation depth and indentation depth versus load for the copper film after exposure to aqueous solution at pH 11.7 are also shown in Figure 5.4. Near the surface of the wafer the nanohardness values are between 3.7-7.3 within a 25 nm indentation depth. The hardness is that of Cu metal for indentation depths greater than 35 nm. The possible states of the copper according to the potential-pH diagram [41] at pH 11.7 are solids in the form of Cu metal, Cu_2O, CuO, and $Cu(OH)_2$, or dissolved in solution as $HCuO_2^-$. The etch rate for this solution was 2.6 nm/min, indicating very little dissolution of the surface. The hardness values of 3.7–7.3 near the surface are higher than that of Cu metal and indicate that a copper oxide (CuO or Cu_2O) may be forming on the surface.

5.4.6 Solutions with Glycine and H_2O_2 (pH~3)

The hardness versus indentation depth and indentation depth versus load data are shown in Figure 5.5 and also listed in Table 5.4. For the samples exposed to solutions containing 0.1 M glycine, the hardness values at a given pH are compared to values of samples from solutions containing both 0.1 M glycine and various concentrations of H_2O_2 at the same pH. For the solution with 0.1 M glycine at pH 3.1 the hardness varies from 1.0–3.5 GPa within 40 nm of the surface. This indicates that films are forming on the surface that are both softer and harder than Cu metal. The softer surface values could be due to the presence of the Cu-glycine complex formation on the surface. This was also observed by Seal et al. in solutions containing glycine at pH 4; they found that the oxide film on the copper surface will dissolve in the presence

of glycine after forming a soluble complex [26]. They also showed the presence of the Cu-glycine complex on the surface using XPS [26].

For solution c at pH~3.0, the hardness varies from 1.0-4.4 GPa within 45 nm of the surface, which is slightly higher than without H_2O_2, and may be due to the H_2O_2 increasing the repassivation rate of the copper surface after dissolution of the Cu-glycine complex [26]. For solution d at pH~3.0, the hardness varies from 2.8–8.2 GPa within 40 nm of the surface, which is significantly harder than without H_2O_2 and indicates the formation of a copper oxide on the surface. For pH 3.0 the potential-pH diagram given in Figure 5.3 shows that copper may exist as a solid in the form of Cu metal, or as a soluble complex in the form of either $CuHL^{2+}$ or CuL^{+}. Under acidic conditions, the most likely reactions occurring in this system include [20, 26]

$$2Cu + H_2O \rightarrow Cu_2O + 2H^{+} + 2e \quad \text{(passivation)} \quad [5.4]$$

$$Cu_2O + 2HL \rightarrow 2CuL\ (s) + H_2O \quad \text{(complex formation)} \quad [5.5]$$

$$2CuL\ (s) \rightarrow 2CuL^{+}\ (l) + 2e \quad \text{(dissolution)} \quad [5.6]$$

The copper surface is first passivated, the Cu-glycine complex then forms on the surface and eventually dissolves into the solution [20, 25, 26]. This is consistent with the hardness measurements. After exposure to the solution containing 0.1M glycine at pH~3.1, the surface hardness measurements (1.0-3.5 GPa) are near that of Cu metal, indicating little oxide formation on the surface, while the low etch rate of this solution indicates very little dissolution of the surface. In this case the complexing reaction (Eq. 5.5) may be limited by the formation of the passivation layer (Eq. 5.4), which may be slow for this slurry solution.

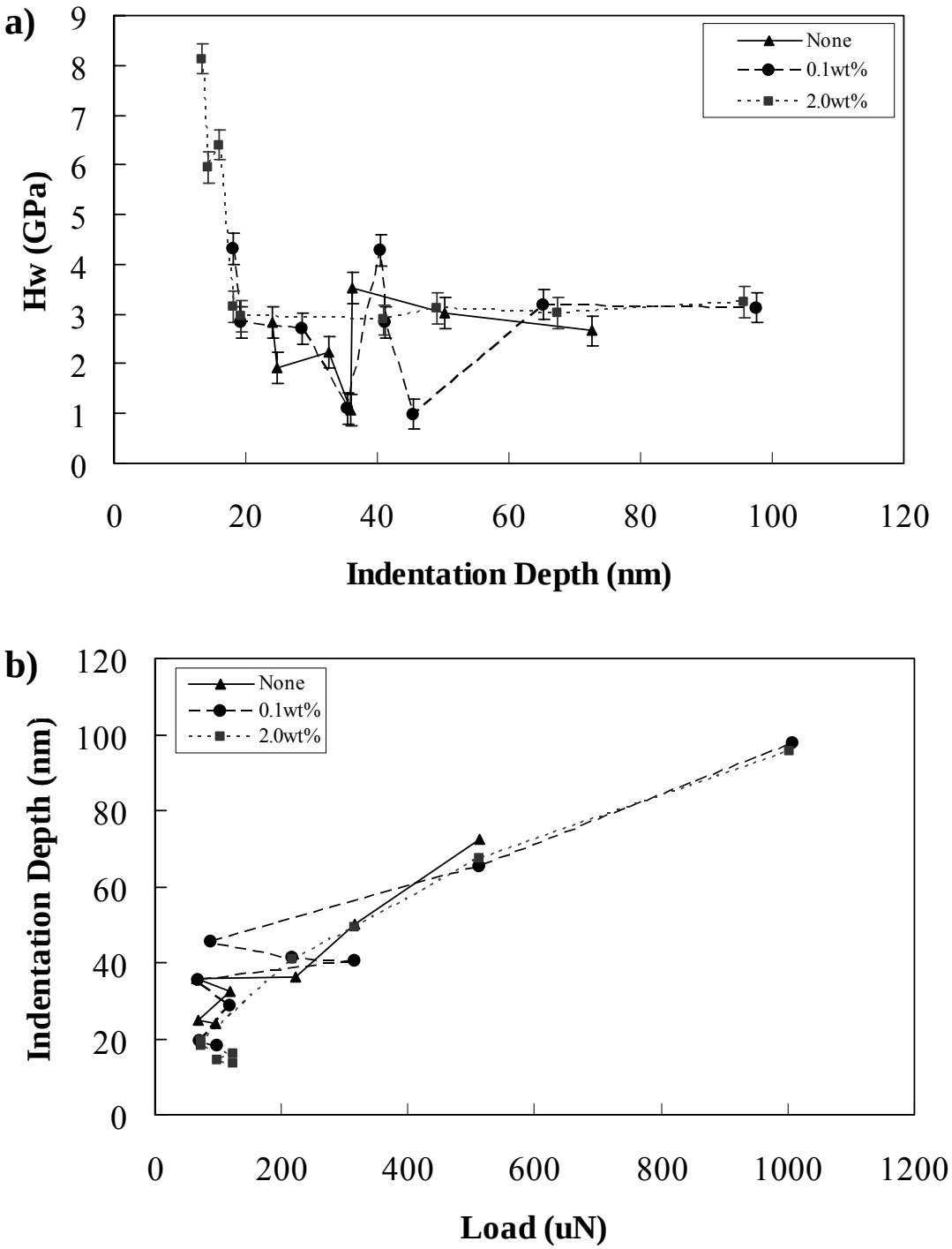

Figure 5.5 a) Nanohardness versus indentation depth and b) indentation depth versus load for the copper film after exposure to aqueous solutions with 0.1 M glycine and various concentrations of H_2O_2 at pH ~3 (error bars indicate ±0.3 GPa variation).

With the addition of 0.1wt% H_2O_2 to the solution the hardness values are slightly higher (1.0-4.4), indicating that a copper oxide layer may be forming, but is quickly complexed with glycine and dissolved. The decomposition of H_2O_2 is given by the following reaction [23]

$$H_2O_2 + e^- \rightarrow OH^* + OH^- \quad \text{(decomposition)} \quad [5.7]$$

which yields a more reactive oxidizer hydroxyl radical that may cause faster oxidation of the surface; excess hydroxyl radical may also accelerate the formation of a thicker passivation layer [25]. This is consistent with the etch rate measurements which are much higher for this solution, 45 nm/min.

Increasing the H_2O_2 concentration to 2.0wt% causes the hardness values to increase to 2.8-8.4 GPa near the surface, indicating the formation of a copper oxide layer. The etch rate is slightly lower, 38 nm/min, at 2.0wt% H_2O_2 compared to 0.1wt% H_2O_2. For this solution the passivation reaction may be very fast due to the higher concentration of H_2O_2, but complex formation and dissolution may be inhibited by the thicker oxide layer. This suggests that there is an optimal H_2O_2 concentration that is needed to passivate the copper surface without inhibiting Cu-glycine complexing, which was also observed by Seal et al. [26]. As previously stated, these films are not spacially uniform and there are most likely different surface films forming at different locations which may be due to both the rate of the reactions on the surface and the diffusion rate of the reaction species to/from the surface.

5.4.7 Solutions with Glycine and H_2O_2 (pH~8.5)

The nanohardness versus indentation depth and indentation depth versus load for the copper film after exposure to solutions containing 0.1 M glycine and various concentrations of H_2O_2 at pH~8.3 are shown in Figure 5.6, where one of the profiles is significantly different than previously observed. For the solution with 0.1 M glycine the hardness varies from 1.6 – 5.2 GPa within 40 nm of the surface and indicates that films are forming on the surface which are both softer and harder than Cu metal. The softer surface values could be due to the presence of the Cu-glycine complex formation on the surface, as was observed on the sample exposed to the same solution but at pH 3.0.

For solution c at pH 8.3, the hardness varies from 2.1 -5.6 GPa within 50 nm of the surface, which is slightly harder than without H_2O_2, and may be due to the H_2O_2 increasing the repassivation rate of the copper surface after dissolution of the Cu-glycine complex [26]. For solution d the hardness varies from 3.8–5.5 GPa within 40 nm of the surface, which is slightly harder than without H_2O_2 and indicates the formation of a copper oxide on the surface. For this solution the hardness values do not equal that of Cu metal as the indentation depth increases, as was observed in most of the previous samples. In this solution the hardness values are <1.0 GPa for indentation depths greater than 70 nm.

For pH 8.3 the potential-pH diagram given in Figure 5.3 shows that copper may exist as a solid in the form of Cu metal and Cu_2O, or as a soluble complex in the form of CuL_2. Xu et al. have shown that the water-soluble glycine complex may be formed with the free copper ions dissolved from the surface and/or with the copper

hydroxide/oxide prior to the dissolution from the surface [26]. The most likely reactions occurring on the surface of the wafer in alkaline conditions are the following [20, 25]:

$2Cu + H_2O \rightarrow Cu_2O + 2H^+ + 2e$ (passivation) [5.8a]

$Cu_2O + H_2O \rightarrow 2CuO + 2H^+ + 2e$ (passivation) [5.8b]

$Cu_2O + 4HL \rightarrow 2CuL_2\,(s) + H_2O + 2H^+ + 2e$ (complex formation) [5.9a]

$CuO + 2HL \rightarrow CuL_2\,(s) + H_2O$ (complex formation) [5.9b]

$CuL_2\,(s) \rightarrow CuL_2\,(l)$ (dissolution) [5.10]

Similar to the reactions occurring in acidic conditions, the surface is first passivated where either CuO or Cu_2O is formed, then a neutrally charged copper-glycinate complex forms (CuL_2) on the surface, and eventually the complex dissolves into the solution.

For the sample exposed to the solution containing 0.1 M glycine at pH 8.5 the hardness values <2.3 may be from the Cu-glycine complex. The hardness values >2.8 GPa may be due to a copper oxide film. The rate of dissolution is slow for this solution, as given by the etch rate of 7.6 nm/min, indicating the rate of the reactions (Eqs. 5.8-5.10) are slow, possibly due to slow passivation of the surface.

Addition of 0.1wt% H_2O_2 to the solution increases the rate of the reactions on the surface (Eqs. 5.8-5.10) as reflected by the larger etch rate of 33 nm/min, which is most likely due to faster passivation with the addition of the oxidizer, H_2O_2. However, the hardness values for the sample exposed to the 0.1M glycine and 0.1wt%H_2O_2 at pH 8.3 solution are similar to the hardness values for sample exposed to the solution with only 0.1 M glycine at pH 8.5. In this case, the rate of the reactions on the surface

increases, which increases the etch rate, but the structure of the surface remains similar with the addition of 0.1wt% H_2O_2. This is consistent with observations by Xu et al., which have shown that the copper-glycine complex further catalyzes the decomposition of hydrogen peroxide to yield a more reactive oxidizer hydroxyl radical (reaction Eq. 5.7) which may cause faster oxidation and dissolution of the surface [25].

Increasing the concentration of H_2O_2 to 2.0wt% increases the hardness values near the surface and decreases the hardness values at larger indentation depths. The high 2.0wt% H_2O_2 concentration may increase the dissolution rate of the Cu-glycine complex, which then increases the decomposition of the H_2O_2, and further accelerates passivation of the surface. Additionally, the hydroxyl radical in Eq. 5.7 is more stable in acidic conditions, which causes the reaction Eqs. 5.8-5.10 to occur faster at higher pH. This is consistent with the very high etch rate for this solution of 56 nm/min. The hardness values larger than that of Cu metal at the surface may be due to the harder copper oxide surface layer from increased passivation and the hardness values <1 GPa for indentation depths >70 nm may be due to the increased Cu-glycine dissolution causing a very porous, soft film.

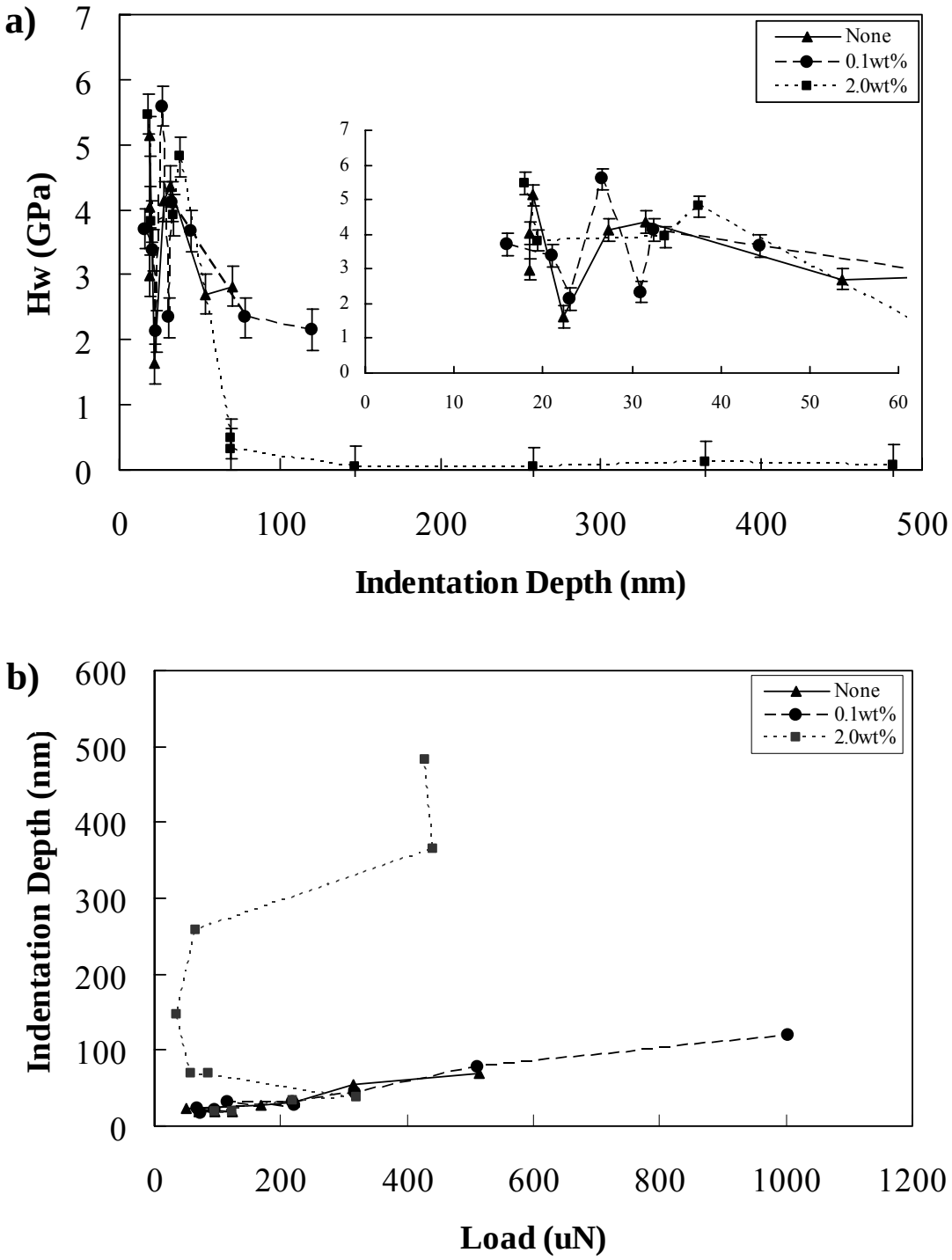

Figure 5.6 a) Nanohardness versus indentation depth and b) indentation depth versus hardness for the copper film after exposure to aqueous solutions with 0.1 M glycine and various concentrations of H_2O_2 at pH ~8.3 (error bars indicate ±0.3 GPa variation).

5.4.8 Solutions with Glycine and H_2O_2 (pH~10.0)

The nanohardness versus indentation depth and indentation depth versus load for the copper film after exposure to solutions containing 0.1 M glycine and various concentrations of H_2O_2 at pH~10.0 are shown in Figure 5.7. Nanohardness data is also listed in Table 5.4. For the solution with 0.1 M glycine the hardness varies from 3.5–16 GPa within 60 nm of the surface. For pH 10.0 the potential-pH diagram given in Figure 5.3 shows that copper may exist as a solid in the form of Cu metal and Cu_2O, or as a soluble complex in the form of CuL_2 or CuL_2^-. The hardness values near the surface are larger than that of Cu metal and indicate that copper oxide is formed on the surface. However, no etching indicates that dissolution of the Cu-glycine complex does not occur (or is very slow). In this solution the formation of the Cu-glycine complex may be the limiting reaction, which could be very slow without the presence of the hydroxyl radical. Additionally, the hardness values near the surface are very high (up to 16 GPa at indentation depth of 5 nm). This may be due to the formation of a much thicker passivation layer given that copper oxides are more stable at higher pH [39].

For solution c at pH 10.1, the hardness varies from 0.34-4.7 GPa within 70 nm of the surface. The addition of 0.1wt% H_2O_2 increases the Cu-glycine complex formation and dissolution on the surface as indicated by the increased etch rate of 14 nm/min. The measured hardness values suggest that this solution causes the surface to become very soft and porous possibly due to the increased dissolution. However, the H_2O_2 concentration is not high enough to cause thick passivation layer formation as indicated by the hardness values remaining less than 4.5 GPa. For solution d at pH

10.0, the hardness varies from 4.2–18 GPa within 60 nm of the surface. The increase in the H_2O_2 concentration to 2.0wt% increases the Cu-glycine complex formation and dissolution as indicated by the increased etch rate of 33 nm/min. At this high concentration of H_2O_2 the hardness values are very high (>15 GPa) near the surface, which is much larger than any of the previous samples. As previously stated, the reduction of H_2O_2 to hydroxyl radical (reaction Eq. 5.7) is faster in higher pH solutions, which could cause a much thicker passivation layer and may explain the higher hardness near the surface. The high hardness values for this sample are consistent with the hardness values of the cuprite sample and suggest that a thick Cu_2O layer may be forming. Other researchers [21, 27, 46] have also shown that in the presence of high concentrations of H_2O_2 the copper may oxidize to form copper sesquioxide (Cu_2O_3) or copper peroxide (CuO_2) which are not considered in the Fig. 5.3 potential-pH diagrams. No information could be found on the hardness of the Cu_2O_3 or CuO_2 films because of their rarity. It is possible that the very high hardness values observed after exposure to this solution may be due to the formation of these rare films (Cu_2O_3 or CuO_2) which may be much harder than Cu_2O or CuO. However, further research is needed to verify the formation of these films.

The hardness measurements at pH 10.0 in the presence of 0.1 M glycine and various concentrations of H_2O_2 further suggest that an optimal H_2O_2 concentration exists which will cause a passive layer to form on the surface that is just thin enough to provide adequate Cu-glycine complex formation and dissolution without causing pitting.

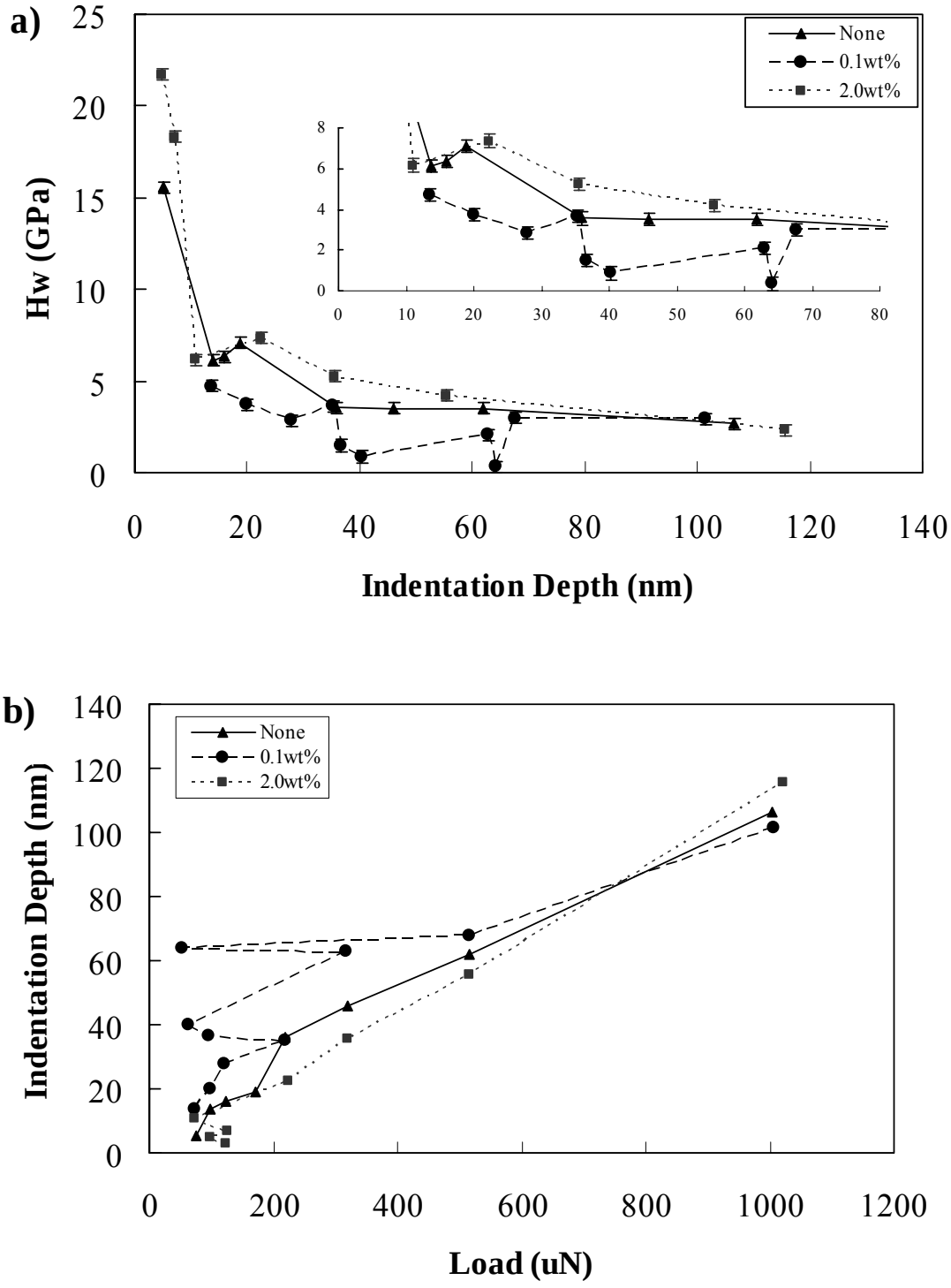

Figure 5.7 a) Nanohardness versus indentation depth and b) indentation depth versus hardness for the copper film after exposure to aqueous solutions with 0.1 M glycine and various concentrations of H_2O_2 at pH ~10.0 (error bars indicate ±0.3 GPa variation).

5.4.9 Combination of Additives

Figure 5.8 shows the nanohardness versus indentation depth and indentation depth versus load for the copper film after exposure to solution e at various pH values. After exposure to the solution at pH 3.1, the hardness varies from 1.2–3.3 GPa within 50 nm of the surface. According to the potential-pH diagrams for the copper-water-glycine system and the copper-water-BTA system [43], at pH 3.1 the copper may exist as Cu metal, or dissolve into solution as either Cu^{2+} or a copper-glycinate complex ($CuHL^{2+}$, CuL^{+}). The formation of the Cu-BTA complex on the surface is unlikely at this low pH [43] and the low etch rate (1.6 nm/min) for this solution indicates very little dissolution of the surface. The hardness values are near that of Cu metal at the surface, with some values slightly less than that of Cu metal. The hardness values less than that of Cu metal are most likely due to the presence of the Cu-glycine complex on the surface [26]. At this pH the hardness values and etch rate are very similar to those observed on the sample exposed to 0.1M glycine and 0.1wt% H_2O_2, which is expected because both BTA and SDS [45] should not have any effect on the copper surface at pH 3.1.

Figure 5.8 also shows the hardness measurements after exposure to solution e at pH~8.4. After exposure to the solution at pH 8.4, the hardness varies from 1.7–5.3 GPa within 40 nm of the surface. According to the potential-pH diagrams [20, 43], at pH 8.4 the copper may exist as a Cu metal, Cu_2O, Cu-BTA, or dissolve into solution as a copper glycinate-complex (CuL_2). No dissolution of the surface occurs, which may be due to the presence of BTA. The hardness values range from slightly softer (1.7 GPa) than Cu metal to harder (5.3 GPa) than Cu metal, which may be due to the formation of

several different states of copper on the surface. The hardness values higher than Cu metal may be from the formation of a copper oxide film, while the hardness values less than Cu metal may be from the Cu-BTA complex.

Figure 5.8 also shows the hardness measurements after exposure to solution e at pH~10.8. After exposure to the solution at pH 10.8, the hardness varies from 2.0–3.0 GPa within 40 nm of the surface. For indentation depths between 40-90 nm the hardness varies from 3.7-4.0 GPa. According to the potential-pH diagrams [20, 43], at pH 10.8 the copper may exist as a Cu metal, Cu_2O, CuO, or $Cu(OH)_2$, or dissolve into solution as a copper glycinate-complex (CuL_2 or CuL_2^-). The etch rate in this solution was 8.6 nm/min and indicates some dissolution of the surface, which is expected because the BTA is not likely to complex with the copper surface at this high pH. The surface hardness values for this solution are near that of Cu metal, while the hardness values at deeper indentation depths (>40 nm) may be indicative of copper oxide. The slightly higher etch rate for this solution compared to the same solution at pH 3.1 and 8.4 suggests Cu-glycine complex formation and dissolution. For this solution the copper surface may have a very thick copper oxide layer, as indicated by the larger hardness values at deep indentation depths, while the dissolution of the surface after Cu-glycine complex formation causes a softer more porous surface film than the underlying film.

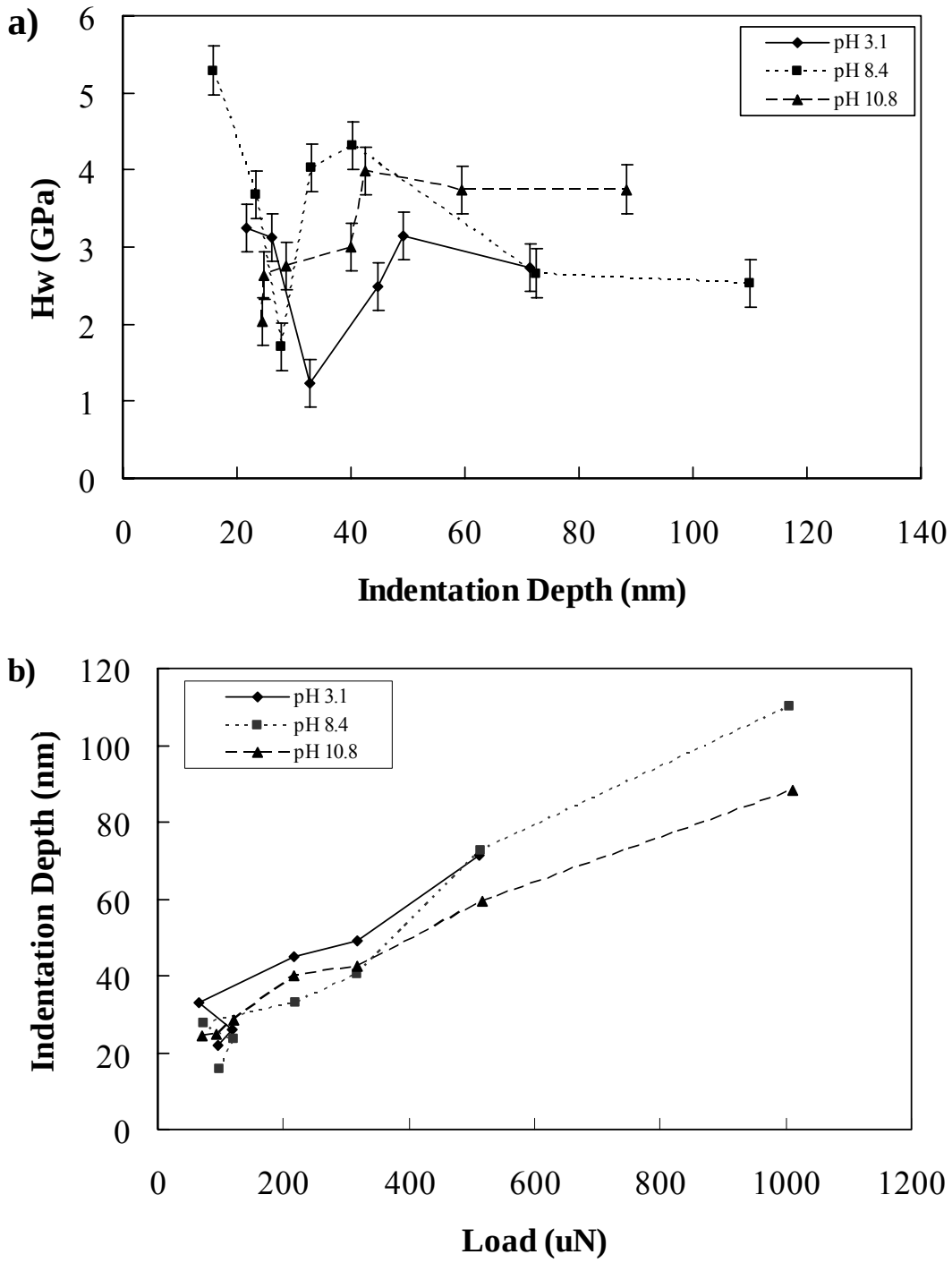

Figure 5.8 a) Nanohardness versus indentation depth and b) indentation depth versus load for the copper film after exposure to aqueous solution with 0.1 M glycine, 0.1wt% H_2O_2, 0.01wt% BTA, and 0.1 mM SDS at various pH values (error bars indicate ±0.3 GPa variation).

Figure 5.9 shows the nanohardness versus indentation depth and indentation depth versus load for the copper film after exposure to solution f at various pH values. For solution f at pH 2.6, the hardness varies from 0.9–10.5 GPa within 50 nm of the surface. According to the potential-pH diagrams for the copper-water-ethylendiamine system [22] at pH 2.6 the copper may exist as Cu^{2+}, Cu-EDTA complex, Cu metal or Cu_2O and the potential-pH diagram for the copper-water-BTA system [43] shows that copper should be in the form of either Cu^{2+} or Cu metal. No dissolution of the surface was measured. The hardness values range from less (0.9 GPa) than the hardness of Cu metal to significantly higher (10.5 GPa) than Cu metal. The hardness measurements that are less than Cu metal may be due to the presence of a Cu-EDTA complex on the surface and the hardness measurements that are higher than Cu metal may be due to the formation of Cu_2O.

For solution f at pH 9.0, the hardness varies from 2.5–8.0 GPa within 50 nm of the surface. According to the potential-pH diagrams [22, 43] at pH 9.0 the copper may exist as a Cu metal, Cu_2O, Cu-BTA, or dissolve into solution as a Cu-EDTA complex. No dissolution of the surface was measured, which may be due to the presence of BTA at this pH. The hardness values range from that of Cu metal to higher than Cu metal, which suggests that a copper oxide may be forming in some places while other areas may be Cu metal that is protected from dissolution (Cu-EDTA formation) by the Cu-BTA complex.

For solution f at pH 10.9, the hardness varies from 2.1–13 GPa within 40 nm of the surface. The potential-pH diagrams [22, 43] at pH 10.9 show the copper may exist as a Cu metal, Cu_2O, CuO, $Cu(OH)_2$, or dissolve into solution as a copper-EDTA

complex. No dissolution of the surface was observed, which may be due to the formation of a thick passivation layer that is much more stable at high pH conditions compared to neutral or acidic conditions [39, 41]. The hardness values range from that of Cu metal to significantly higher than Cu metal, indicating that a thick passivation layer (Cu_2O) quickly forms on the surface most likely due to the exposure at high pH.

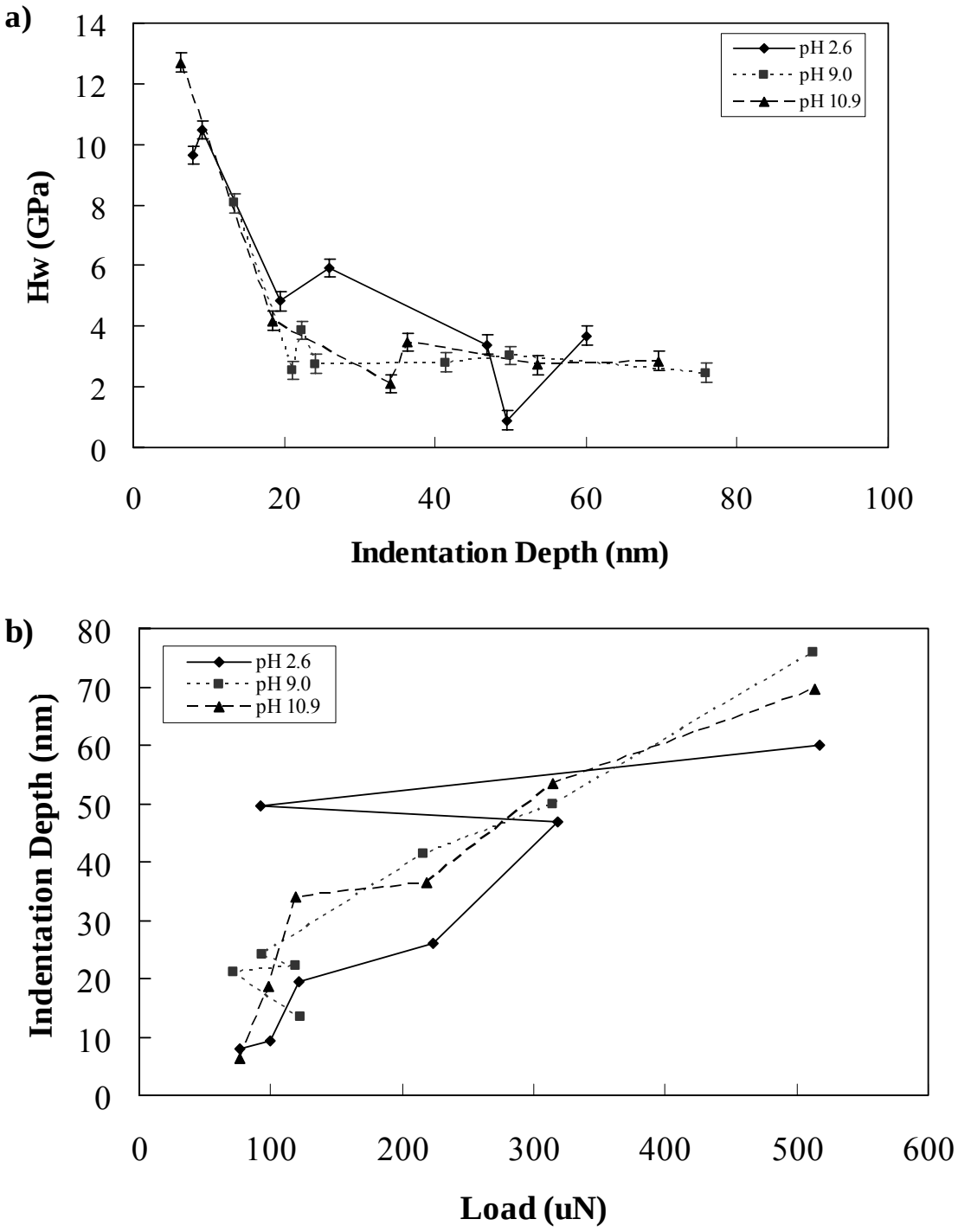

Figure 5.9 a) Nanohardness versus indentation depth and b) indentation depth versus load for the copper film after exposure to aqueous solution with 0.01 M EDTA, 0.1wt% H_2O_2, 0.01wt% BTA, and 0.1 mM SDS at various pH values (error bars indicate ±0.3 GPa variation).

5.4.10 Nanohardness versus Exposure Time

The hardness values listed in Table 5.4 show that the hardness of the copper surface varies significantly after exposure to various slurry chemistries. The formation of different surface films, as well as the pitting caused by dissolution, has a large effect on the hardness measurements, which may cause large differences in the MRR during CMP. The measurements in this study were performed under quiescent conditions with a 10 min exposure time, while during CMP the wafer would be exposed to flowing slurry. Researchers have suggested that one mechanism of removal during copper CMP may be from growth of a passivation layer, mechanical abrasion of the passive layer, and then regrowth [2]. For this removal mechanism, the chemical reaction time on the fresh substrate surface between abrasions may be shorter than the 10 min exposure time used in this study, and the surface products formed during CMP may be due to only fast reactions, while the surface products formed in this study may also be from slower reactions. Figure 5.10 shows the nanohardness versus indentation depth for a copper sample after immersion in 0.1M glycine, 0.1wt% H_2O_2, and 1mM KNO_3 solution at pH 7.0 for various exposure times. This solution was chosen because it had a large etch rate indicating this solution was very chemically active. The figure shows that the hardness near the surface (within <200 nm indentation depth) is ~0.8 GPa after exposure for only 1 min, which may be due to a hydroxide formation (Cu metal→$Cu(OH)_2$) or etching (Cu metal→Cu^{2+} or Cu^{+}) reactions. After exposure to the solution for 5 min, the hardness increases to ~1.0 GPa near the surface, possibly due to oxide formation reactions (Cu metal → CuO or CuO_2). After exposure to solution for 10 min, the hardness decreases to ~0.5 GPa, possibly due to the dissolution of the

copper-oxide/glycine complex reaction (CuO or $CuO_2 \rightarrow CuL_2$). Therefore, the measurements in this study may not be entirely representative of the hardness that occurs on the surface during CMP. However, these measurements show the range of possible values and also provide some insight to the types of films that form due to exposure to these chemistries. Additional experiments to measure the nanohardness after a shorter exposure time to the solutions, as well as after exposure to a flowing slurry containing abrasives may provide a better understanding.

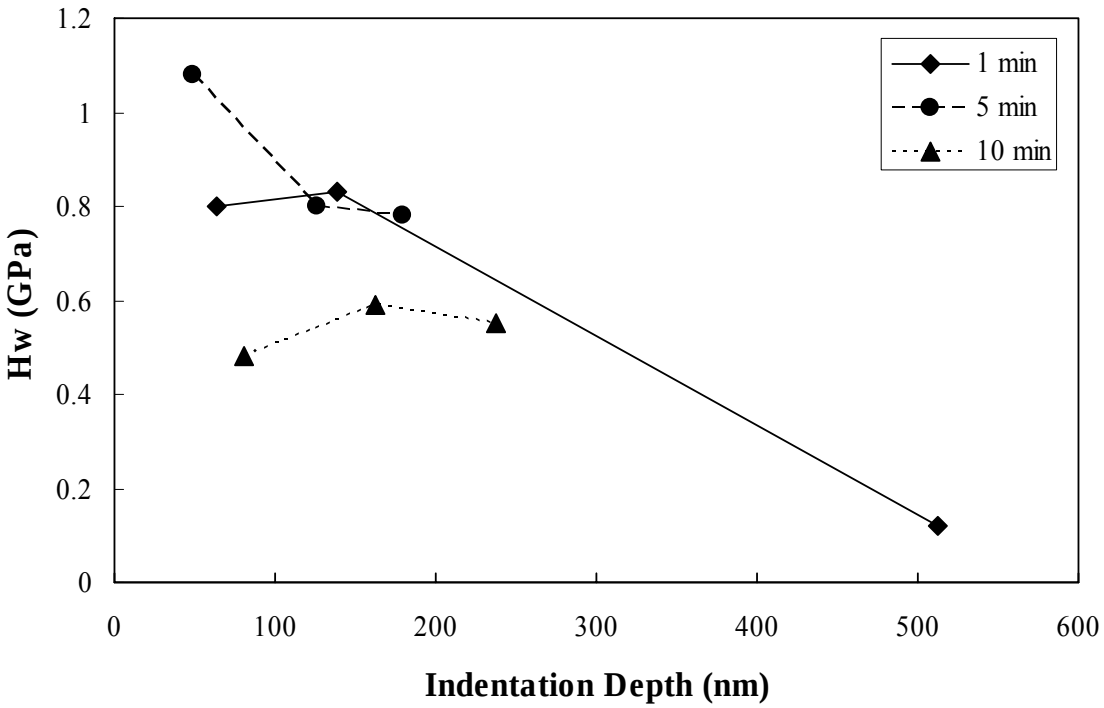

Figure 5.10 Nanohardness versus indentation depth for a copper sample after immersion in 0.1M glycine, 0.1wt% H_2O_2, and 1mM KNO_3 solution at pH 7.0 for various exposure times.

For each condition studied an explanation of the compounds formed from exposure to the solutions was proposed using the potential-pH diagrams, literature and the measured nanohardness values. Currently, work is being done to characterize the sample surfaces using XPS, which could aid in determining the surface films with their hardness values. However, the binding energies for the different states of the copper surface films are very similar [47], which makes it difficult to differentiate by XPS. Also, as shown in this study, the surface films may be very inhomogeneous for some samples. More work is needed to characterize the surface films. To explain the results of the experiments in this study, the potential-pH diagrams for copper in each of the chemistries from the literature [19-22, 41, 43] were used which only provide information on the thermodynamic equilibrium of the system; kinetics of the reactions was not considered [20].

5.5 Conclusions

The addition of chemical additives and changes in the pH of the slurry solution significantly affected the nanohardness of the copper surface due to the formation of different surface films, such as CuO, Cu_2O, or $Cu(OH)_2$, and/or changes in the compactness of the surface film from complexing reactions or dissolution. In general, when the pH was low, the hardness values were near that of Cu metal or slightly harder due to a thin passivation layer. As the pH increased, hardness values varied from softer than Cu metal when hydroxides may have formed, to harder than Cu metal when oxides formed. At very high pH values, the copper surface can become much harder (>7.0

GPa) than that of Cu metal most likely due to formation of a very thick passivation layer.

The addition of glycine to the solution caused the film to be softer than Cu metal in some places (0.9–2.0 GPa) due to the presence of the Cu-glycine complex on the surface and/or a decrease in the compactness of the surface layer due to pitting. Addition of H_2O_2 increased the passivation rate and dissolution of the surface causing hard oxides to form (>10 GPa) in some areas and very porous soft films (<1.0 GPa) in other areas. The addition of BTA only prevented surface dissolution after exposure to solution at pH 8.4, and did not affect the hardness of the surface. Dissolution of the surface was not prevented at pH 3.1 and 10.8 in the presence of BTA, which is consistent with the potential-pH diagrams. The addition of SDS to the solution had no effect on the hardness of the copper surface, as was expected of this surfactant [45]. The hardness measurements of the samples exposed to solutions containing EDTA were similar to the measurements of the samples exposed to glycine solutions.

In general, the hardness measurements indicated the formation of surface films and dissolution of the surface were consistent with the potential-pH diagrams [19-22, 41, 43]. However, there were several samples, such as the sample exposed to the solution with no additives at pH 2.9, that seemed to have hardness values that were inconsistent with the surface films predicted by the potential-pH diagrams. This suggests that the equilibrium phases may not be reached in the 10 min exposure time.

The slurry chemistries studied in this research were used in CMP experiments on 100 mm Cu wafers to obtain MRR data [4, 8]. These experimental MRR data were then compared to MRR predictions from the Luo and Dornfeld CMP model using

measured agglomerate size distributions of the alumina abrasives, where the hardness of the wafer surface was assumed to be equal to that of Cu metal [8]. It was found that for most cases the model predictions did not agree well with experiment, most likely due to the use of a constant surface hardness of Cu metal for all of the chemistries and also neglecting the chemical etch rate of each of the slurries. Future work will incorporate the hardness and etch rate measurements in this study to predict MRR with the Luo and Dornfeld model and compare to our experimental MRR data.

5.6 Acknowledgements

This work was sponsored by FLCC Consortium through a UC Discovery grant. The authors gratefully acknowledge all the companies involved in the UC Discovery grant: Advanced Micro Devices, Applied Materials, ASML, Atmel Corporation, Cadence, Canon, Cymer, Cypress, Dupont, Ebara Technologies Inc., Hitachi Global Storage Technologies, Intel Corporation, KLA-Tencor, Mentor Graphics, Nikon Research Corporation of America, Novellus Systems Inc., Panoramic Technology, Photronics, Synopsys, and TEL USA. The collaboration of Professors Komvopoulos, Dornfeld, and Doyle and their research groups from the University of California, Berkeley is greatly appreciated. Professor Bavarian and his research group from California State University, Northridge, provided the Hysitron Instrument for our experiments and their time and expertise is very much appreciated. Additional thanks to Professor Arrhenius from University of California, San Diego for providing the cuprite samples and Evelyn York for the EDX analysis.

This chapter is a reprint of the material as it appears in the Journal of the Electrochemical Society, Robin Ihnfeldt and Jan B. Talbot, Vol. 155, Issue 6 (2008), also with some additional information. The dissertation author was the primary investigator and author of this paper.

REFERENCES

1. S. Chang, T. Chang, and Y. Lee, *J. Electrochemical Soc.*, **152**, C657 (2005).

2. A. Jindal and S.V. Babu, *J. Electrochemical Soc.*, **151** (10), G709-G716 (2004).

3. M.R. Oliver, *Chemical-Mechanical Planarization of Semiconductor Material*, Springer-Verlag, Berlin, Germany (2004).

4. R. Ihnfeldt, Masters Thesis, University of California, San Diego (2005).

5. R. Ihnfeldt and J. B. Talbot, *J. Electrochemical Soc.*, **153**, G948 (2006).

6. J. Luo and D. Dornfeld, *IEEE Trans. Semi. Manuf.*, **14**, 112 (2001).

7. J. Luo and D. Dornfeld, *Integrated Modeling of Chemical Mechanical Planarization (CMP) for Integrated Circuit Fabrication: from Particle Scale to Feature, Die and Wafer Scales*, Report, University of California, Berkeley (October 2003).

8. R. V. Ihnfeldt and J. B. Talbot, *J. Electrochemical Soc.*, **154**, (12) H1018 (2007).

9. T. Gopal and J. B. Talbot, *J. Electrochemical Soc.*, **154**, H507 (2007).

10 N. Ye and K. Komvopoulos, *J. Tribology*, **125**, 685 (2003).

11. M. A. Meyers and K. K. Chawla, *Mechanical Behavior of Materials*, Prentice-Hall Inc., Upper Saddle River, New Jersey (1999).

12. D. Beegan, S. Chowdhury, and M. T. Laugier, *Thin Solid Films*, **466**, 167 (2004).

13. D. Beegan, S. Chowdhury, and M. T. Laugier, *Surface and Coatings Technology*, **176**, 124 (2003).

14. T. Fang and W. Chang, *Microelectronic Engineering*, **65**, 231 (2003).

15. Y. Liu and A. H. W. Ngan, *Script Mater.*, **44**, 237 (2001).

16. D. Beegan, S. Chowdhury, and M. T. Laugier, *Surface and Coatings Technology*, **201**, 5804 (2007).

17. M. Hakamada, Y. Nakamoto, H. Matsumoto, H. Iwasaki, Y. Chen, H. Kusuda, and M. Mabuchi, *Materials Science and Engineering A*, **457**, 120 (2007).

18. Y. M. Soifer, A. Verdyan, M. Kazakevich, and E. Rabkin, *Scripta Materialia*, **47**, 799 (2002).

19. S. Aksu and F. M. Doyle, *J. Electrochemical Soc.*, **149**, (6) G352 (2002).

20. S. Aksu and F. M. Doyle, *J. Electrochemical Soc.*, **148**, (1) B51 (2001).

21. S. Aksu, L. Wang, and F. M. Doyle, *J. Electrochemical Soc.*, **150**, (11) G718 (2003).

22. S. Aksu and F. M. Doyle, *J. Electrochemical Soc.*, **149**, (7) B340 (2002).

23. T. Du, D. Tamboli, V. Desai, and S.Seal, *J. Electrochem.Soc.*, **151**, (4) G230 (2004).

24. J. Chen, S. Lin, and W. Tsai, *Applied Surface Science*, **233**, 80 (2004).

25. G. Xu, H. Liang, J. Zhao, and Y. Li, *J. Electrochemical Soc.*, **151**, (10) G688 (2004).

26. S. Seal, S.C. Kuiry, and B. Heinmen, *Thin Solid Films*, **423**, 243 (2003).

27. Y. Eli, E. Abelev, and D. Starosvetsky, *Electrochimica Acta*, **49**, 1499 (2004).

28. C. Wang, P. Sherman, and A. Chandra, *International Journal of Manufacturing Technology and Management*, **7**, (5/6) 504 (2005).

29. Hysitron Inc. Product Form, Trade Name Triboscope® Nanomechanical Test Instrument, Minneapolis, MN (2007).

30. Hysitron Inc., Triboscope® Users Manual, Minneapolis, MN (2005).

31. M. Ueda, C. M. Lepienski, E.C. Rangel, N. C. Cruz, and F. G. Dias, *Surface and Coatings Technology*, **156**, 190 (2002).

32. A. Szymanski and J. M. Szymanski, *Hardness Estimation of Minerals Rocks and Ceramic Materials*, Elsevier Science Publishers B. V., New York, NY (1989).

33. R. B. Ross, *Metallic Materials Specification Handbook*, E. & F. N. Spon Ltd, New York, New York (1968).

34. C. A. Klein and G. F. Cardinale, *Diamond and Related Materials*, **2**, 918 (1993).

35. Z. Zhang, G. Lin, S. Zhang, and J. Zhou, *Mat.Sci.and Eng.A*, **457**, 313 (2007).

36. J. H. Bechtold, *Acta Metallurgica*, **3**, 249 (1955).

37. G.L. Pearson, W.T. Read Jr., and W.L. Feldmann, *Acta Metallurgica*, **5**, 181 (1957).

38. Hysitron Incorporated, Tip Selection Guide, NRL-M-003 v2.0, Minneapolis, MN (2004).

39. Y. Feng, K. Siow, W. Teo, K. Tan, and A. Hsieh, *Corrosion (Houston)*, **53**, 389 (1997).

40. C. Klein and C.S. Hurlbut, *Manual of Mineralogy*, John Wiley & Sons, New York, New York (1993).

41. M. Pourbaix, *Atlas of Electrochemical Equilibria in Aqueous Solutions*, National Association of Corrosion Engineers, Houston, Texas (1974).

42. S. S. Tan, M. Ye, and A. G. Milnes, *Solid-State Electronics*, **38**, 17 (1995).

43. S. Tamilmani, W. Huang, S. Raghavan, and R. Small, *J. Electrochemical Soc.*, **149**, G638 (2002).

44. U. B. Patri, S. Aksu, and S. V. Babu, *J. Electrochemical Soc.*, **153**, (7) G650 (2006).

45. T. Gopal and J. B. Talbot, *J. Electrochemical Soc.*, **153**, G622 (2006).

46. N. P. Shevelev, N. G. Klyuchinikov, and I. G. Gorichev, *Uchenye Zapiski Uchenye Zapiski Omskii Gosudarstveniy Pedagogitchesky Institut*, **74**, 111 (1973).

47. J.F. Moulder, W.F. Stickle, P.E. Sobel, and K.D. Bomben, *Handbook of X-ray Photoelectron Spectroscopy*, Physical Electronics, Inc. Eden Prairie, Minnesota (1992).

CHAPTER 6

MODELING MATERIAL REMOVAL RATES FOR COPPER CMP USING COPPER NANOPARTICLES AND ETCH RATES

6.1 Abstract

Measurements of copper nanohardness and etch rate were used with alumina agglomerate size distributions in a model to predict material removal rates (MRR), which were then compared to experimental copper CMP data. Generally, model predictions improved using measured nanohardness compared to predictions using a constant nanohardness of Cu metal. When the slurry pH was acidic (<4) the model overpredicted the MRR. An increase in the slurry pH (>7) increased the nanohardness, and MRR predictions agreed with experimental results. For slurries with small etch rates (<8nm/min), the nanohardness had little affect on the MRR predictions, and the model agreed with experiment. The model was very sensitive to the nanohardness for slurries with large etch rates (>8nm/min), and was unable to predict the MRR.

6.2 Introduction

Chemical mechanical planarization (CMP) is used in integrated circuit manufacturing to remove excess material and provide a globally planarized wafer surface. The CMP process uses a slurry which provides both mechanical action with nanometer-sized abrasive particles and chemical action from the solution additives with a synergistic effect that causes material removal [1, 2]. Various materials, such as copper, tantalum, tungsten, and oxides, are polished with different slurries. Because

copper has become the interconnect material of choice and an understanding of the polishing behavior of copper continues to be important, the focus of our research is on copper CMP [1]. The effects of common slurry additives on the colloidal behavior of alumina suspensions used for copper CMP has been investigated by measurement of zeta potential and agglomerate size distribution [3, 4]. It was found that the presence of copper can increase or decrease the agglomeration of the alumina depending on the chemical additions and pH of the solution [4]. The state of the copper in the solution was typically consistent with the potential-pH equilibrium (Pourbaix) diagrams [4]. The agglomerate size distributions, which were measured under quiescent conditions, were incorporated into an existing model of CMP of Luo and Dornfeld [5, 6]. It was determined that the agglomerated abrasive particles are strong enough to withstand the shear force during CMP, so that they do not break up, and therefore the measurements are applicable in the Luo and Dornfeld model [7]. The MRR predictions were compared to experimental copper CMP data using the same slurry chemistries and as a function of pH [7]. The study showed that the predictions using data from alumina in the presence of copper agreed better with the experimental MRR than the measurements done without copper [7]. In our previous study the hardness of the copper surface was assumed constant and the chemical etch rate of the copper film was neglected [7]. Recently, we have investigated the effects of common slurry additives and pH of the solution on the nanohardness and etch rate of the copper surface and found that the solution chemistry significantly affects these measurements [8]. In this study, the objective was to also incorporate these nanohardness and etch rate measurements of the

copper surface into the model of CMP of Luo and Dornfeld and then compare to our experimental copper CMP data.

The CMP process consists of rotating a polishing pad against a rotating wafer surface while a polishing slurry is passed between the two surfaces. The pad is typically a polyurethane material which applies pressure and transports slurry to the wafer surface [9]. A conditioning disk is rotated across the pad surface to roughen it before and during the CMP process [1]. Previous work summarized the process variables that can affect the MRR [7]. The polishing slurry, which consists of a dispersion of abrasive particles in aqueous media with additives (glycine, H_2O_2, etc.), can have a large affect on the polishing performance. The addition of chemical additives in the slurry can affect the agglomeration and thus, size distributions of the abrasive particles [3, 4, 10, 11]. Agglomeration is also affected by the presence of copper in the slurry, which is removed from the wafer surface during CMP [3, 4]. Various studies of copper CMP have shown that changes in the colloidal behavior of the abrasives can affect the MRR [5, 6, 12-16]. Additionally, many studies have shown that the addition of chemical additives which cause the formation of different copper surface films (Cu metal, CuO, Cu_2O, etc.) also can significantly affect the MRR [17-23]. Jindal and Babu showed that changes in the pH of the slurry affect the structure and compactness of the layer that is formed, thus affecting its nanohardness [17]. The changes in the surface film due to chemical addition and pH variation of the slurry can cause significant changes in the MRR [17].

6.3 Luo and Dornfeld Model

Numerous models of CMP have been proposed and a summary of these models is given elsewhere [7, 24]. In this study the CMP model of Luo and Dornfeld is used to predict MRR [5, 6]. The Luo and Dornfeld model is a mechanical model of CMP [5, 6], which incorporates both particle-particle and particle-surface interactions of the abrasives and the wafer surface through the average abrasive size (x_{avg}), the standard deviation of the abrasive size distribution (σ), and the wafer surface hardness (H_W), in order to predict the MRR [5]. A detailed derivation of the Luo and Dornfeld model can be found elsewhere [5, 6]. The MRR (in thickness/time) as a function of the abrasive size distribution (x_{avg} and σ) and the wafer and pad hardness (H_W and H_P) is given by the following equation:

$$MRR = \underbrace{\left(\frac{B_1}{H_W^{3/2}}\right)\left(\frac{1}{x_{avg}} + \frac{6\sigma}{x_{avg}^2} + \frac{9\sigma^2}{x_{avg}^3}\right)}_{\text{Thickness Removed}}\underbrace{\left[1 - \Phi\left(3 - B_2\left(\frac{1}{H_P} + \frac{2}{H_W}\right)\frac{\left(x_{avg} + 3\sigma\right)}{\sigma}\right)\right]}_{\text{Probability of Active Abrasives}} + \underbrace{C_0}_{\text{Etch Rate}} \quad [6.1]$$

where B_1 and B_2 include properties of the slurry, pad, wafer, and polishing conditions. Definitions and values for the parameters in B_1 and B_2 can be found elsewhere [7]. In Eq. 6.1, Φ is the normal probability density function. The product of the first two terms of Eq. 6.1 represents the thickness removed per unit time while the third term represents the probability of active abrasives (abrasives actively removing material). The last term in Eq. 6.1 is the chemical etch rate of the slurry, C_0, which is often neglected because it is usually small (<5%) compared to the overall MRR [5, 6]. In this study of copper CMP the etch rate is included. As shown in Eq. 6.1, this model has a complicated

dependence on the wafer hardness with a dependence to the -3/2 power in the first term and inversely in the probability density function. The hardness of the copper wafer surface is on the order of 0.05 – 20 GPa [8], while the hardness of the pad used is 100 MPa [6]. Although the influence of the H_W parameter in Φ on the MRR is small (<10%) when H_W >5 GPa, it becomes significant (>20%) when H_W<2 GPa [5, 6]. The probability of active abrasives must be less than 0.5 (so that Φ>0.5), because the model assumes a Gaussian particle distribution and the size of the abrasives actively removing material must be greater than the average abrasive size, x_{avg} [5, 6, 7]. This term is then limited according to the following criteria:

$$\frac{x_{avg}}{\sigma} < \frac{3\left(1 - B_2\left(\frac{1}{H_P} + \frac{2}{H_W}\right)\right)}{B_2\left(\frac{1}{H_P} + \frac{2}{H_W}\right)} . \qquad [6.2]$$

In the model when the value of the left side approaches that of the right side of Eq. 6.2, the MRR predictions become very large and unreasonable.

The Luo and Dornfeld model dependence of MRR on its parameters has been only verified conceptually, that is, they have shown that the trends of the model MRR predictions follows that of the experimental data [6]. This is typically done using experimental data to determine the unknown parameters (B_1, B_2, etc.) in the model, and then using these fitted parameters to make predictions. While this does not experimentally verify the model for any CMP process, it does show that the model MRR behaves similar to experiment with changes in the physical parameters. This conceptual verification for the dependence of the MRR on down pressure, wafer

velocity, pad hardness, abrasive size, and standard deviation of the abrasive size distribution has been done for CMP of SiO_2 [6]. However, the MRR dependence on H_W is complicated as the slurry chemistry not only affects hardness but the abrasive size distribution. Luo and Dornfeld investigated the dependence of their model MRR on H_W by assuming the wafer surface consisted of a bilayer structure where the bottom layer was a harder passive film and the upper layer was a softer porous film due to the slurry chemical etching [6]. By increasing the concentration (by weight) of the abrasives, the MRR increased linearly. At a certain concentration the MRR is equal to the generation rate of the upper softer layer and the softer layer is removed as soon as it is generated. Further increase of the concentration of the abrasives increases the MRR linearly, but at a different slope due to the abrasives now removing the harder bottom material. This transition of slope for the two material removal regions has been observed for SiO_2, tungsten, copper and tantalum CMP [6]. The Luo and Dornfeld MRR predictions were compared to experimental MRR for tungsten with abrasive concentration increasing from 2 to 15% where this change in slope was observed, and the model was able to successfully predict these changes by fitting several data points to obtain the unknown parameters (B_1, B_2, H_W) and then using these in the model to make predictions [6].

The goal of our research is to incorporate the chemical effects of the slurry into the Luo and Dornfeld model through hardness and abrasive size distribution measurements. Prediction of MRR for CMP of copper is more complicated than of SiO_2 or tungsten due to the complex chemical and electrochemical reactions between the slurry and the copper during polishing, and the coupled effect of these on the mechanical properties of the surface [25]. Therefore, our approach has been to

investigate the effects of chemical additives in the slurry by experimentally measuring the abrasive size distribution, nanohardness, and etch rates of copper in these solutions, which are then included in the model. The motivation for further development of this model is to improve the understanding of the copper CMP process and also to provide a tool to predict MRR and compare to experimental data.

It should be noted that the experimental copper CMP data used in this study is limited to only one set of polishing conditions (1 psi down pressure, 30 rpm platen and wafer rotational speed, 150 ml/min slurry delivery rate, and 2 min polish time) using 100 mm silicon wafers sputter deposited with 1 μm copper on 30 nm tantalum with the same slurry chemistries and as a function of pH [7]. A detailed procedure for the copper CMP experiments can be found elsewhere [3, 7]. Further comparison of the model to experimental copper CMP data over a wider range of conditions (various P_0, H_P, v, etc.) is needed to better validate this model for the copper CMP process. However, the comparisons in this study provide a better understanding of the copper CMP process.

6.4 Results and Discussion

6.4.1 Parameters Used in Luo and Dornfeld Model

The parameters used in Eq. 6.1 were chosen to correspond to the CMP experiments that were performed. In this study B_1 in Eq. 6.1 is 3.18×10^7 $nm^2GPa^{1.5}/min$ and B_2 is 1720 kPa. The hardness of the IC1000 pad is 100 MPa [6]. The parameters x_{avg}, σ, H_W, and C_0 in the Luo and Dornfeld model are dependent upon the chemistry in the slurry, and thus, were experimentally measured. In this study only

the x_{avg} and σ values from the distributions with copper in the solution will be used [7]. Table 6.1 lists the agglomerate size (x_{avg}) and the standard deviation of the size distribution (σ) for the alumina agglomerates in 1mM KNO_3 and 0.12mM copper solution with various additives and at different pH values. Also listed in Table 6.1 are the nanohardness (H_W) and the etch rate (C_0) of the copper film measured after exposure to each of the solutions. The previous study investigated the nanohardness of the copper surface over a wide range of indentation depths (5-120 nm) by varying the maximum applied load between 50-3000 μN [8]. The H_W value used in this study was an average of 2-3 of the nanohardness values measured with a maximum applied load between 50-100 μN. This range was the lowest applied load range possible, which yielded measurements with fully developed plastic deformation, and is therefore, the smallest indentation depth that can be measured using this technique. However, the indentation depths of our measurements (>5 nm) are still greater than that of the abrasive particle into the wafer during CMP (<1 nm) [6]. A detailed discussion of these measurements can be found elsewhere [4, 8].

Table 6.1 Average agglomerate size and standard deviation of the alumina in solution, average surface nanohardness and etch rate of the copper film after exposure to solution, and nanohardness values necessary to obtain the experimental MRR.

Solutions	pH	x_{avg}* (nm)	σ* (nm)	C_0 (±4 nm/min)	H_W (±0.3 GPa)	H_N (GPa)
a) 1 mM KNO_3	2.9	235	9	0.7	4.55	>16
	8.3	1870	445	0.0	4.76	>3
	11.7	3750	2510	2.6	5.40	>5
b) 1 mM KNO_3, 0.1 M glycine	3.1	219	9	1.2	2.38	>17
	8.5	3750	319	7.6	2.99	>2
	10.0	4760	820	0.0	15.6	1 - 11
c) 1 mM KNO_3, 0.1 M glycine, 0.1 wt% H_2O_2	3.0	199	15	45.0	3.58	***
	8.3	1430	97	33.0	2.92	0.7
	10.0	2380	241	14.0	0.61	0.4
d) 1 mM KNO_3, 0.1 M glycine, 2.0 wt% H_2O_2	3.0	167	11	37.5	3.05	5 - 6
	8.3	1570**	12**	55.5	0.28	0.3
	10.0	1280	124	33.1	6.16	1
e) 1 mM KNO_3, 0.1 M glycine, 0.1 wt% H_2O_2, 0.01 wt% BTA, 0.1 mM SDS	3.0	341	74	1.6	3.24	>12
	8.4	1150	94	0.0	5.29	>3
	10.8	957	93	8.6	2.04	0.8
f) 1 mM KNO_3, 0.01 M EDTA, 0.1 wt% H_2O_2, 0.01 wt% BTA, 0.1 mM SDS	2.6	508	58	0.0	9.65	>7
	9.0	1930	136	0.0	2.54	>3
	10.9	883	142	0.0	12.7	>4

*measurements used solutions which also contained 0.12 mM copper nanoparticles

**Measured x_{avg} and σ values approach the limit of Eq. 6.2, therefore assumed probability of active abrasives=0.2%

***cannot obtain exp. MRR

The MRR predictions are very sensitive to the x_{avg}, σ, and H_W parameters and small changes in these parameters can cause large changes in the values. As previously stated, changes in chemistry will affect the H_W and C_0 parameters as well as the agglomerate size distribution, x_{avg} and σ. First, the behavior of x_{avg} and σ will be discussed. Figure 6.1a shows the dependence of the probability of active abrasives (3rd term in Eq. 6.1) on the x_{avg} and σ parameters. This figure shows that when all other parameters are held constant with σ=10 nm and x_{avg} is increased, the probability of active abrasives increases to the maximum value of 0.5. This is because as x_{avg} increases, the active abrasive size, which is equal to $x_{avg} + 3\sigma$, approaches x_{avg}. When all parameters are held constant with x_{avg} =200 nm and σ is decreased, the probability of active abrasives increases to 0.5 also because the active abrasive size approaches x_{avg}.

Examination of the second term of Eq. 6.1 shows that the MRR decreases as x_{avg} increases and increases as σ increases. Figure 6.1b shows the MRR dependence on x_{avg} and σ values where each parameter is varied while all other parameters are held constant. This figure shows three curves using different σ values (σ= 10, 50, 200 nm) where x_{avg} is varied, and one curve with x_{avg} =200 nm where σ is varied. The MRR has a U-shape dependence on the x_{avg} parameter where the second term of Eq. 6.1 is dominant (resulting in large MRR) when x_{avg} is small, and the third term is dominant when x_{avg} is large. Similarly, the MRR has a U-shape dependence on the σ parameter, but the second term of Eq. 6.1 is dominant when σ is large, and the third term is dominant when σ is small. For both x_{avg} and σ, the MRR is at a minimum when the second and third terms of Eq. 6.1 are similar. The three curves with different σ values with varied x_{avg} show that the minimum MRR decreases as σ increases.

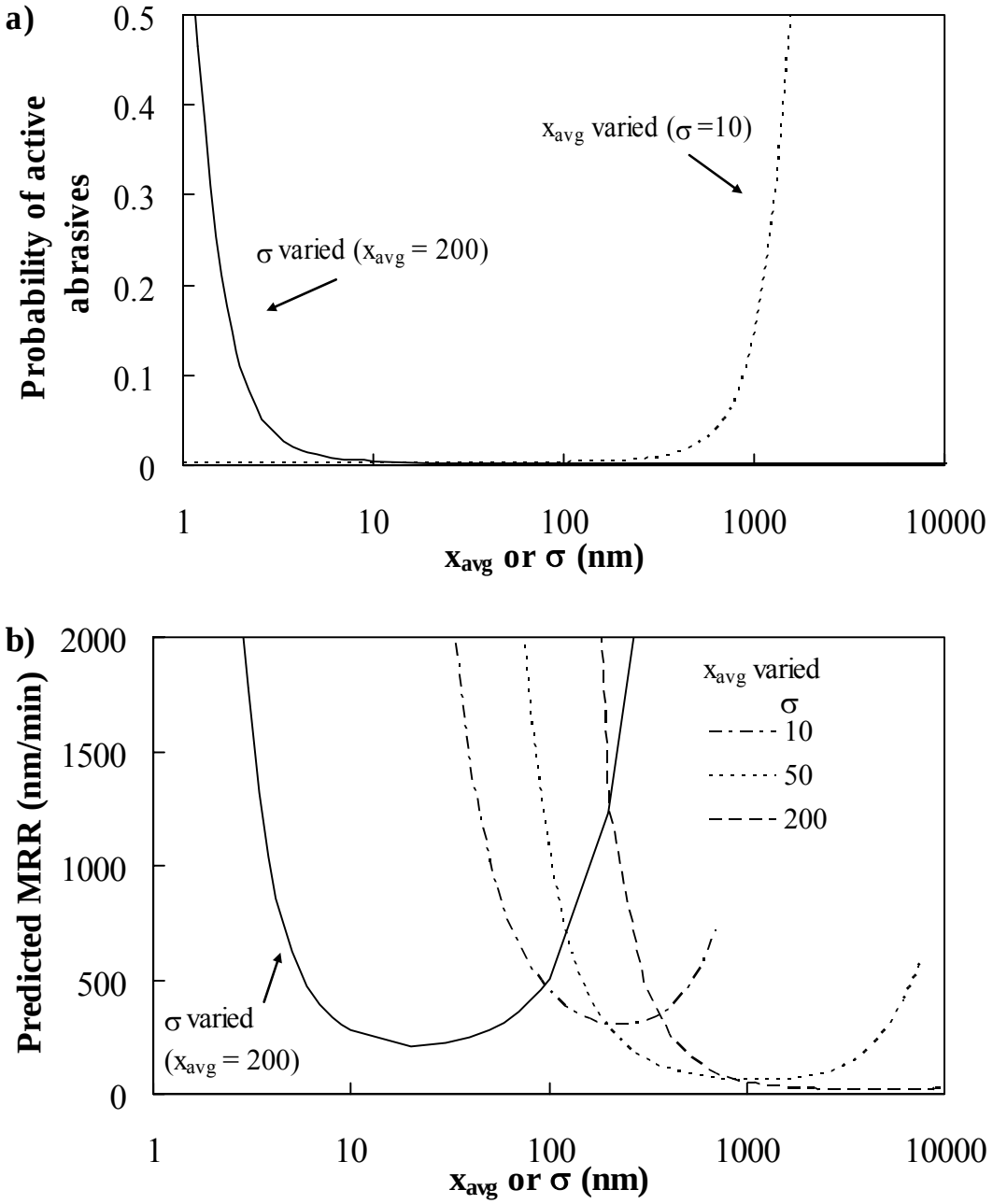

Figure 6.1 a) Probability of active abrasives and b) predicted MRR from Eq. 6.1 versus either x_{avg} or σ, with all other values held constant (H_W=2.3 GPa, C_0=0 nm/min).

Examination of Eq. 6.1 shows that increasing H_W causes both the first and third terms to decrease as previously discussed. Figure 6.2 shows the predicted MRR versus

H_W for various sets of x_{avg} and σ, with all other values held constant. Figure 6.2a shows that at small H_W values the MRR is very sensitive to H_W, and when H_W is large, the MRR is relatively insensitive to it. For three values of x_{avg} (100, 200, and 1000 nm), when x_{avg} is increased from 100 to 200 nm, the MRR predictions decrease, but when x_{avg} is increased from 200 to 1000 nm, the MRR predictions increase. As discussed, this is due to the U-shape dependence of the MRR on the x_{avg} parameter as shown in Fig. 6.1. Similarly, Figure 6.2b shows the sensitivity of the MRR predictions versus H_W for three different values of σ (10, 50, and 200 nm). When H_W becomes very large ($H_W \rightarrow \infty$) in Eq. 6.1, the MRR is equal to the chemical etch rate, C_0. Understanding the behavior of the variables of interest (x_{avg}, σ and H_W) in this model will be useful in the following explanation of the model predictions for our copper system.

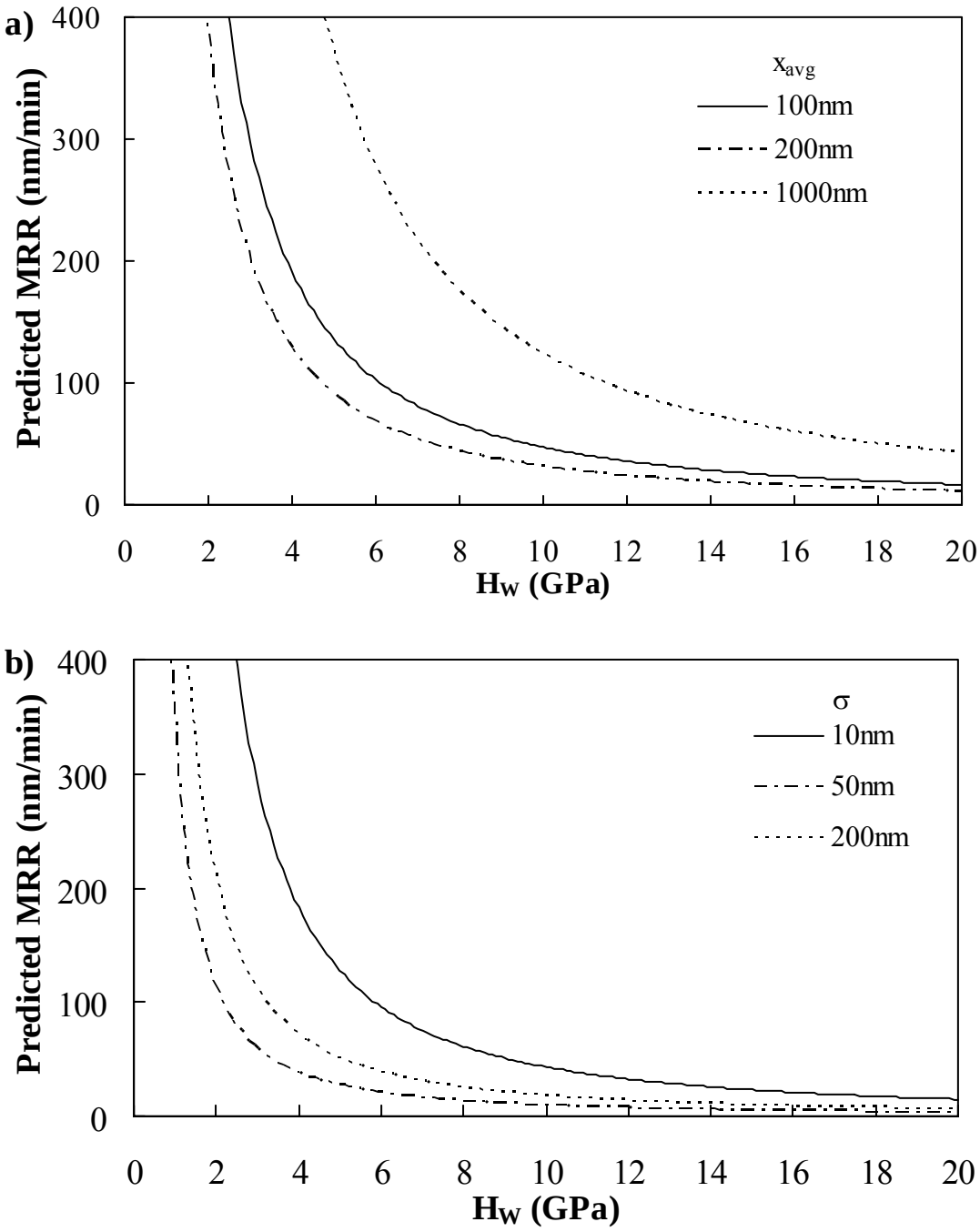

Figure 6.2 Predicted MRR versus H_W from Eq. 1 for a) various x_{avg} values with σ=10nm and b) various σ values with x_{avg}=500nm, with all other values held constant (C_0=0 nm/min).

Our previous modeling work incorporated measured x_{avg} and σ into the Luo and Dornfeld model for each of the slurry chemistries using a constant surface H_W value of 2.3 GPa, found in the literature for Cu metal [26, 27], and neglected the chemical etch rate (i.e. C_0=0) [7]. Table 6.2 lists the experimental MRR data for each of the slurry chemistries, the model predictions using the constant H_W value [7], and the model predictions using the measured H_W values and chemical etch rates. Comparison of the model predictions to the experimental MRR shows that for almost all cases the MRR prediction using measured H_W and C_0 is in better agreement with the experimental MRR than the prediction using constant H_W. However, the predicted MRR for several of the solutions, even using the measured H_W and C_0, do not agree with experiment. To explain the model predictions, the data are divided into three categories. The first category is for all solutions with pH <3.1, where model predictions were much larger than experimental MRR. The second category is for solutions with pH>8 and smaller etch rates, C_0<8 nm/min (solutions a, b, and f with pH>8, and e with pH 8.4), where the model predictions agreed well with experiment. The third category is for solutions with pH>8 and larger etch rates, C_0>8nm/min (solutions c and d with pH>8, and e with pH 10.8), where the model disagrees with experiment. Furthermore, to help understand the model predictions, additional calculations were performed to determine the hardness value necessary (H_N) in the Luo and Dornfeld model to obtain a prediction in agreement with the experimental MRR. Table 6.1 lists the hardness values necessary to obtain the experimental MRR (H_N) within the experimental error of ±14 nm/min. Previous experimental work has shown that hardness values between ~0.05 – 20 GPa are physically possible for the copper surface with formation of different films (Cu_2O, CuO,

Table 6.2 Experimental MRR and Luo and Dornfeld model predictions of MRR using various slurries at different pH.

Solutions*	pH	Experimental MRR (±14 nm/min)	Model MRR w/ constant H_W [7] (nm/min)	Model MRR w/ measured H_W and C_0 (nm/min)
a	2.9	4	344	117
	8.3	4	30	10
	11.7	0	39	13
b	3.1	2	320	304
	8.5	9	12	16
	10.0	15	10	1
c	3.0	8	244	167
	8.3	287	35	57
	10.0	350	19	178
d	3.0	113	303	232
	8.3	289	NR	343**
	10.0	166	35	41
e	3.0	0	155	93
	8.4	11	41	11
	10.8	242	47	65
f	2.6	2	88	10
	9.0	9	26	22
	10.9	8	53	4

*As listed in Table 6.1I

**Measured x_{avg} and σ values approach the limit of Eq. 6.2, therefore assumed probability of active abrasives=0.2%

etc.) and changes in compactness due to etching and passivation [8]. Therefore, Table 6.1 only gives values in this physically reasonable range.

6.4.2 Solutions with pH<3.1

Comparing the model predictions in Table 6.2 with the experimental MRR shows that for all solutions with pH<3.1, the model overpredicts the MRR using both the constant H_W and using the measured H_W and C_0, except for solution f. The major difference in the experimental data for the solutions with pH<3.1 are the measured x_{avg} and σ values. For the solutions with pH<3.1, the x_{avg} values are <510 nm and the σ values are <75 nm, while the x_{avg} and σ values for the solutions with pH>8 are much larger (x_{avg}>800 nm, σ>90 nm). Figure 6.3a shows the predicted MRR versus H_W for the solution with 1mM KNO_3 (solution a) at three pH values. The curve for pH 2.9 is

significantly higher than the curves for the pH values >8, which is due to the smaller x_{avg} and σ values. Similar behavior is observed for solutions b-f where the model MRR curve is higher for the low pH value compared to those at higher pH values. Copper CMP experiments performed by Matijevic et al. have shown that increasing the particle size, when using the same number of particles, increases the MRR [28]. However, increasing the particle size, while holding the weight percent of particles constant, decreases the MRR, as was shown by Bielmann et al. [29] for tungsten CMP, and is consistent with the Luo and Dornfeld model behavior shown here. The experimental MRRs for the solutions with pH<3.1 are all small, <8 nm/min, except for solution c, which has an experimental MRR of 113 nm/min at pH 3.0. As shown in Figure 6.3b, to obtain small MRR predictions, the H_W values must be large (the surface must be hard). However, the measured H_W values shown in Table 6.1 are not significantly harder for the solutions with pH<3.1 as compared to the solutions with higher pH. According to the potential-pH diagram for the copper-water system [30] at pH 2.9 the copper surface should be in the form of Cu metal. According to literature the hardness of Cu metal is ~2.3 GPa [26, 27]. On the Moh's hardness scale the hardness decreases from Cu_2O > CuO > Cu metal > $Cu(OH)_2$ [31]. The measured H_W value of 4.6 GPa for solution a at pH 2.9 suggests the formation of an oxide layer on the surface, which is inconsistent with the potential-pH equilibria [30]. However, several researchers propose that a very thin layer of copper oxide exists on the copper surface at all pH ranges in the copper-water system and as the pH increases the compactness of the oxide layer increases [32]. This is consistent with our hardness measurements shown in Table 6.1, which increase as the pH increases for solution a. For solution a at pH 2.9, the MRR prediction is

improved using the measured H_W, but is still much larger than the experimental MRR of 4 nm/min. Listed in Table 6.1 and also shown in Figure 6.3b is the hardness value necessary to obtain the experimental MRR, which for solution a at pH 2.9, the H_N must be >16 GPa.

The addition of glycine did not have much effect on the etch rate or experimental MRR, and the model predictions for solution b at pH 3.1 were similar to that of the copper-water system, solution a. In solution b, the glycine forms soluble complexes with the copper in certain pH ranges [33]. At pH 3.1 the measured H_W was 2.4, which is similar to the hardness of Cu metal, and there was very little improvement in the model prediction with the measured H_W. The H_N values to obtain MRR predictions in agreement with the experimental MRR at pH 3.1 were >16 GPa, which is similar to the slurry with no additives.

The addition of H_2O_2, solution c, significantly increased the etch rate. The potential-pH equilibria for solution c is similar to that of the copper-water-glycine system with the addition of H_2O_2 increasing the redox potential which would cause the copper to more likely form the soluble copper-glycinate complex [33, 34]. This is consistent with the larger etch rate for solution c, however, it is larger than the experimental MRR. Therefore, it is not possible to obtain MRR predictions in agreement with the experimental MRR as from Eq. 6.1, as $H_W \rightarrow \infty$, the MRR is equal to C_0.

Increasing the H_2O_2 concentration, solution d, caused the experimental MRR to increase at pH 3.0 and the etch rate remained large for this system. For solution d at pH 3.0 the model prediction is improved with the measured H_W, but not within the

experimental MRR error. The hardness to obtain an MRR prediction in agreement with the experimental MRR is H_N~5 - 6 GPa, which is a fairly narrow range and indicates that the model is more sensitive to the H_W value for this solution.

In solution e, BTA is a corrosion inhibitor that can bind to the copper surface and prevent dissolution [34]. SDS is a surfactant which will affect the alumina agglomeration and distribution, but it should not affect the copper surface [10]. The H_2O_2 will increase the formation of soluble complexes as well as increase the surface oxidation [34]. The etch rate for solution e at pH 3.0 indicates little dissolution of the surface. The MRR prediction is improved using the measured H_W value, but not within the experimental MRR error. The H_N to obtain the experimental MRR is H_N>12 GPa.

In solution f, EDTA behaves similarly to the glycine, in that it forms soluble complexes with copper in certain pH ranges [25]. Using the measured H_W value improves the MRR prediction, which agrees with the experimental MRR.

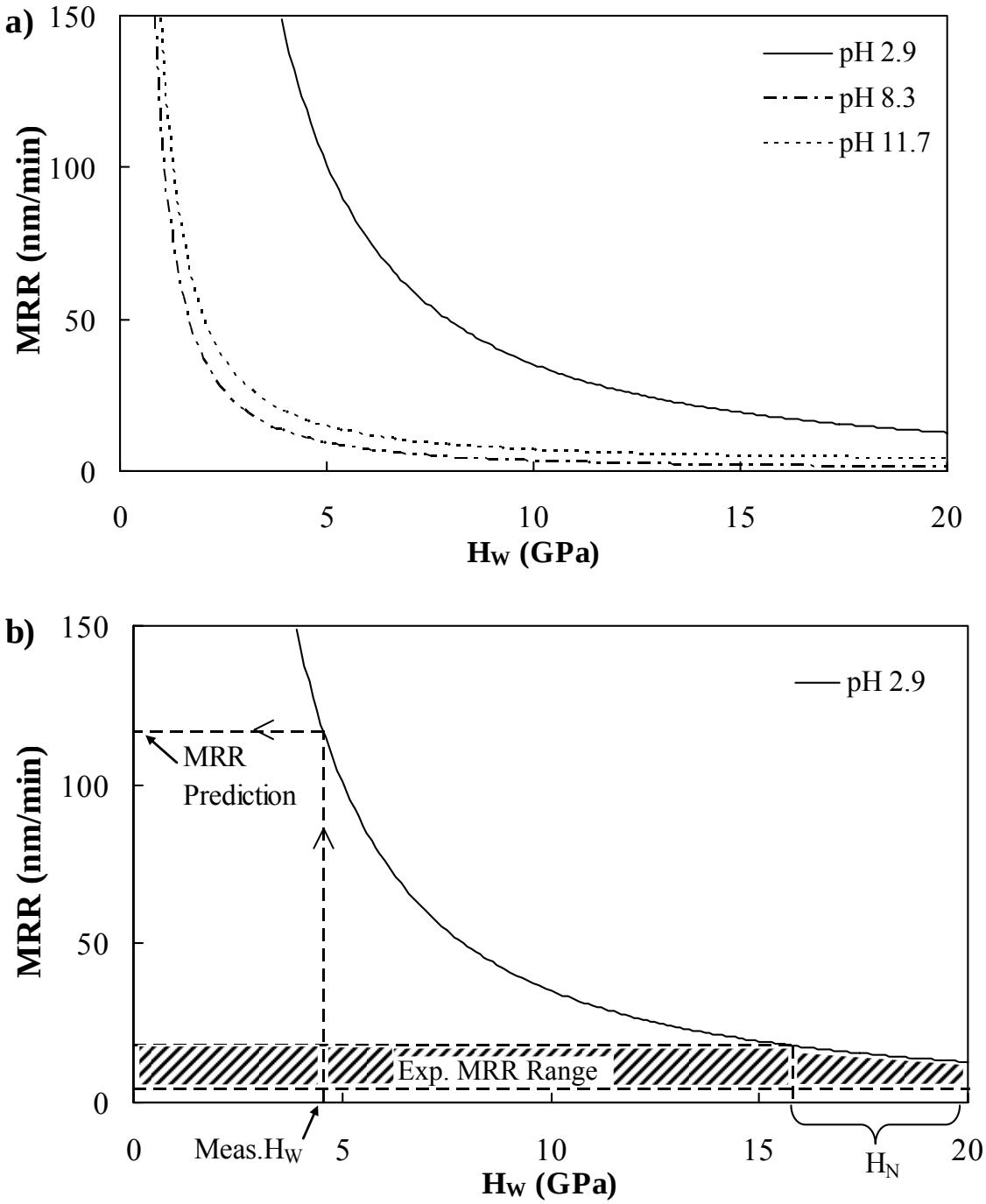

Figure 6.3 MRR versus H_W for an alumina slurry with 1mM KNO_3 at a) all pH values and b) pH 2.9 using x_{avg}, σ, and C_0 from Table 6.1.

For solutions a-e at pH<3.1, the hardness required to obtain the experimental MRR, H_N, was much larger than the measured H_W value. For these solutions, it is

possible that a copper oxide layer formed on the surface that is so thin it cannot be measured using the technique in this study. It may also be possible that the film formed on the surface under quiescent conditions is not the same as the film formed during CMP. For solution f, the measured H_W value at pH 2.6 was much larger than for the previous systems, indicating that a thicker passivation layer may have formed which our nanohardness measurement technique is capable of detecting.

6.4.3 Solutions with pH>8 and Small Etch Rates

For the solutions with pH>8 and etch rates <8 nm/min, the model predictions agreed well with experiment. The small etch rate (C_0) may be indicative of a less active surface, which is consistent with our copper CMP data that shows when C_0<8 nm/min, the MRR is also small, <15 nm/min. As shown in Figure 6.3b, to obtain small experimental MRRs, the H_W values need to be larger (typically >3 GPa to obtain MRR<15 nm/min), and thus are in the region where the model is not as sensitive to the H_W value.

For solution a, the etch rates were small at both pH 8.3 and 11.7. The model predictions at both pH values improved when the measured H_W was used, and are in agreement with the experimental MRR. For these pHs, the range of H_N values to obtain MRR predictions within the experimental MRR error is very wide because the model is insensitive to the H_W value for these solutions.

Solution b is very similar to solution a, with small etch rates and experimental MRRs at pH 8.5 and 10.0. The small etch rate at pH 10.0 suggests very little dissolution/complexation of the copper surface, whereas the slightly larger etch rate at

pH 8.5 suggests some dissolution of the surface, most likely in the form of a soluble copper-glycinate complex [33, 34]. At these pHs the MRR predictions were in agreement with the experimental MRR using both the constant H_W and measured H_W. The wide range of H_N values that produce MRR predictions in agreement with the experimental MRR illustrate further that the model is insensitive to the H_W parameter for these solutions.

For solution e there was no surface dissolution and the experimental MRR was small at pH value 8.4. The model prediction improves using the measured H_W and agrees with the experimental MRR. At pH 8.4 the model is not as sensitive to the H_W value.

For solution f there was no dissolution of the surface for all pH values, and the experimental MRR values were also small. At pH 9.0, the model predictions using constant H_W and measured H_W were similar and agreed with experiment. At pH 10.9, the model prediction improved using measured H_W, which also agreed with experiment. For both pHs, the model is not sensitive to the H_W parameter.

6.4.4 Solutions with pH>8 and Large Etch Rates

For the solutions with pH>8 and etch rates >8nm/min, the model predictions did not agree with experiment. These solutions were more chemically active, and the experimental MRR values were also larger, >100nm/min. Figure 6.4 shows the model MRR versus H_W for solution c at pH 8.3. The figure shows that for MRR predictions that are larger, the model is more sensitive to the hardness parameter and a single value is needed to predict the experimental MRR.

For solution c, the experimental MRRs for pH values 8.3 and 10.1 were much larger than the copper-water-glycine system without H_2O_2. Using the measured H_W values in the model improves the MRR predictions, however, the model MRR disagrees with the experimental MRR increase as the pH increases. For these solutions the H_N to obtain MRR predictions in agreement with the experimental MRR is a single value, indicating that the model is very sensitive to the H_W value. This slurry is more chemically active and has larger etch rates and experimental MRRs than the slurry with no additives or with just glycine. The predicted MRR may have disagreed with experiment because the measured H_W values are not representative of the H_W of the surface during CMP.

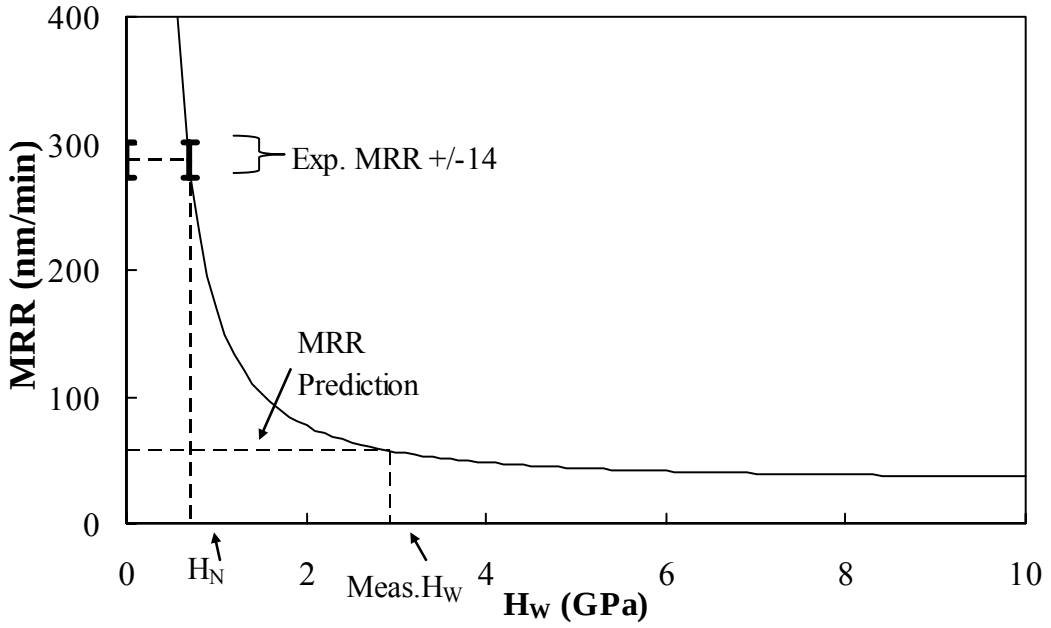

Figure 6.4 MRR versus H_W for an alumina slurry with 0.1M glycine, 0.1wt% H_2O_2, and 1mM KNO_3 at pH 8.3 using x_{avg}, σ, and C_0 from Table 6.1.

For solution d, all predictions using either constant H_W or measured H_W disagree with experiment. However, the predictions are significantly improved using the measured H_W value and incorporating the etch rates. At pH 8.3 the model prediction was outside of the limit of Eq. 6.2, and caused the model to give unreasonably large MRR predictions (>1200 nm/min). According to Luo and Dornfeld, the probability of active abrasives is typically ~0.2% which was determined by solving Eq. 6.1 using experimental down pressures and corresponding MRR values [6]. From our previous study the calculated probability of active abrasives ranged from ~0.17-0.27% for the MRR predictions that were within the limit of Eq. 6.2 [7]. To obtain a reasonable MRR prediction at pH 8.3 the second term in Eq. 6.1 was assumed to be 0.2%. This gave a much improved MRR prediction at pH 8.3. At pH 10.0, using the measured H_W did not improve the MRR prediction, however, incorporation of the etch rate did improve it. At both pHs, the H_N to obtain MRR predictions in agreement with the experimental MRR was a single value. For pH 10.0, the large difference in the measured H_W of 6.2 GPa, which is consistent with the formation of a copper oxide, and the H_N of ~1.0 GPa, which is much softer than Cu metal, suggests that a very different surface film may be forming during CMP compared to the film formed under quiescent conditions.

For solution e at pH 10.8, the etch rate was smaller than those of solutions c and d, however, the experimental MRR value was still large. The model prediction improved using measured H_W. The H_N of ~0.8 GPa at pH 10.8 suggests that the copper surface may be much softer during CMP than it is under quiescent conditions, possibly due to increased etching from the flowing slurry, which can cause increased pitting and a decrease in the compactness of the surface.

The MRR predictions in Table 6.2 show that the Luo and Dornfeld model was unable to predict the experimental MRR for several conditions. There are several reasons that may have caused the model to disagree. The H_W values were measured under quiescent conditions. Also, the technique used to measure the hardness is only capable of measuring at indentation depths >5nm, which is deeper than the indentation of an abrasive into the wafer surface during CMP [6]. Therefore, the H_W values used may not be entirely representative of the surface that occurs during polishing. Additionally, the Luo and Dornfeld model incorporates the hardness of the surface through a single H_W parameter which is assumed constant during the entire duration of the polish [5, 6]. Researchers have suggested that one mechanism of removal during copper CMP may be from growth of a passivation layer, mechanical abrasion of the passive layer, and then regrowth [17]. For this type of removal mechanism the copper surface hardness is most likely not constant during polishing. However, additional work is needed to obtain H_W values more representative of the copper surface during CMP.

To explain the results of the experiments in this study the potential-pH diagrams for copper in each of the chemistries from the literature [25, 30, 33, 34] were used. It should be noted that these diagrams only provide information on the thermodynamic equilibrium of the system [33] and kinetics of the reactions was not considered. Furthermore, this study infers the state of the copper surface using the potential-pH diagrams [25, 30, 33, 34], the measured H_W value, and literature [17, 31, 32] observations. A more quantitative analysis of the surface layer, such as x-ray

photoelectron spectroscopy (XPS), is needed to verify the state of the copper on the surface for each of the chemistries.

6.5 Conclusions

The incorporation of the measured copper surface nanohardness and chemical etch rates into the Luo and Dornfeld model improved the agreement between the MRR predictions and the experimental MRR only under certain conditions. When the pH of the slurry was acidic, the model overpredicted the MRR because the measured hardness of the surface was too small, possibly due to a very thin, harder passivation layer which could not be measured. As the pH increased the hardness increased, which may be due to the thickness of the passivation layer on the copper surface increasing, and the model predictions agreed much better with experiment. Addition of glycine to the solution affected the hardness of the surface but did not affect the MRR, and the MRR predictions were similar to the slurry without additives; which were overpredicted at acidic pH, and agreed with experiment as the pH increased. Addition of H_2O_2 significantly increased the etch rates and experimental MRRs, and the model was unable to predict the MRR.

In general for the chemically-inactive slurries (etch rate <8 nm/min), the model was not very sensitive to the hardness parameter, and model predictions were in fairly good agreement with experimental MRR. For slurries that were chemically active (etch rate >8 nm/min), the model was very sensitive to the hardness parameter and, therefore, was unable to predict the MRR. The small discrepancies in the hardness of the surface measured under quiescent conditions and the hardness of the surface during CMP

caused large differences in the predicted MRR. However, in all cases the MRR predictions were improved using the measured H_W and etch rates compared to the predictions using the constant H_W of Cu metal and neglecting the etch rates [7]. It should also be noted that while the model was unable to predict the MRR for the very chemically-active slurries, the model gave reasonable values that followed the trend of the experimental MRR data with respect to pH.

The nanohardness and etch rate measurements were done under quiescent conditions and may not represent the surface that occurs during polishing. However, the nanohardness measurements provide information on the range of physically possible values that may occur during processing and are an improvement to using a constant surface hardness. It is possible that the Luo and Dornfeld model may provide very reasonable MRR predictions as long as the measured abrasive size and distribution, x_{avg} and σ, of the dispersion, and the H_W parameter are representative of the copper surface during polishing and if such measurements are possible.

6.6 Acknowledgements

This work was sponsored by FLCC Consortium through a UC Discovery grant. The authors gratefully acknowledge all the companies involved in the UC Discovery grant: Advanced Micro Devices, Applied Materials, ASML, Atmel Corporation, Cadence, Canon, Cymer, Cypress, Dupont, Ebara Technologies Inc., Hitachi Global Storage Technologies, Intel Corporation, KLA-Tencor, Mentor Graphics, Nikon Research Corporation of America, Novellus Systems Inc., Panoramic Technology,

Photronics, Synopsys, and TEL USA. The collaboration of Professors Komvopoulos, Dornfeld, and Doyle from the University of California, Berkeley is greatly appreciated.

This chapter, in full, has been submitted for publication of the material as it may appear in the Journal of the Electrochemical Society, Robin Ihnfeldt and Jan B. Talbot, 2008. The dissertation author was the primary investigator and author of this paper.

REFERENCES

1. M. R. Oliver, *Chemical-Mechanical Planarization of Semiconductor Material*, Springer-Verlag, Berlin, Germany (2004).

2. G. Yehiel and R. Kistler, *Electrochemical 198th Society Meeting Abstracts*, **2000-2**, 496 (2000).

3. R. Ihnfeldt, Masters Thesis, University of California, San Diego (2005).

4. R. Ihnfeldt and J. B. Talbot, *J. Electrochemical Soc.*, **153**, G948 (2006).

5. J. Luo and D. Dornfeld, *IEEE Trans. Semi. Manuf.*, **14**, 112 (2001).

6. J. Luo and D. Dornfeld, *Integrated Modeling of Chemical Mechanical Planarization (CMP) for Integrated Circuit Fabrication: from Particle Scale to Feature, Die and Wafer Scales*, Report, University of California, Berkeley (October 2003).

7. R. Ihnfeldt and J. B. Talbot, *J. Electrochemical Soc.*, **154** (12), H1018 (2007).

8. R. Ihnfeldt and J. B. Talbot, *J. Electrochemical Soc.*, to be published (2008).

9. A. K. Babel and R. A. Mackay, *Mat. Res. Soc. Symp. Proc.*, **566**, 135 (2000).

10. T. Gopal and J. B. Talbot, *J. Electrochemical Soc.*, **153**, G622 (2006).

11. T. Gopal, PhD Thesis, University of California, San Diego (2004).

12. Z. Li, K. Ina, P. Lefevre, I. Koshiyama, and A. Philipossian, *J. Electrochemical Soc.*, **152** (4), G299 (2005).

13. A. R. Mazaheri and G. Ahmadi, *J. Electrochemical Soc.*, **150** (4), G233 (2003).

14. G. B. Basim, I. U. Vakarelski, and B. M. Moudgil, *J. Colloid and Interface Science*, **263,** 506 (2003).

15. K. Osseo-Asare, *J. Electrochemical Soc.*, **149** (12), G651 (2002).

16. G. B. Basim and B. M. Moudgil, *J. Colloid and Interface Science*, **256**, 137 (2002).

17. A. Jindal and S. V. Babu, *J. Electrochemical Soc.*, **151** (10), G709 (2004).

18. S. Ramarajan, Y. Li, M. Hariharaputhiran, Y. S. Her, and S. V. Babu, *Electrochemical and Solid-State Letters*, **3** (5), 232 (2000).

19. G. Xu, H. Liang, J. Zhao, and Y. Li, *J. Electrochemical Soc.*, **151** (10), G688 (2004).

20. M. K. Carter and R. Small, *J. Electrochemical Soc.*, **151** (10), B563 (2004).

21. T. Du, A. Vijayakumar, and V. Desai, *Electrochemica Acta*, **49**, 4505 (2004).

22. S. Deshpande, S. C. Kuiry, M. Klimov, Y. Obeng, and S. Seal, *J. Electrochemical Soc.*, **151** (11), G788 (2004).

23. Y. Wang, R. Bajaj, G. Lam, Y. Dordi, D. Bennet, and F. Redeker, *Mat. Res. Soc. Symp. Proc.*, **671** (2001).

24. T. Gopal and J. B. Talbot, *J. Electrochemical Soc.*, **154**, H507 (2007).

25. S. Aksu and F. M. Doyle, *J. Electrochemical Soc.*, **149** (7), B340 (2002).

26. S. Chang, T. Chang, and Y. Lee, *J. Electrochemical Soc.*, **152** (10), C657 (2005).

27. D. Beegan, S. Chowdhury, and M.T. Laugier, *Surface and Coatings Technology*, **210**, 5804 (2007).

28. E. Matijevic and S. V. Babu, *J. Colloid and Interface Science*, (2007), doi:10.1016/j.jcis.2007.11.057

29. M. Bielmann, U. Mahajan, and R. K. Singh, *Electrochemical and Solid-State Letters*, **2**, (8) 401 (1999).

30. M. Pourbaix, *Atlas of Electrochemical Equilibria in Aqueous Solutions*, National Association of Corrosion Engineers, Houston, Texas (1974).

31. A. Szymanski and J. M. Szymanski, *Hardness Estimation of Minerals Rocks and Ceramic Materials*, Elsevier Science Publishers B. V., New York, NY (1989).

32. Y. Feng, K.S. Siow, W. K. Teo, K. L. Tan, and A. K. Hsieh, *Corrosion*,**53**, 389, (1997).

33. S. Aksu and F. M. Doyle, *J. Electrochemical Soc.*, **148** (1), B51 (2001).

34. S. Tamilmani, W. Huang, S. Raghaven, and R. Small, *J. Electrochemical Soc.*, **149** (12), G638 (2002).

CHAPTER 7

COPPER SURFACE ANALYSIS

7.1 Introduction

By exposing a copper surface to various solution chemistries, the surface nanohardness value can vary from 0.05 to 20 GPa [1, 2]. This is due to the formation of different types of films, such as oxides, hydroxides, and complexes, and/or etching of the surface leading to porous, less compact films [2]. In Chapter 5, the state of the copper on the surface were infered using the measured nanohardness, potential-pH equilibrium diagrams, and other observations from literature. The following section discusses the surface analysis of copper samples before and after exposure to a solution of 0.1M glycine, 2.0wt% H_2O_2, and 1mM KNO_3 at pH 10.0. This solution was chosen because the film formed on the surface was much harder (>15GPa) than any of the other samples studied in Chapter 5.

Surface analysis by x-ray photoelectron spectroscopy (XPS), also known as electron spectroscopy for chemical analysis (ESCA), is accomplished by irradiating a specimen with monoenergetic soft x-rays and energy-analyzing the emitted electrons. Each element has a unique elemental spectrum, and the spectral peaks from a mixture are approximately the sum of the elemental peaks from the individual constituents. Since the mean free path of the electrons is very small, the electrons that are detected originate from only the top few atomic layers. Quantitative data can be obtained from the peak heights or areas, and identification of chemical states can be made from the exact positions and separations of the peaks, as well as certain spectral contours [3].

7.2 Experimental

Surface analysis was performed by electron spectroscopy for chemical analysis (ESCA) using a Perkin-Elmer 5400 ESCA from Physical Electronics, Inc. Two copper film (1000 nm) sputter deposited on 30 nm tantalum on pieces of silicon wafer (~1 cm^2) were analyzed. One copper sample was not exposed to any solution, and the other was immersed for 10 min in 100 mL of an aqueous solution of 0.1M glycine, 2.0wt% H_2O_2, and 1mM KNO_3 with pH adjusted to 10.0 using KOH. After immersion, this sample was air dried and immediately placed into the ESCA chamber for measurement.

7.3 Results and Discussion

Figure 7.1 shows the ESCA spectra for the copper sample before and after exposure to 0.1M glycine, 2.0wt% H_2O_2, and 1mM KNO_3 at pH 10.0. For the copper surface before exposure to solution, the broad peak between binding energies of 933.7 and 935.1 eV is consistent with the formation of both CuO and $Cu(OH)_2$ [3, 4]. The shifted peaks near 943 and 963 eV confirm the presence of CuO [3-6]. The peak between 953.5 and 955.2 may be due to the formation of either CuO and $Cu(OH)_2$. This is consistent with the research of Du et al. who suggest that the copper surface forms a duplex structure made up of CuO/$Cu(OH)_2$ followed by Cu_2O [7]. However, the results for the sample before exposure do not show Cu_2O, which may be due to Cu_2O existing below the depth of technique (~3-5 nm), or it simply may not be there [3].

For the copper surface after exposure to solution, all peaks (933.7, 943, 953.5, and 963 eV) are consistent with the formation of CuO [3]. For this sample there is no

indication of hydroxide formation. The hardness measurements reported for this sample in Chapter 5 suggested that the surface may have had a very thick, hard layer with a hardness of >15 GPa which is consistent with the formation of a copper oxide [1].

ESCA analysis is a useful tool to determine the state of the copper at the surface of the wafer when the surface layer is spatially uniform [3]. However, as suggested by our hardness measurements, after exposure to the various solutions, the surface layers of most of our samples most likely are inhomogeneous and may have different films and/or various compactness of the surface film [2]. As shown in Figure 7.1, the binding energies for the different states of copper are very similar [3, 4], which makes it difficult to differentiate by ESCA, and therefore, ESCA analysis of additional samples was deemed inadequate to provide further discriminating information about the surface state of the copper films.

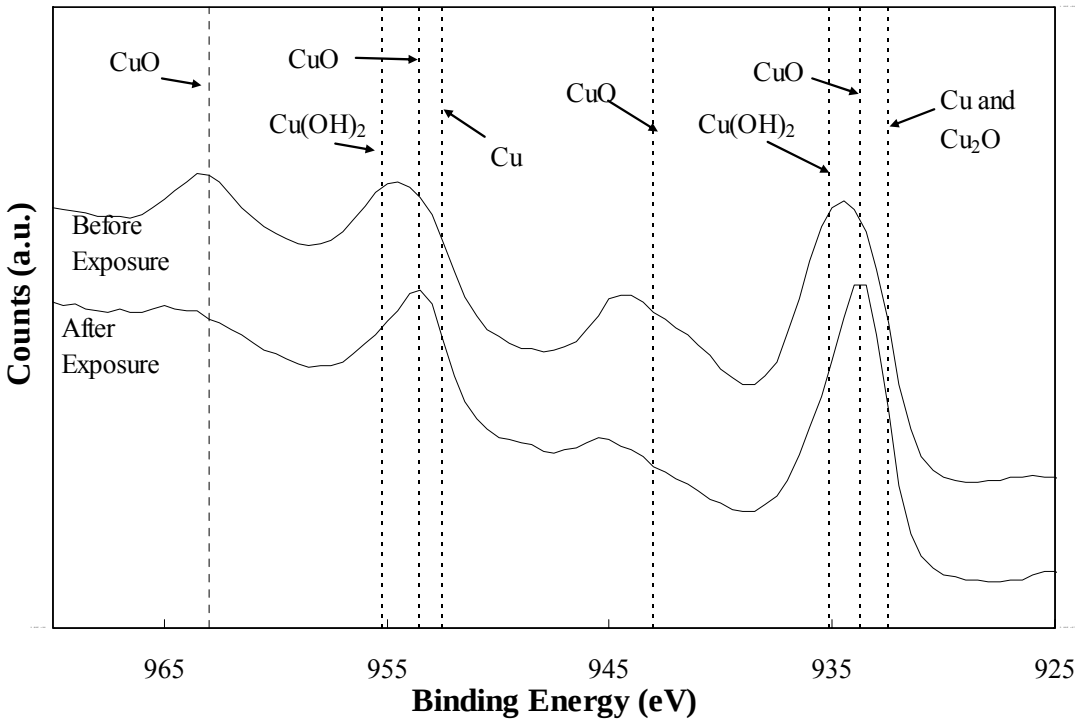

Figure 7.1 ESCA analysis of copper samples before and after exposure to an aqueous solution with 0.1M glycine, 2.0wt% H_2O_2, and 1mM KNO_3 at pH 10.0. Reference for bonding energies from [3-6].

REFERENCES

1. R. V. Ihnfeldt and J. B. Talbot, *J. Electrochemical Soc.*, **155**, 6 (2008).

2. A. Jindal and S.V. Babu, *J. Electrochemical Soc.*, **151** (10), G709-G716 (2004).

3. J.F. Moulder, W.F. Stickle, P.E. Sobel, and K.D. Bomben, *Handbook of X-ray Photoelectron Spectroscopy*, Physical Electronics, Inc. Eden Prairie, Minnesota (1992).

4. M. Kulkarni, D. Ng, M. Baker, H. Liang, and R. Her, *Wear*, **263**, 1470 (2007).

5. D.E. Mencer, M.A. Hossain, R. Schennach, T. Grady, H. McWhinney, J.A.G. Gomes, M. Kesmez, J.R. Parga, T.L. Barr, and D.L. Cocke, *Vacuum*, **77**, 27 (2004).

6. M. C. Kang, H. Nam, H.Y. Won, S. Jeong, H. Jeong, and J.J. Kim, *Electrochemical and Solid-State Letters*, **11**, (2) H32 (2008).

7. T. Du, D. Tamboli, V. Desai, and S.Seal, *J. Electrochem.Soc.*, **151**, (4) G230 (2004).

CHAPTER 8

CONCLUSIONS AND FUTURE WORK

8.1 Conclusions

Since planarization during CMP is achieved through a combination of surface modification by chemical reaction and mechanical abrasion, an understanding of the effects of slurry chemistry on the colloidal behavior of the abrasives and the hardness of the surface is important. This dissertation is a continuation of the preliminary work of Tanuja Gopal whom investigated the colloidal aspects of CMP slurries [1]. In this research, the role of chemical additives as well as the effect of copper particles on the colloidal properties of the alumina abrasives were examined by measurement of zeta potential and agglomerate size distribution. Additionally, the effects of common slurry additives and pH of the solution on the nanohardness and etch rate of the copper surface were also studied. The experimental results were incorporated into a model of CMP to predict material removal rate (MRR) and predictions were compared to experimental copper CMP data.

It was found that the addition of copper nanoparticles to the slurry affects the colloidal properties of the alumina abrasives. Even with a small amount of copper in the slurry solutions, an increase or decrease in agglomeration of the alumina is observed depending on the state of the copper in the solution, which is generally consistent with potential-pH equilibrium diagrams from literature [2]. With the addition of chemical additives and changes in the pH of the solution, the nanohardness of the copper film was observed to range from 0.05 – 20 GPa, due to the formation of different films

(CuO, Cu_2O, etc.) and/or changes in the compactness of the surface film from complexing reactions or dissolution.

The experimentally measured agglomerate size distributions, hardness and etch rates were used in the Luo and Dornfeld model of CMP to predict MRR [3]. The model assumes that material removal occurs due to the plastic deformation of the wafer surface by a spherical abrasive. In this research the size and standard deviation of the abrasives were measured under quiescent conditions. For these measurements to be applicable in the model, it is assumed that the agglomerated abrasive particles must be strong enough to withstand the shear force of the wafer during CMP. Therefore, the shear force of the wafer sliding over the agglomerate must be less than the force required to break up the agglomerate. Previous studies of the Luo and Dornfeld model have either neglected agglomeration of the abrasives by assuming the shear force on the abrasives was large enough to break apart the agglomerates, or have assumed the shear force was small so that measured agglomerate sizes could be used [1, 3, 4]. In this research, a criteria was developed to determine the shear force on the abrasives during CMP which was compared to the force required to break apart the agglomerates. For the CMP conditions of this study, it was found that the agglomerated abrasive particles would not break apart during CMP, hence the agglomerate size measurements could be used in the CMP model.

This is the first time this model has been applied to the copper CMP process to directly compare with experimental CMP data. Initial modeling work incorporated the agglomerate size and distribution measurements both with and without the presence of copper nanoparticles in the solution into the model to predict MRR, where the hardness

of the copper surface was assumed constant, that of Cu metal ~2.3 GPa, and the chemical etch rate was neglected. The model predictions only agreed with experimental copper CMP data under certain conditions. Further modeling work incorporated the copper nanohardness and etch rate measurements into the model, which improved the agreement with experiment.

The Luo and Dornfeld model accounts for the chemical activity of the slurries through the abrasive size and distribution, hardness and chemical etch rate parameters. The model overpredicted the MRR when the pH was less than 4; as the nanohardness of the surface measured may be much lower than that of a very thin passivation layer (<5nm). As the pH increased to >8 the hardness increased, which may be due to the thickness of the passivation layer on the copper surface increasing; then the model predictions agreed much better with experiment. Addition of glycine and H_2O_2 to the solution increased the etch rates and the experimental MRRs significantly, and the model was unable to predict the MRR. As the nanohardness and etch rate measurements were done under quiescent conditions, they may not fully represent the surface during polishing. However, the nanohardness measurements provide information on the range of physically possible values that may occur during CMP. The Luo and Dornfeld model may be able to provide reasonable MRR predictions as long as the abrasive size and distribution of the dispersion, and the hardness parameter are representative of the copper surface during polishing and if such measurements are possible.

8.2 Future Work

With the continuous decrease in device sizes in IC manufacturing, there are new challenges and improvements to the CMP processes. It is believed that CMP will continue to enable IC manufacturing for the next couple of decades, and therefore, it is important to understand the effects of the different consumables (slurries, pads, process conditions, etc.) on the CMP process [5]. Future work should continue to develop a basic understanding of the agglomeration/dispersion effects on CMP. Various chemical additives and exposure to materials (i.e. copper) can alter the dispersion characteristics of a slurry. An initial study on the rate of agglomeration of the abrasives after addition of chemical additives is given in this research (Chapter 3), however, more work is needed to understand the change of agglomerate distributions over time and the effects of additives on these distributions. Modeling the agglomerate size distributions over time of polishing as a function of chemistry would also be useful in developing more robust CMP models.

In industry, the CMP machines are typically operated continuously, with up to thousands of wafers processed per consumable set (pad, conditioner, etc.) [6]. The temperature of the consumables has been observed to increase over time from 24 to 38 ^{0}C, which could have significant affects on the CMP process, especially for a highly reactive process such as copper CMP, where the reaction rates are very sensitive to temperature [7]. A study on the effects of heating (temperature) on the agglomeration of the abrasives and the wafer surface hardness as a function of chemistry is needed.

In a typical CMP process the wafer is exposed to flowing slurry for ~5-10min [6]. The nanohardness measurements in this research, were performed after a 10 min

exposure time to solution under quiescent conditions. The results of the hardness of a copper sample after immersion in a solution for various exposure times is reported in Chapter 5, which showed that the exposure time can have significant effects on the surface hardness. Further studies on the hardness with exposure time in solution may help to determine the rate of formation of different surface films (CuO, $Cu(OH)_2$), etc.), and aid in determining the chemical reactions of importance to CMP (fast reactions versus slow reactions). Measuring nanohardness after exposure to flowing slurry may provide values that are more representative of the surface during CMP. Additionally, future work may require using a different type of AFM tip, or adjusting other equipment or parameters on the AFM tool, in order to probe within 1-5 nm of the surface. This may also provide values more representative of the surface that the abrasive particle encounters during CMP, compared to the measurements of this study which were done within >5nm of the surface.

In this research, only the Luo and Dornfeld model was used to predict MRR. More recently developed CMP models, such as the model proposed by Chandra et al. [8], certainly have some significant improvements and future work may be able to incorporate the experimental results of this research into other models. For copper CMP processes with low down pressures, the hydrodynamic models have also worked well, mainly because these models account for the chemical reactivity of the slurry with the copper surface. However, when polishing copper with standard down pressures (>1psi) the hydrodynamic models are unable to predict MRR because they do not account for the synergistic effect of the abrasive particles and slurry chemistry. The models that assume solid-solid contact mode typically only account for the effects of

the chemicals in the slurry through a wafer surface hardness parameter, which does not account for the variation in hardness over time nor the inhomogeneous films that typically form during copper CMP. Also these models define the physical process parameters by interpolating or extrapolating from experimental MRR [3, 8]. To date, no CMP models have been developed which account for both the abrasive size effect, such as the Luo and Dornfeld model [3], and the chemical reactions with the copper surface, such as the Paul et al. model [9]. Future copper CMP models may be able to combine these two approaches.

REFERENCES

1. T. Gopal, "Colloidal Aspects of Chemical Mechanical Planarization", PhD Thesis, University of California, San Diego (2004).

2. S. Tamilmani, W. Huang, S. Raghavan, and R. Small, *J. Electrochemical Soc.*, **149**, G638 (2002).

3. J. Luo and D. Dornfeld, *IEEE Trans. Semi. Manuf.*, **14**, 112 (2001).

4. T. Gopal and J. B. Talbot, *J. Electrochemical Soc.*, **154 (6)**, H507-H511 (2007).

5. K. Cadien, "Is There a Future For CMP?" Proceedings for the 13th International CMP for ULSI Multilevel Interconnection Conference (CMP-MIC), Keynote presentation, Fremont, California, March 4, 2008.

6. M. R. Oliver, *Chemical-Mechanical Planarization of Semiconductor Material*, Springer-Verlag, Berlin, Germany (2004).

7. D. Kwon, H. Kim, and H. Jeong, *Journal of Materials Processing Technology*, **178**, 82 (2006).

8. C. Wang, P. Sherman, and A. Chandra, *Int. J. Manufacturing Technology and Management,* **7** (5), 504 (2005).

9. E. Paul, F. Kaufman, V. Brusic, J. Zhang, F. Sun, and R. Vacassy, *Journal of the Electrochemical Society*, **152** (4), G322 (2005).